Modelling the soil-structure interaction of 60 m long piles under gradual loading during construction of a high-rise building in Rotterdam

Diana Margarita Portillo Arreguin

TU Delft

Gemeente Rotterdam

Modelling the soil-structure interaction of 60 m long piles under gradual loading during construction of a high-rise building in Rotterdam

by

Diana Margarita Portillo Arreguin

to obtain the degree of Master of Science in Civil Engineering

at Delft University of Technology.

Student number:	5476860	
Project duration:	December 1st, 2022 – September 26th, 2023	
Thesis committee:	Dr. ir. M. Korff,	TU Delft, supervisor
	Dr. ir. R. Spruit,	Gemeente Rotterdam
	ing. R. Schippers,	Geobest BV
	ir. R. Crielaard,	TU Delft
	Dr. ir. K. Gavin,	TU Delft

TU Delft

Gemeente Rotterdam

Acknowledgements

I express my infinite gratitude to the individuals and organizations who played a vital role in the development of my thesis:

To the Municipality of Rotterdam, for granting me the invaluable opportunity to work and learn in their dynamic environment.

To Rodriaan Spruit, for offering me to be part of this project, for his unwavering support, enthusiasm, and encouragement in this journey, and for pushing me to learn Dutch.

To Mandy Korff, for her constant guidance and insightful advice that shaped the direction of this project.

To Robert Schippers, for generously sharing his knowledge on the POST Rotterdam project, high-rise building foundations, and Plaxis 3D modelling.

To Roy Crielaard and Ken Gavin, I extend my appreciation for their valuable feedback and support during the meticulous revision process.

To the companies involved in the fibre optic instrumentation of POST Rotterdam foundation: Fundex Verstraeten BV, Geobest BV, Besix, Gemeente Rotterdam, and TNO.

To Roman van Os for supporting me with access to the POST Rotterdam construction site, and to Willem van Bommel (Municipality of Rotterdam) for his assistance with the FO measurements on-site.

To Dirk de Lange and Kevin Duffy for sharing their wisdom and insights into the intricate world of soil-structure interaction.

To Nadevah, Zanyar, and Freyre for the companionship that has made my time in the Municipality of Rotterdam truly enjoyable.

To my loving family, my long-time friends, and to the new friends I have made along my master's journey, my heartfelt thanks.

Abstract

This thesis examines the load distribution on 60 m long piles under gradual static loading, considering the POST Rotterdam high-rise building as the study project. The research employs fibre optic (FO) instrumentation on site to monitor strain changes in the piles over time and assess load transfer mechanisms. This data is integrated into a Plaxis 3D model of the building's foundation to validate existing approaches on soil structure interaction (SSI), optimize SSI modelling, and assess the high-rise building's impact on nearby structures. Results show that at early stages, the resistance contribution comes from the shaft in contact with the Pleistocene sand layer. However, as loading progresses and the Kedichem clay layer consolidates, most of the resistance shifts to the tip and the shaft located in the deeper sands. The FO strain measurements follow a similar trend to the site stratigraphy, but there is high uncertainty about the results at early load stages. The latter requires further investigation to corroborate once the building is finalised. The piles were incorporated into the Plaxis 3D model by means of EBR with a layer-dependent force distribution. The resulting spring stiffness of various pile groups reveals the significance of the group effect. Regarding the impacts of POST loads on the adjacent Old Post Office building, an angular distortion of 1/555 in 50 years was obtained, which indicates a conservative result of slight damage in the structure. For the Timmerhuis building, a resulting angular distortion of 1/1428 indicates no damage. This study addresses gaps in understanding load distribution in 60 m long piles, offering a practical modelling approach and recommendations for future research. It contributes to optimizing design and safety protocols as the use of such piles becomes more common in Rotterdam. By utilizing advanced sensing techniques like FO, this research may lead to more accurate pile design and criteria, potentially reducing construction costs and enhancing safety for high-rise buildings and their surroundings.

Nomenclature

Abbreviations

$3D$	Three-dimensional
$BOTDA$	Brillouin Time Domain Analysis
$BOTDR$	Brillouin Time Domain Reflectometry
$c-c$	Centre-to-centre
CPT	Cone Penetration Test
EBR	Embedded beam row
FC/APC	Ferrule Connector/Angled Physical Contact
FE	Finite element
FO	Fibre optic
HS	Hardening Soil
NAP	Amsterdam Ordnance Datum or Normaal Amsterdams Peil
SLS	Serviciability limit state
SSC	Soft Soil Creep
SSI	Soil structure interaction
SSM	Soft Soil Model
ULS	Ultimate limit state

Suffixes

b	Base
$conc$	Concrete
lat	Lateral
$pile$	Pile
$ref50$	Reference secant
$refoed$	Reference oedometer
$refur$	Reference unload/reload
sat	Saturated

Symbols

α_p	Factor for base resistance calculation
α_s	Factor for shaft resistance calculation
$\Delta\sigma$	Stress increment
ΔF_b	Tip resistance increment
ΔF_s	Shaft resistance increment
Δs	Soil displacement increment
Δu	Pile displacement increment
Δu_b	Pile tip displacement increment
$\Delta u_{rel,b}$	Soil-pile tip relative displacement increment
Δu_{rel}	Soil-pile relative displacement increment

$\Delta u_{s,b}$	Soil displacement increment at the pile tip
γ	Soil unit weight
$\kappa*$	Modified swelling index
$\lambda*$	Modified compression index
$\mu*$	Modified creep index
ν	Poisson's ratio
ϕ'	Friction angle
ϕ_{inter}	Friction angle of the interface
ψ	Dilatancy angle
$\sigma'p$	Preconsolidation stress
$\sigma'v$	Effective stress
τ	Unit shaft resistance
ε	Strain
A	Area
c'	Cohesion
c_{inter}	Cohesion of the interface
D	Diameter
D_b	Material stiffness matrix of the pile tip
Dr	Relative density
E	Stiffness
F_b	Tip force
F_s	Shaft resistance
f_s	Cone sleeve friction
H	Layer thickness
I	Moment of inertia
K_0^{nc}	H/V stress ratio in normally consolidated 1D compression
m	Power for stress-level dependency of stiffness
N	Axial force
OCR	Overconsolidation ratio
POP	Pre-overburden pressure
q_b	Unit base resistance
q_c	Cone tip resistance
Q_{ult}	Ultimate bearing capacity
R_{inter}	Relative stiffness between modelled pile and soil
s	Settlement
t	Thickness
T_{skin}	Material stiffness matrix of skin interface
u	Pile displacement

Contents

List of Figures

List of Tables

1

Introduction

1.1. Problem statement

The escalating trend of constructing tall buildings in densely populated urban areas is increasingly shaping the contemporary urban landscape. In the Netherlands, Rotterdam is the leader of this transformative wave, in which the increment of high-rise buildings in the city aims to improve the quality of urban living while addressing the housing shortage.

However, the pursuit of vertical expansion is accompanied by geotechnical challenges. A typical soil profile in Rotterdam is composed of intercalations of dense sands and compressible clays. While piles reaching the Pleistocene sand layer at -30 m NAP have long served as the foundation solution for various structures in Rotterdam, this approach becomes unsuitable for high-rise buildings in the city centre, where the building density is significant. The elevated stress concentration in the Pleistocene sand could trigger important consolidation within the underlying Kedichem clay layer, leading to unfavourable differential settlements (Schippers et al., 2021) that could damage the surrounding buildings over time. Consequently, the demand for innovative foundation methodologies has prompted the exploration of alternatives, i.e., the installation of screw-displacement piles that penetrate the deep dense sand layer at approximately -65 m NAP.

Nonetheless, this alternative presents additional challenges; when loaded, the deep clay layers will undergo consolidation gradually, leading to changes in the soil-structure interaction (SSI) behaviour. With this, the accuracy of the currently available modelling techniques becomes uncertain, and existing knowledge on these unique foundations is limited for the Dutch ground conditions.

1.2. Scope and objective of research

This thesis addresses the soil-structure interaction within the context of foundation engineering for high-rise buildings. The main objective is to study load distribution along 60 m long piles subjected to gradual loading during construction, considering the POST Rotterdam high-rise

building as the study project. Through the application of FO instrumentation on the POST site, the study aims to capture the strain development of these piles over time, and thus evaluate load transfer mechanisms. This information will contribute to verify what is the best way to model the 60 m long piles, in order to predict their behaviour in the short and long term. With more high-rise projects to be constructed in Rotterdam, understanding the load distribution of this foundation alternative is vital.

1.3. Research questions

The research questions to be answered are shown below.

- How does stress distribute in very long piles, in the short and long term, considering Rotterdam's soil profile?
- How accurate are the predictions of stress distribution of the current existing approaches?
- What is the best way to model the soil-structure interaction of these very long piles?

These questions will be reconsidered in the last chapter based on the obtained results.

1.4. Outline

The thesis is developed as follows. Chapter 2 examines definitions of soil-structure interaction, Dutch pile design, and recently proposed adjustments to the methodology, plus their application in currently designed Rotterdam's high-rise buildings.

Then, in Chapter 3, the study project is presented. POST Rotterdam's project details, including soil profile and pile installation, are mentioned, along with a description of the instrumentation process on site, and interpretation procedures.

Next, Chapter 4 includes the construction of simplified single spring models using NEN methodology, comparing INTER and D-Pile Group software results, and assessing parameter sensitivity. Parameters marked by a high uncertainty in soil-structure interaction calculations are analysed, and their effect on final load distribution and pile displacement outcomes is discussed, aiming to optimize further complex modelling.

Subsequently, Chapter 5 covers Plaxis 3D modelling, including general aspects, constitutive models and soil parameters, progressing from single pile to group modelling.

Following, Chapter 6 presents fibre optic measurement interpretation, their correlation with group models, and identifies the optimal pile modelling method.

Further, Chapter 7 includes the final complete high-rise foundation model, predicting long-term behaviour and structural impact on the adjacent buildings.

Finally, Chapter 8 concludes and offers recommendations, contributions, and future impacts.

2

Literature review

2.1. Soil structure interaction

Soil structure interaction (SSI) accounts for the connection between a foundation or structure and the soil or rock under it. When a structure is built, it transmits the loads to the soil underneath it, thus, the soil responds to these loads by deforming and exerting reaction forces on the structure (Kausel, 2010).

In pile foundations, piles are installed in order that the tip reaches a competent deep soil layer where it can develop optimum base and shaft resistance forces while minimizing reaction deformations on the structure and the surroundings. Thus, the soil-structure interaction becomes a complex iterative system in which, when the piles are loaded, they need some displacement with respect to the soil in order to develop skin friction (with the surrounding soil) and therefore give resistance to the building through the shaft. Likewise, piles can also develop base resistance at the tip by moving against the ground. Furthermore, there are two types of skin friction to consider for SSI analyses: On one side, positive skin friction is an upward force that contributes to the reaction forces against structural loads. On the other side, negative skin friction is a downward force that occurs when the shallow soft soil layers on site consolidate and act as a down drag on the foundation (Rajapakse, 2016).

There are several methodologies for calculating resistance, however, this thesis will focus on the α method described by NEN 9997-1 (2017), as it is the most widely used in the Netherlands.

2.2. Current Dutch design approach

The pile design established in the NEN 9997-1 (2017) is based on the use of cone penetration tests (CPT) tip resistance, and constant reduction factors for the determination of tip and shaft bearing capacity. These values account for the maximum resistance the pile can develop:

$$\tau_f = \alpha_s q_c \tag{2.1}$$

$$q_b = \alpha_p q_c \tag{2.2}$$

where:
τ_f: unit shaft resistance (kPa)
q_b: unit base resistance (kPa)
α_s: factor for calculating shaft resistance in compression (-)
α_p: factor for calculating base resistance (-)
q_c: CPT tip resistance (kPa)

The ultimate axial bearing capacity (Q_{ult}) is given by the sum of shaft and base resistance[1].

$$Q_{ult} = \tau_f A_{lat} + q_b A_b \tag{2.3}$$

where:
A_{lat}: lateral area (m^2)
A_b: area of pile base (m^2)

Bearing capacity can be affected by several factors (Bica et al., 2014), such as the soil type and its stress state, the installation method, the degree of soil displacement during installation, residual loads, the geometry of the pile, and set-up and time-related effects. The installation method is considered in the NEN 9997-1 (2017) methodology by the α_s factor as stated in Table 2.1.

Table 2.1: Reduction factors for pile resistance calculation (adapted from Gavin et al., 2021).

Pile type	α_p	α_s	α_t
Pre-cast concrete closed-end	0.7	0.01	0.007
Steel tube closed-end	0.7	0.01	0.007
Steel tube open-end	0.7	0.006	0.004
Screw injection pile	0.63	0.009	0.009
Continuous flight auger	0.56	0.006	0.0045
Bored pile	0.35	0.006	0.0045

In the Dutch approach (NEN 9997-1, 2017), the normalized load-settlement curves (Figure 2.1) are used to calculate the pile settlement under different load magnitudes depending on the pile types, which are classified as follows:

1. Type 1: Displacement piles.

[1]Unit shaft and unit base resistances can be transformed into force when multiplied by the pile lateral area or the pile base cross-section, respectively.

2. Type 2: Partial displacement piles, in which the soil is partly removed around the pile shaft during installation.

3. Type 3: Piles whose installation results in a significant disturbance to the surroundings, but also provide a large bearing capacity.

With this, it is possible to determine the safe load-carrying capacity and estimate the expected settlement under specific design loads. In Figure 2.1, the first graph shows the relationship between the force on the pile tip and its sag, both as normalized values[2]. Likewise, the second graph presents the relationship between shear force (normalized value) and tip displacement (in mm).

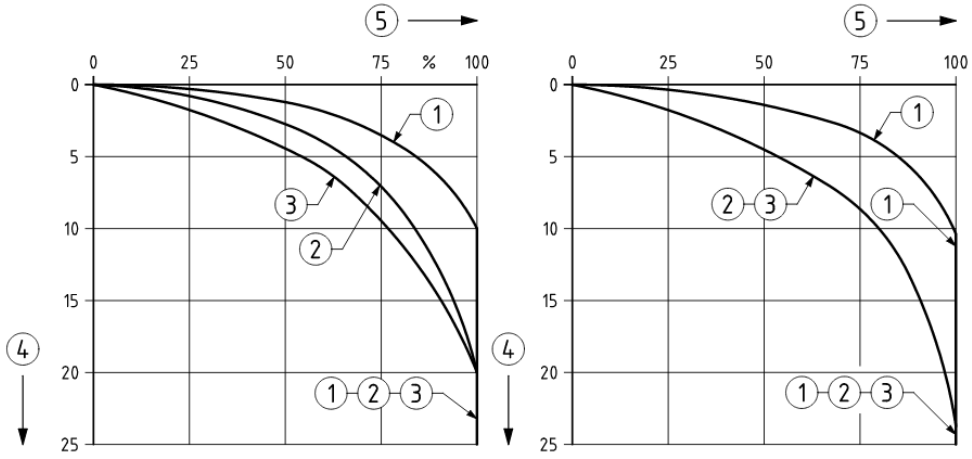

Legenda

1 last-zakkingslijn 1 volgens tabel 7.c
2 last-zakkingslijn 2 volgens tabel 7.c
3 last-zakkingslijn 3 volgens tabel 7.c
4 $\frac{s_b}{D_{eq}}$, in %
5 $\frac{R_{b;k}}{R_{b;k;max}}$, in %

Figuur 7.n — Relatie tussen de kracht op de paalpunt (R_b), in % van de maximumkracht op de paalpunt ($R_{b;max}$) bij de uiterste grenstoestand of de bruikbaarheidsgrenstoestand en de zakking van de punt (s_b), in % van D_{eq}

Legenda

1 last-zakkingslijn 1 volgens tabel 7.c
2 last-zakkingslijn 2 volgens tabel 7.c
3 last-zakkingslijn 3 volgens tabel 7.c
4 s_b, in mm
5 $\frac{R_{s;k}}{R_{s;k;max}}$, in %

Figuur 7.o — Relatie tussen de schuifkracht op de paalschacht (R_s), in % van de maximumschuifkracht op de paalschacht ($R_{s;max}$) bij de uiterste grenstoestand of de bruikbaarheidsgrenstoestand en de zakking van de punt (s_b), in mm

Figure 2.1: Load settlement curves of piles (NEN 9997-1, 2017).

Translation note: Figure 7.n: Relationship between the force on the pile tip, expressed in percentage of the maximum force on the pile tip at the ultimate limit state or serviceability limit state and the sag of the tip, as a percentage of equivalent pile diameter. Figure 7.o: Relationship between the shear force on the pile shaft, as a percentage of the maximum shear force on the pile shaft, at the ultimate limit state or the serviceability limit condition and the sag of the tip in mm.

It must be emphasized that the load-settlement curves are intended for safe design purposes (Frissen, 2020) and therefore may not fully capture the complexities of real conditions at all

[2]In the first graph of Figure 2.1, axes correspond to normalized values; the force is expressed as a percentage of the maximum force on the tip, and the sag of the tip is included as a percentage of the pile diameter.

times. NEN 9997-1 (2017) was calibrated by means of experimental data (Ter Steege, 2022) obtained from typical Dutch foundation projects and subsoil conditions, but uncertainty is introduced when either the project specifications or the site materials are out of the scope.

In addition, Duffy, Gavin, Askarinejad, et al. (2022) and Ter Steege (2022) present research on screw displacement piles with grout injection by means of the interpretation of existing load tests, performed in several sites in the Netherlands. The main improvement proposals for the designed process are discussed as follows: First, it is stated that the measured load tests data has a better fit to the load-settlement curve of type 2 piles (Figure 2.1), differing from the indications of NEN 9997-1 (2017) to follow a type 1 behaviour. This indicates that there is a softer mobilisation of shaft fiction and the base mobilisation is larger than 10% of the cross-section diameter. Second, it is shown that limiting the q_c values on the bearing capacity calculations results in a more conservative design but deviates the calculations from the measured data. Third, the calculated α_p values from load tests result in values ranging from 0.23 to 0.35, which are considerably lower than the value stated in the code for screw-displacement piles (0.63). Results show the load-settlement curve of NEN 9997-1 (2017) overestimates the base resistance (as shown in Figure 2.1), and therefore α_p values should be lowered.

2.3. Group effect

When piles are installed in groups, the individual behaviour can be influenced by the presence of the neighbouring piles, depending on spacing, soil properties and structural requirements (Poulos, 1968).

When soil pressures overlap in the pile cluster, their behaviour gets affected. On one side, the group gains efficiency: When pile groups are closely spaced, there is an overall increase in the bearing capacity of the individual piles (Poulos, 1968), as there is a more efficient load distribution between them. On the other side, neighbouring piles can also cause negative interference (Bowles, 1997); if there is excessive compaction of the soil among the group, its stiffness will increase, which can decrease the relative soil-pile displacement from the inner piles and therefore reduce their capacity. Likewise, the settlement of an individual pile can induce additional settlement or changes in load distribution on the adjacent piles (Poulos, 1968). Further, the group effect may also have impacts in the presence of lateral loads; depending on the pile spacing, geometry, and soil conditions, lateral stiffness and resistance can be altered. Increasing the spacing between piles in a group results in a decrease in the stress intensity from overlapping stressed zones. However, large pile spacings are impractical in reality, as pile groups are commonly covered by a pile cap to support the column base and distribute the load to multiple piles within the group (Bowles, 1997).

Estimating soil stresses from multiple piles in a group is challenging for several reasons. Pile caps often introduce uncertainty as they share the load with all the piles within the group (Bowles, 1997). The distribution of friction effects along the piles is often unknown, making it hard to recognize specific loads. Assessing the overlap of stresses from neighbouring piles is difficult, as well as considering the impact of pile driving on the surroundings. Moreover, time-related factors such as consolidation, changing loads, and groundwater level variations further complicate load estimation.

2.4. High-rise buildings design experience in Rotterdam

This section describes the experience of building in Rotterdam and applying the above guidelines, as well as the considerations that have been made according to stratigraphic conditions and project requirements. The soil profile in this area typically consists of several distinct layers (Woestenburg, 2020): Near the surface, there is a sandy layer of 3 m thick extending until approximately -6 m NAP. Below this, there is a soft soil sequence comprising clay and peat, forming a layer of 7 m in thickness, from -6 m to approximately -18 m NAP, known as the Holocene pack. Subsequently, there is a 20 m thick layer of dense sand, commonly referred to as the Pleistocene sand layer, ranging from approximately -18 m to -33 m NAP. Underneath lies the Kedichem clay, occupying a depth from -33 m to -45 m NAP, characterized by alternating layers of hard overconsolidated clay and dense sand. Further exploration reveals the presence of a dense sand layer with hard clay from -45 m to -58 m NAP, followed by a very dense sand layer (part of the Wad formation) extending from -58 m to -85 m NAP[3].

While most of the existing structures in Rotterdam are founded on piles whose tip reaches the Pleistocene sand layer, this is not a viable solution for high-rise buildings. The large additional stresses could cause significant consolidation of the Kedichem clay layer, which would lead to settlements on all the layers above Kedichem that will mainly affect the surrounding structures (Schippers et al., 2021), with special attention on the Old Post Office historical building. Consequently, it has been necessary to look for alternatives, such as the construction of diaphragm walls (Robbemont and Janssen, 2018), or the installation of special foundations, the latter being the most popular in the design of upcoming high-rise projects. Due to this, a foundation alternative was defined, which involves the installation of screw-displacement piles that reach the deep dense sand layer, at approximately -65 m NAP. This solution has been implemented in major high-rise building projects, such as Zalmhaven (Schippers et al., 2021), De Sax and Tree House Rotterdam.

These buildings, until now, have followed a bearing capacity calculation methodology based on the NEN 9997-1 (2017) with some modifications considering the pile installation, as shown in Figure 2.2. When grout injection is applied during drilling, it is assumed that the borehole diameter in the lower sand layers corresponds to the pile tip diameter (0.95 m). This assumption is based on the fact that the sand layer above this diameter is fully mixed with grout and remains stable during drilling. The α_s value specified in NEN 9997-1, 2017 for type 1 is employed for this purpose. For the intermediate clay layers, an increased shaft friction coefficient is applied. To address potential issues related to incomplete mixing and clay layer deformation during grout hardening, a reduction in pile diameter is necessary. In this case, the average casing and pile tip diameter of 0.85 m is utilised. Regarding the upper section of the pile, factors such as the installation method, grout cover thickness and quality and precise pile diameter cannot be definitively determined. Consequently, a reduced α_s value is adopted for the upper sands, taking into account the smallest value provided in NEN 9997-1, 2017. Similarly, a conservative assumption is made, setting the pile diameter equal to 0.762 m in the upper clay layers (negative skin friction zone).

[3]The last dense sand layer hereby mentioned corresponds to the deepest registered geotechnical explorations done for the aforementioned high-rise buildings.

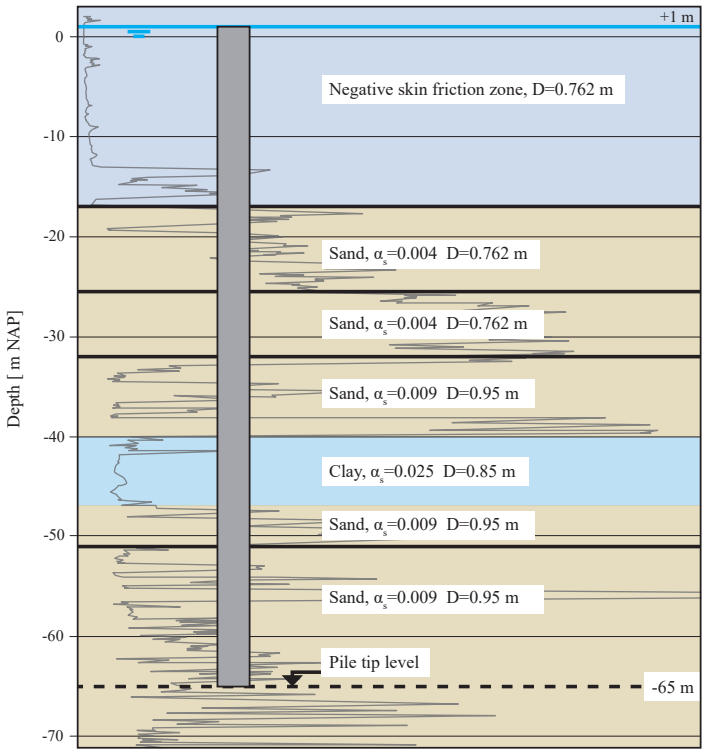

Figure 2.2: Current bearing capacity calculation methodology for high rise buildings (adapted from Schippers et al., 2021).

3

Study project

3.1. General aspects

The study project consists of the restoration of the old Post Office building and the construction of a 155 m tall high-rise building in its courtyard. The new concept, shown in Figure 3.1, will convert the site into a multicomplex including a hotel, apartments, catering, shops and a public passage (POST, 2021).

Figure 3.1: POST Rotterdam (POST, 2021).

The site is located in the city centre of Rotterdam, as shown in Figure 3.2. The City Hall and the Stadhuisstraat lie to the north, while Meent street and the World Trade Center are located to the south. Rodezand street, Timmerhuis building, and local businesses are situated to the east, and Coolsingel street is found to the west. The project will occupy an area of approximately 936 m^2.

Figure 3.2: Project location (adapted from Google Maps).

3.2. Soil profile

To investigate the site stratigraphy, six CPT up to a depth of -75 m NAP were carried out between 2018 and 2021 (Schippers and Broekens, 2021). The complete ground investigation, as well as the location of the CPT, is available in Appendix A. The soil profile is described below.

- **Clean sand.** From ground level to -6.8 m NAP, fine clean sand is shown, with an average cone resistance of 5 MPa.
- **Holocene pack.** From -6.8 m NAP to -16.0 m NAP, a series of soft materials are found. First, a sandy clay is shown, with a cone resistance of 0.8 MPa. Following, peat is found with a cone resistance of 0.8 MPa. Further, the soundings present a soft clay with an average cone resistance of 0.7 MPa.
- **Pleistocene sand.** From -16.0 m NAP to -34.0 m NAP, a medium-dense to dense sand is found, with an average cone resistance of 15 MPa.
- **Kedichem clay.** From -34.0 m NAP to -48.2 m NAP a layer is found that consists of sandy clays interspread with packed sand, with an average cone resistance of 4 MPa. It must be highlighted that from -36.4 m NAP to -38.2 m NAP, a medium-dense sand is present, whose cone resistance is 12 MPa.

- **Deep dense sand.** From -48.2 m NAP to the final CPT depth a very dense sand is found, with a variable cone resistance from 12 MPa to 30 MPa.

Likewise, based on the drainage recommendation of the project (Schippers and Broekens, 2021), a water level of -1.4 m is assumed.

3.3. Geotechnical overview

3.3.1. Piled foundation

Since the high-rise building construction will lead to important differential settlements in the area, in order to reduce them, the foundation design considers the installation of piles that reach the deep dense sand layer. The degree of differential settlement is important for the Old Post Office not only for its historical value, but predicted economic losses related to damage to buildings range from 5 to 45 billion euros by 2050 in the country (Hoogvliet et al., 2012; Van den Born et al., 2016; Kok and Angelova, 2020).

In accordance with the project specifications (Schippers and Broekens, 2021), soil displacement screw piles with lost steel casing and grout injection were implemented, commercially known as Tubex piles with grout injection. They have a shaft diameter of 762 mm and a tip diameter of 950 mm. The pile tip is set to be at -65.0 m NAP, while the pile head will be at the bottom of the basement (-5.0 m NAP), which means the piles are 60 m long. Soil displacement piles are vibration-free, soil-displacing concrete piles, consisting of a permanent steel tube that is screwed to depth (Fundex Verstraeten BV, 2021). As the foundation is not driven, but drilled, noise and vibration nuisance in the surroundings is minimized. Likewise, since the permanent steel casing does not need to be extracted, it is possible to install them at significantly deep levels (Ter Steege, 2022).

3.3.2. Geotechnical construction stages

Construction stages were planned as follows, according to Schippers and Broekens (2021) and The POST Bouw (2023). Appendix B includes a detailed photographic report.

1. Demolition of the existing wall adjacent to Rodezand street.
2. Installation of the four sheet pile walls to form the building pit.
3. Installation (and instrumentation) of screw-displacement piles.
4. Lowering of the water level from -1.0 m NAP to -2.5 m NAP.
5. Excavation from 0.75 m NAP to -2.0 m NAP.
6. Installation of struts at -2.0 m.
7. Lowering the water level to -7.0 m NAP.
8. Excavation until -5.6 m NAP.
9. Casting of the concrete slab.
10. Removal of the struts.
11. Construction of basement and ground floor.

12. Construction of the rest of the building.

3.3.3. Pile installation

For the standard pile installation (Figure 3.3) first, a steel tube that has a steel drill tip (with a diameter slightly larger than the tube) is placed on the ground level. Next, the pipe is screwed by applying an axial pressure and a torque, until desired tip level is reached. Parallelly, a grout mixture is injected from the base to reduce friction while screwing (Ter Steege, 2022), and to fill the overcut, since the pile tip has a larger diameter than the shaft. Later, the steel tube can be cut to the exact height. The reinforcement cage is placed inside the tube, and concrete is poured (Fundex Verstraeten BV, 2021).

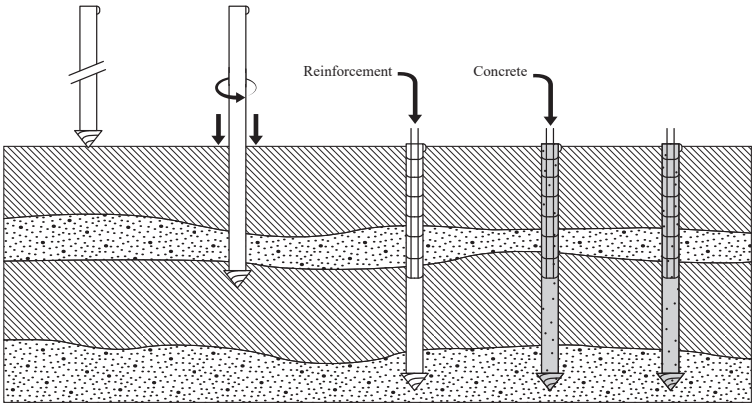

Figure 3.3: Installation of Tubex piles (adapted from Fundex Verstraeten BV, 2021).

Since the Tubex piles have a maximum length of approximately 30 m, for this project, the installation was done in two sections, as described by Schippers and Broekens (2021). The pile tip level is on average at -65.0 m NAP, and the pile head level must be at approximately -5.0 m NAP (at the basement level). A scheme of the pile installation is shown in Figure 3.4.

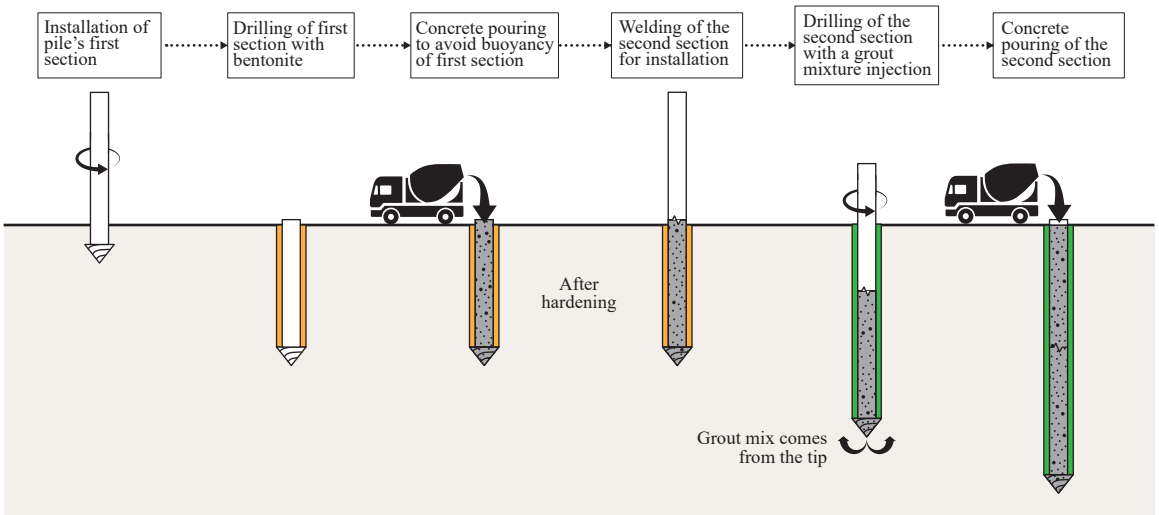

Figure 3.4: Installation process of piles on site (adapted from Schippers and Broekens, 2021).

The first pile section of 33 m in length was drilled to depth implementing bentonite, and later filled with concrete to avoid buoyancy. Further, the second section was welded to the first. After some hardening of the concrete (usually on the next working day), the second section is drilled in, injecting the shaft from the drilling tip with cement grout during drilling to the final depth.

During installation, the following uncertainties arise:

- First, the installation of the piles is carried out in two parts that follow different procedures. In the lower part, from -65.0 m to -33.0 m NAP, the pile is screwed and grout is directly injected. However, the grout injection comes from the bottom when installing the upper part of the pile. Therefore, there is uncertainty in the thickness and quality of the grout fill (Schippers et al., 2021).
- Second, there is uncertainty about the quality of the attachment of the two parts of the pile.
- Third, due to the heterogeneous soil profile, the grout diameter may vary along the pile depending on the surrounding soil (Schippers and Broekens, 2021). At the sand layers, the diameter may approximate the tip diameter, as the grout envelope forms around the case during the downward drilling of the pile. However, at the parts in contact with clay, the soil may push back after screwing, leading to grout deformation and reduction of its cross-section during hardening.
- Fourth, the Tubex piles consist of concrete, the steel casing and grout, with the concrete being the material that occupies the largest percentage of the cross-section. While all of the materials are prefabricated and account for specific design strength and stiffness values, it is possible that slight variations in the concrete's stiffness impact the final performance of the pile.

3.4. Pile instrumentation

3.4.1. Background

The project of POST Rotterdam was an opportunity to carry out a study on stress distribution along very long piles by means of fibre optic (FO) instrumentation. The goal is to measure the strain development of the piles in time, as the structure is being built on top. With this, the load transfer from the pile to the soil is studied and therefore, it can be understood how stress distributes along these piles (in time) in the city centre of Rotterdam. Thus, current design approaches will be verified, and suggestions to improve their accuracy, along with their implications, will further be developed.

The instrumentation was done jointly by the piling company (Fundex Verstraeten BV), the foundation design bureau (Geobest BV), the main contractor (Besix) and the instrumentation providers (Gemeente Rotterdam and TNO).

3.4.2. Fibre Optic (FO)

FO consists of a glass core, an outer layer called cladding and a plastic coating around it (van Overstraten Kruijsse, 2019). The cladding has a refractive index slightly smaller than the glass core. Consequently, if a light pulse is sent through the FO, when it hits the cladding at a shallow enough angle, it can be completely reflected by it instead of passing through. Therefore, the light pulse travels in a zigzag pattern until it reaches the end of the fibre (Kechavarzi et al., 2019).

While it is possible to obtain information on temperature and strain with the FO, for this project, the technology is implemented for strain measurement only, by means of the reflectometry interrogation methods Brillouin Time Domain Reflectometry (BOTDR) and Brillouin Time Domain Analysis (BOTDA). In both processes a light pulse is sent through a silica fibre, generating a Brillouin scattering signal (Bilgen and Günday, 2021). Part of the light pulse is reflected back, while the rest propagates along the rest of the fibre. As the scattered light travels back, it has a nonlinear interaction with strain-induced acoustic waves (van Ravenzwaaij et al., 2018), which can alter the light frequency. This process is recorded in time throughout the entire fibre length to extract the Brillouin frequency shift (Duffy, Gavin, Lange, et al., 2022). With this, it is possible to determine the strain distribution. A scheme of the measuring mechanism is shown in Figure 3.5.

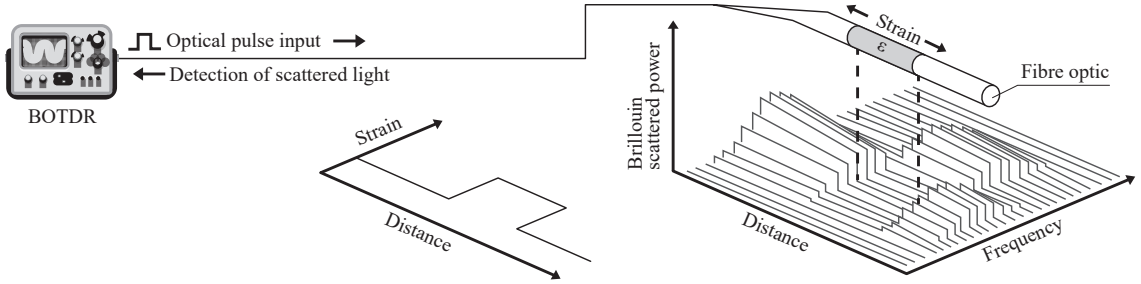

Figure 3.5: Measurement mechanism (adapted from Zhang et al., 2004).

The difference between BOTDR and BOTDA is that when applying BOTDA, a second light pulse is sent from the opposite end of the fibre, in order to amplify the reflection that is generated within the cable. Due to the amplification, the signal of BOTDA is stronger and therefore, the measurements have a longer sensing range, a higher resolution, and more sensitivity towards strain measurements, as well as a faster reading (Ismail et al., 2019). Nonetheless, it is only possible to apply it when there is access to both ends of the FO. In contrast, BOTDR provides a lower reading resolution, but can be applicable when only one end of the fibre is reachable (Bilgen and Günday, 2021), which is common in geotechnical engineering. Additionally, measurements can still be taken even if the cable breaks.

The implementation of FO represents several advantages such as spatial resolution, long sensing distances and the ability to provide a profile of continuous data at a low cost per reading (de Battista et al., 2016). This technology has had multiple applications of monitoring in geotechnical and structural engineering in recent years, such as local strain measurements in foundations and geogrids, pipe deformation, load distributions along anchors, tracking of the

casting process, reactivation of old inclinometer casings, and could also be used as an alternative to traditional extensometers (van Ravenzwaaij et al., 2018). Nonetheless, its use involves challenges such as equipment selection and integration, accurate data interpretation, and FO careful handling at all stages.

3.4.3. Instrumentation on site

Instrumentation consisted of the installation of FO cables throughout the whole length of four piles on site, referred as piles 18, 31, 92 and 97 in the piling plan shown in Figure 3.6.

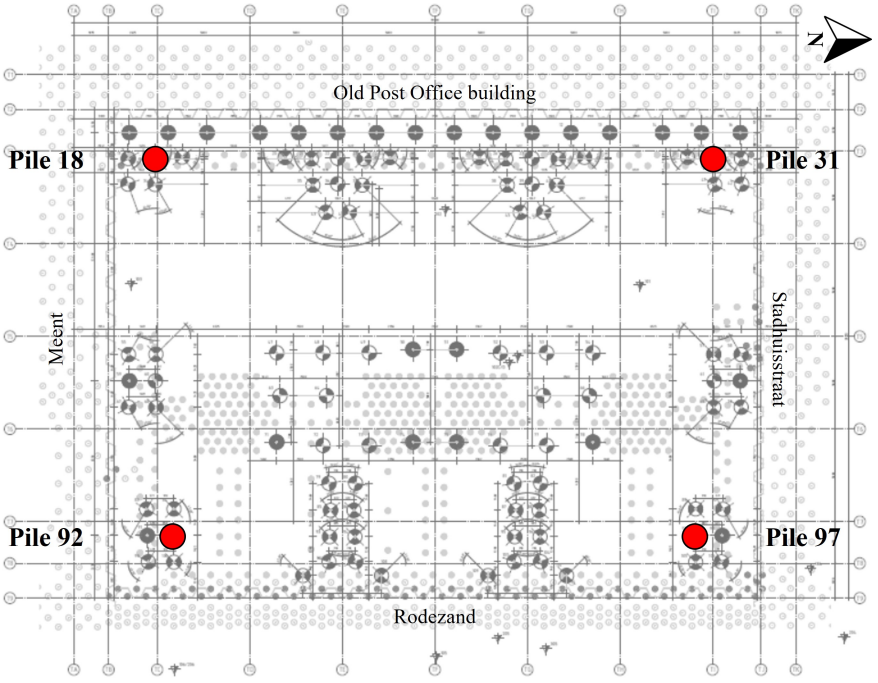

Figure 3.6: Location of instrumented piles on site (adapted from Pieters Bouwtechniek, 2021).

The instrumentation was carried out after the installation of the second section of the pile, while the grout was not hardened yet. The FO was attached to a 65 m rebar and introduced into the grout-injection tube by means of a crane until reaching the end of the pile. While the piles were planned to be constructed until the bottom of the basement level (-5 m NAP to -7 m NAP), the instrumented piles were extended to surface level, and cut, to be able to take measurements at the desired level, after excavation of the basement (Figure 3.7a). Special attention had to be taken in order to cut the steel case without damaging the FO. Likewise, the FO included an extra PVC layer for protection. FO inside of the pile can be seen in Figure 3.7b.

(a) Pile cutting while protecting the FO. **(b)** FO inside the pile.

Figure 3.7: Process of pile cutting and protection of the FO.

It is worth noting that in a regular pile load test, the basic measurements to be taken are load-displacement and load-transfer (Bica et al., 2014). However, in this case study, only load-transfer instrumentation is available. Although valuable information about the load distribution on piles can be obtained, it would be ideal to have instrumentation to quantify and verify pile displacement.

3.4.4. Measuring process

Depending on the construction works the access to the piles has been different, i.e. when the baseline measurements were taken the top of the piles were exposed to the surface (Figure 3.8a), as there was nothing built on top. However, as the construction works progressed, the piles were covered by the basement slab and by load-bearing walls and columns, and therefore, a small box was built inside the structures to facilitate access to the FO of each pile (Figure 3.8b). In the future, the Municipality of Rotterdam plans to make an installation to recover strain data remotely, however, during the development of this project, all data was gathered physically on site.

(a) FO access on the surface. **(b)** Connection box inside a wall.

Figure 3.8: Access to the FO on site.

The measuring process is shown in Figure 3.9. First, the pile is located (Figure 3.9a and subsequently, the cable is cut, and the plastic coat is removed in order to expose the fibre (Figure 3.9b). The FO is attached to a set of pigtails, so that it can be connected to the interrogator through an FC/APC Patch cable. The cables used in this project include two fibres (blue and red coloured) to measure strain, and therefore it is advised to make pigtail connections to both for redundancy. When the set-up is finalised (Figure 3.9c), real-time readings can take place (Figure 3.9d), in which all data is sent to the reading unit and gathered in a laptop. FO interrogation, the sensing cable and the installation technique must be appropriately adjusted to guarantee the quality of the measurement results (Monsberger et al., 2020). Likewise, it is important to avoid sharp bends along the FO cables to avoid loss of signal (Kania and Sorensen, 2020), and to keep the working area at a warm temperature to prevent cable damage due to cold[1].

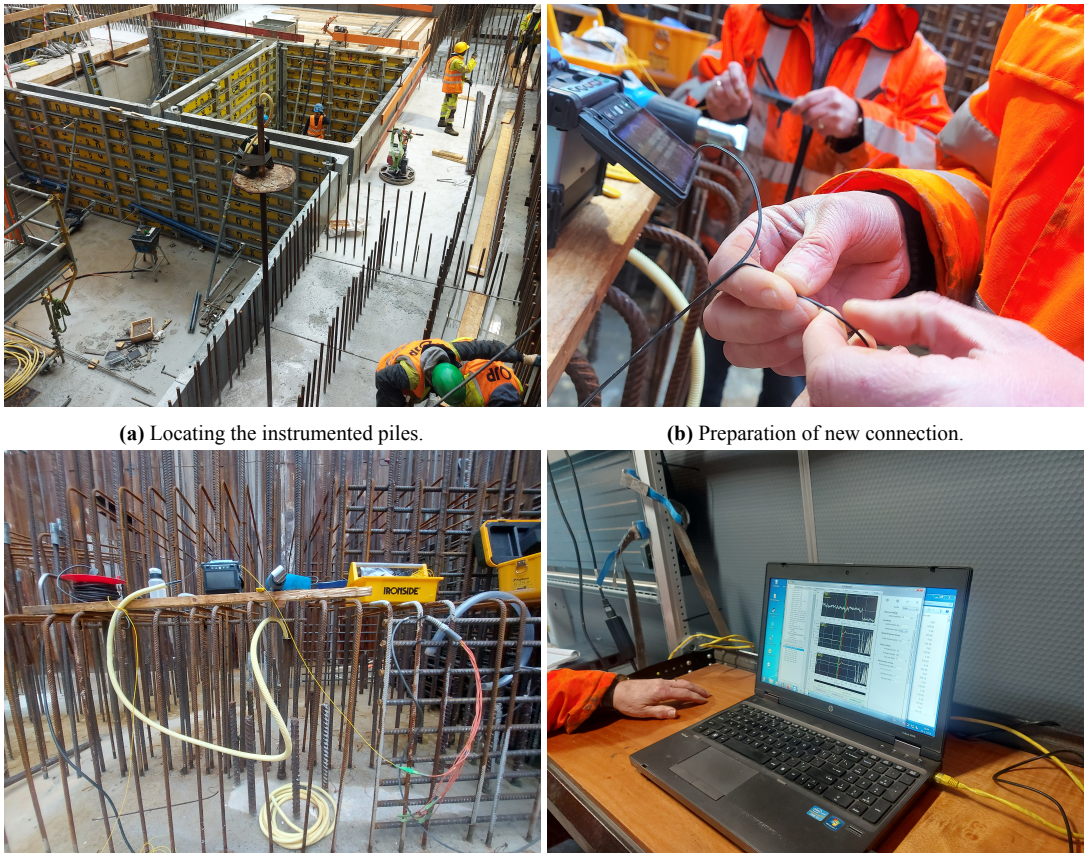

(a) Locating the instrumented piles.

(b) Preparation of new connection.

(c) Cable setup for FO measurements.

(d) Gathering data

Figure 3.9: Process of gathering FO data of pile 97 on site.

[1]While there is not a specific minimum temperature at which FO cables can be manipulated, it is recommended to maintain a controlled temperature in which the cable remains flexible and thus, less susceptible to damage. The specific temperature tolerance of every cable may depend on its composition and the manufacturer's specifications.

3.4.5. Interpretation of FO readings

The pile is expected to show displacement downwards during loading, and therefore developing shaft and base resistance. Shortening occurs along the pile (Matic et al., 2019), which is captured by the FO as strains and can be transformed into axial force as:

$$N = \varepsilon E_{pile} A_{pile} \tag{3.1}$$

where:
N: axial force (kN)
ε: strain ($\mu\varepsilon$ - microstrain)
E_{pile}: pile stiffness (kPa)
A_{pile}: pile cross-section (m^2)

4

Single spring models

4.1. General aspects

The goal of this chapter is to investigate SSI on single spring models, as stated by NEN 9997-1 (2017). By gaining a deeper understanding of these factors, it will be possible to better interpret FO measurements and develop more accurate finite element models in the next steps. This chapter presents an analysis of single spring models built in INTER and D-Pile Group programs, simulating the study project conditions. In addition, the performance of both programs is compared. Further, a series of sensitivity analyses are carried out on the parameters whose uncertainty is higher, and their impact on the final SSI results is assessed.

4.2. INTER

INTER is a code developed in the 1990s with the aim of better describing SSI. Since its initial development, the program has played an important role in predicting the load-deformation behaviour of piles in various projects. The following data is used as input:

- Diameter of the pile.
- Equivalent diameter of steel in the pile.
- Pile type to be considered at the shaft and at the tip (NEN 9997-1, 2017).
- Depth levels of each soil layer.
- Maximum shear force to be mobilised at each defined depth level.
- Maximum end bearing capacity.
- Loads acting at the pile head.
- Soil settlements per layer.

An in-depth description of the operation of the program is given by van Dalen et al. (2014). With the input information, INTER creates a pile that is divided into smaller elements, each with a specific relationship between the specified mobilised shear force and deformation relative to the ground. The program calculates the shortening or elongation of each element and

the respective mobilised shear force based on the deformation and axial force at the top of each element. The iterative process begins with an estimated deformation of the pile head to which a known axial force (pile loading) is applied. By performing the iteration process, a load-deformation diagram of the pile is calculated.

4.3. D-Pile group

D-Pile Group is a software program part of Deltares' D-series designed to analyse individual piles and groups, along with their interactions with the cap and surrounding soil under specified loads. The program represents the SSI by means of axial and lateral soil springs along the pile length (Deltares, 2020). It establishes the non-linear correlation between force and displacement by means of a standard methodology (i.e. API or NEN Dutch standard) or through custom force-displacement curves. In D-Pile Group, the interaction analysis involves the connections between the cap, as well as the adjacent soil, considering various interaction models (Poulos, Plasti-Poulos, cap-soil interaction, cap-layered interaction, dynamic model). These interaction models are based in linear elasticity and can be combined with the aforementioned pile-soil relationships, finding a balance between the accuracy of the results and efficiency in computation time. The following data is used as input:

- Selection of the interaction model.
- Soil materials and selection of their force-displacement correlation method.
- Depth levels of each soil layer.
- Pile material, stiffness and geometry.
- Pile tip curve values.
- Position of the pile and cap.
- Load stages acting at the pile head.
- Soil displacement profiles.

4.4. Comparison of software features

Several distinctive aspects emerge in both programs that could influence their applicability and results.

First, INTER is a user-friendly code with a straightforward interface and simple data input requirements. Compared to D-Pile Group, INTER needs fewer user interactions and selections. D-Pile Group offers a wider range of features and options, which comes with a steeper learning curve.

Second, when considering the application of horizontal loads, INTER offers limited adaptability, as it only considers vertical loads, settlements and displacements in the z-direction. While this simplifies the input, it also limits its adaptability for horizontal load cases. In contrast, D-Pile Group delivers results in 3D, offering a wider comprehension of pile behaviour[1]. Nonetheless, to study static conditions, it is only possible to input loads and bending moments

[1] Horizontal load cases are out of the scope of the graduation project.

at the pile top or cap for both softwares (except for the dynamic model in D-Pile Group, as stated by Deltares, 2020). For the analyses hereby presented, the cap interaction model from D-Pile Group is the one comparable with INTER, the rest of the interaction models cannot be used.

Third, the calculations on INTER rely on the load-settlement curves specified by NEN 9997-1 (2017), which is a limitation when confronting design standards outside the realm of NEN. In contrast, in D-Pile Group is possible to carry out analyses implementing NEN 9997-1 (2017) curves, API methodology, or any user-specified load-settlement behaviour (Deltares, 2020).

Fourth, INTER operates with shaft force values which require recalibration every time parameters such as layer depths or pile diameters. Moreover, it considers constant pile properties and geometry throughout its whole length, which simplifies modelling but fails to capture variations that could occur throughout the pile length. While it is possible to add this feature in the code, this increases the complexity of the input. In contrast, D-Pile Group offers a simpler approach to modifications in the model by considering unit shaft and tip resistance, and normalized curves in the analysis, as well as the ability to input pile segments with different defined properties. This serves to enhance the precision and authenticity of the model.

Fifth, hysteresis is considered in INTER by specifying a percentage of mobilisation from the NEN 9997-1 (2017) load-settlement curves (van Dalen et al., 2014). This behaviour is captured by some interaction models of D-Pile Group, which offer several interaction models for users to choose from, including simpler cap interaction models, as well as more intricate alternatives that even incorporate FEM. In addition, iteration parameters in INTER should be calibrated before starting calculations since they could alter the accuracy of results.

Finally, both programs share several common attributes in their single spring pile models. These include a constant unit weight of water, the exclusion of sloping ground surfaces from calculations, the disregard of excess pore water pressure effects, and the representation of the pile as a linear elastic beam capable of addressing compression and bending.

4.5. Standard single pile model

4.5.1. Building the standard model

The process of creating a standard single spring pile model in INTER and D-Pile Group is described below.

4.5.2. Program input

For this calculation, the characteristics of the project foundation were considered: A pile of 0.762 m in diameter and 60 m in length, whose tip reaches -65 m NAP in a typical Rotterdam soil profile.

The soil layers and maximum shear force to be mobilised are detailed in Table 4.1 for IN-

TER. The soil profile was defined according to the available site information, while the shaft resistance of sand layers was calculated as stated by NEN 9997-1 (2017) for screw displacement piles (type 1 shaft and tip curves), considering the α_s and q_c values hereby presented. Moreover, the maximum mobilised shear force from clay layers was obtained considering the sleeve friction (f_s), as presented in Table 4.2. In both cases, the force to be input in INTER was calculated by multiplying shaft resistance by the lateral area of each pile element.

Table 4.1: Soil layers and maximum mobilised shear force for sand layers (INTER input).

Layer	Depth (m NAP)		α_s	q_c (MPa)	τ (kPa)	Fs (kN)
Sandy clay	-5.0	-7.1			-	
Peat	-7.1	-9.6			-	
Soft clay	-9.6	-16.0				
Pleistocene sand	-16.0	-34.0	0.009	10	90	3878.1
Kedichem clay I	-34.0	-36.4			-	
Kedichem sand	-36.4	-38.2	0.009	12	108	465.4
Kedichem clay II	-38.2	-48.2			-	
Dense silty sand	-48.2	-56.1	0.009	12	108	2042.5
Dense sand	-56.1	-65.0	0.009	20	180	3835.0

Table 4.2: Maximum mobilised shear force for clay layers (INTER input).

Layer	Depth (m NAP)		f_s (MPa)	Fs (kN)
Sandy clay	-5.0	-7.1	0.03	150.8
Peat	-7.1	-9.6	0.05	299.2
Soft clay	-9.6	-16.0	0.02	306.4
Kedichem clay I	-34.0	-36.4	0.10	574.5
Kedichem clay II	-38.2	-48.2	0.06	1436.3

Likewise, tip resistance was defined according to NEN 9997-1, 2017 for type 1 piles, determined in the usual traditional way with Koppejans' method. Therefore, an α_s value of 0.63 was chosen, getting a pile tip force equal to 5746 kN. Further, the stiffness of the piles was calculated considering a weighted average of the concrete, the steel casing and the surrounding grout as explained in Table 4.3. For the concrete, short and long term stiffnesses were varied (Gilbert, 2013).

Table 4.3: Calculation of pile stiffness.

	Diameter (m)	t (mm)	E (kPa)	A (m^2)	I (m^4)	EA (kN)	EI (kN m^2)
Grout	0.856	0.0470	2.0x10^6	0.119	9.81x10^{-3}	2.39x10^5	1.96x10^4
Tube	0.762	0.0088	2.0x10^8	0.021	1.48x10^{-3}	4.16x10^6	2.95x10^5
Concrete (short term)	0.744	-	3.1x10^7	0.435	1.51x10^{-2}	1.30x10^7	4.70x10^5
Concrete (long term)			2.0x10^7				
Total (short term)			2.97x10^7	0.570	2.64x10^{-2}	1.79x10^7	7.82x10^5
Total (long term)			2.34x10^7			1.30x10^7	6.16x10^5

The model set-up of D-Pile Group is equivalent to the one specified in INTER, with some considerations accounting for the software differences. In order to make both models equivalent, the simple cap interaction model was chosen, as it only considers cap interaction with elastoplastic pile-soil interaction (Deltares, 2020). Additionally, each soil layer was defined with a specific load-settlement curve, which was built considering the maximum mobilised shear force (Tables 4.1 and 4.2) and the normalised shaft curve from NEN 9997-1 (2017) (Figure 2.1). Likewise, the pile tip force is not an input value like in INTER, but is introduced as a load-settlement curve. The latter was defined similarly to the shaft load-settlement curves, by considering a maximum mobilised force of 5746 kN and the normalised tip curve from NEN 9997-1 (2017) shown in Figure 2.1[2].

Several combinations of loads and soil settlements were carried out to study different SSI scenarios and will be further described.

4.5.3. Load input

For the standard single pile model, a load of 6700 kN will be considered, which is the maximum load discharged from the finished building, in accordance with Schippers and Broekens (2021).

4.5.4. Settlement input

The settlement profile, referred to as the *greenfield condition*, was calculated considering a load of a 0.5 m tall embankment of sand with a unit weight of 20 kN/m^3. This load is a representation of a standard fill and levelling in the centre of Rotterdam, which could occur on the POST site surroundings over the years. The settlement profile was calculated in Plaxis 3D for the short term (right after the embankment was finished) and for the long term (after 20,000 days, when consolidation and creep occurred on the clay layers). Further, it was verified by means of the 1D equation:

$$s = \frac{\Delta\sigma}{E_{oed}} H \tag{4.1}$$

where:
s: settlement (m)
$\Delta\sigma$: stress increment (kPa)
E_{oed}: oedometric stiffness (kPa)
H: layer thickness (m)

For the above, the stiffness of all the materials of the soil profile was defined based on laboratory test results, the site CPTs and the available information of other projects in Rotterdam. The stiffness parameters are shown in Table 4.4, and the greenfield settlement profile is shown in Figure 4.2. It must be noted that this settlement profile is a starting point for the single pile analyses since SSI is a complex phenomenon that requires iteration between input loads and

[2]It must be noted that INTER works with force units (kN), while the D-Pile Group input considers unit shaft and tip resistance (kN/m).

soil displacements.

Table 4.4: Stiffnesses of soil profile (for settlement calculation).

Layer	Depth (m NAP)		E_{50} (MPa)
Backfill sand	1.0	-4.7	20
Sandy clay	-4.7	-7.1	3
Peat	-7.1	-9.6	3
Soft clay	-9.6	-16.0	4
Pleistocene sand	-16.0	-34.0	60
Kedichem clay I	-34.0	-36.4	25
Kedichem sand	-36.4	-38.2	60
Kedichem clay II	-38.2	-48.2	25
Dense silty sand	-48.2	-56.1	60
Dense sand	-56.1	-65.0	100

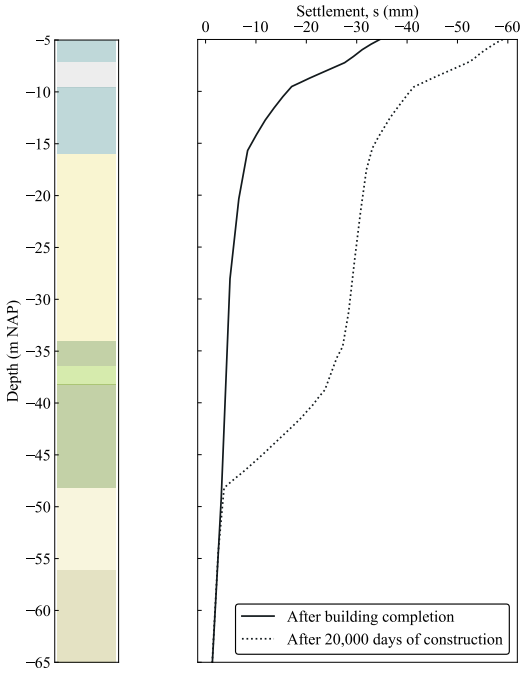

Figure 4.1: Standard settlement profile.

4.5.5. Results from the standard model

Both calculations were first calibrated without a settlement profile, as shown in Figure 4.2. At this stage, both programs display equivalent results of a pile displacement of 11 mm.

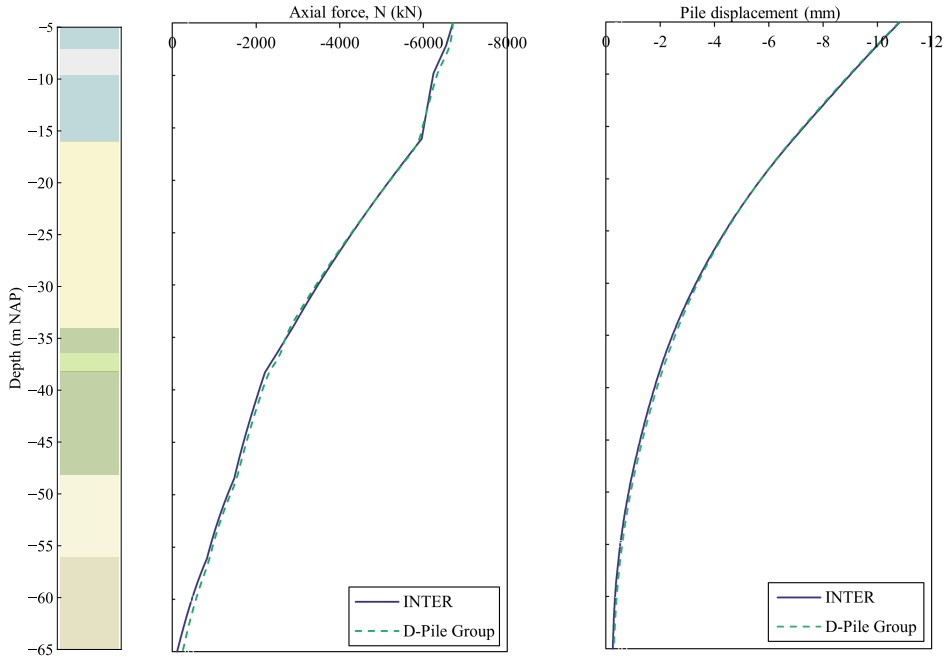

(a) Axial force vs depth. **(b)** Pile displacement vs depth.

Figure 4.2: Results of the standard single pile model without displacement profile, using INTER and D-Pile Group.

Further, Figure 4.3 presents SSI results in the short term for INTER and D-Pile Group. It can be seen that pile behaviour is consistent in both programs; in the short term, the largest force development occurs in the Pleistocene sand, while the deeper sand layers barely develop shaft and tip resistance. Figure 4.3a shows some differences in axial force distribution in the Holocene pack and the first Kedichem clay: For instance, at the first Kedichem clay results of D-Pile Group show there is little to no contribution of said layer, while INTER presents some force mobilisation at the same depth. Nonetheless, Figure 4.3b shows both programs calculated a similar pile displacement, with 1.6% of difference between each other.

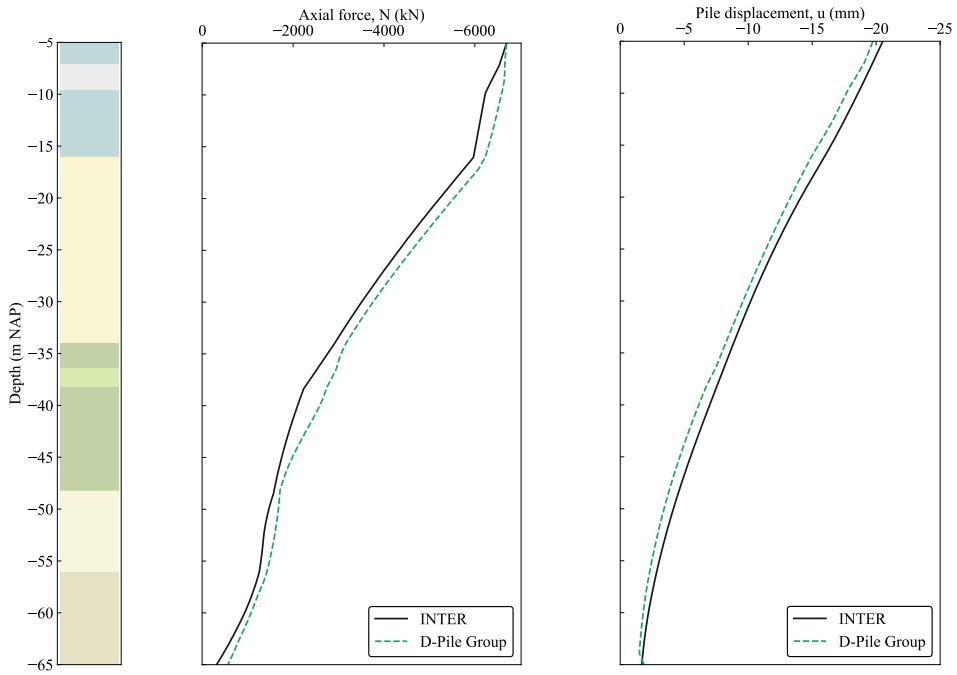

(a) Axial force vs depth **(b)** Pile displacement vs depth

Figure 4.3: Results of the standard single pile model in the short term, using INTER and D-Pile Group.

Likewise, Figure 4.4 presents results for the long term for INTER and D-Pile Group. In both cases, over time, there is a shift of stresses from the Pleistocene sand layer to the deeper sand layers, and the pile displacement is approximately double than in the short term. This occurs because when the Kedichem clay consolidates and settles, it affects the Pleistocene layer. As the sand also settles, its contribution to shaft resistance development is reduced. Consequently, the pile has to carry more weight than initially and therefore it requires larger pile displacement to mobilise such resistance.

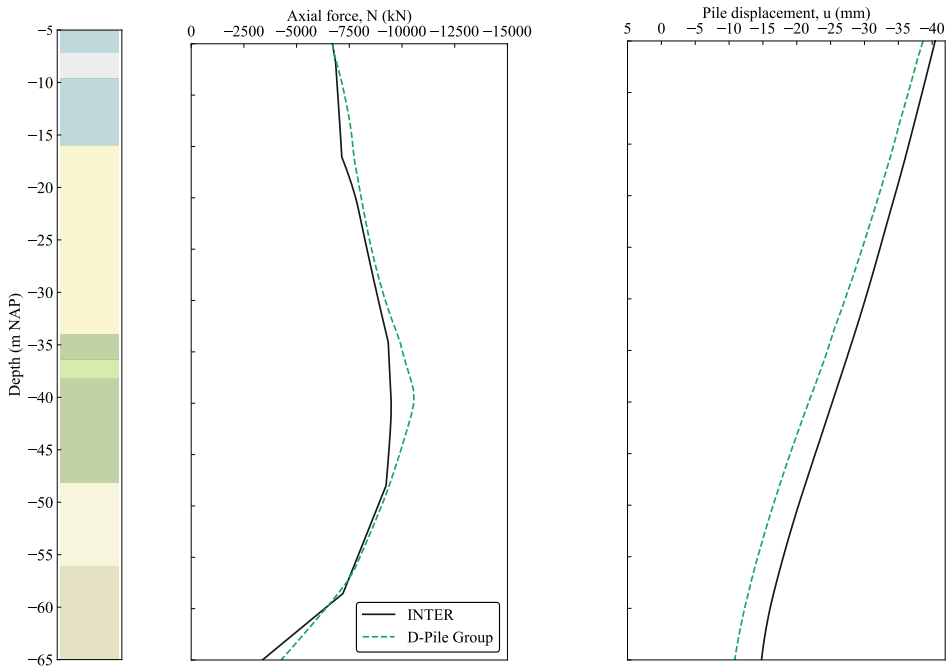

(a) Axial force vs depth **(b)** Pile displacement vs depth

Figure 4.4: Results of the standard single pile model in the long term, using INTER and D-Pile Group.

Both programs exhibit numerical differences when a settlement profile is input, which may be attributed to the incorporation of hysteresis in INTER's code; it attempts to recover the initial state before the application of the settlements and then calculates the SSI. Moreover, there is uncertainty in the coding of hysteresis in D-Pile Group. Nonetheless, in the short and the long term, both programs showed the same SSI behaviour, where there is a shift of stresses from the shaft to the pile tip over time.

4.6. Sensitivity analyses

While some of the parameters involved in the foundation modelling are fixed and given by the project design, such as the dimensions of the piles or loads of the structure, others contain high uncertainty. Due to this, sensitivity analyses were made with the purpose of studying the effect of their variations on the load distribution and pile displacement results, and thus approach the optimal modelling. The parameters considered are:

- The stiffness of clay layers.
- Factors of tip resistance.
- Factors of shaft resistance.
- Pile diameter.
- Pile stiffness.

The first sensitivity analyses were made by implementing the single spring model in INTER, as single spring models are a simple and resourceful tool for studying SSI. The effects of certain parameters will further be explored by Plaxis 3D.

4.6.1. Clay stiffness

First, a sensitivity analysis of the stiffness of the clay materials present at the site was performed, i.e. the Holocene and Kedichem layers. For this, the greenfield settlement profile was considered (section 4.5.4).

Further, the stiffness of the clay layers was changed independently, to calculate different settlement profiles to be compared to INTER, and therefore study their effect on the final results of axial force and pile displacement. The standard settlement profile against which the comparisons are made is shown in Figure 4.1.

Holocene clay
The Young modulus of the Holocene clay layer was varied with values of 0.5 MPa, 1 MPa, 2 MPa, 3 MPa, 6 MPa and 10 MPa (being 3 MPa the original set value). With this, the settlement profile was recalculated. Results are shown in Figures 4.5 and 4.6 for the short term and the long term (20,000 days after the construction finalised) respectively. When inputting a smaller stiffness, the axial force plots exhibit a larger negative skin friction, and consequently, the pile displays a softer behaviour. Likewise, since the pile is carrying an additional load, the total pile displacement increments approximately 9% in short and long term, when reducing the Young modulus by 16%.

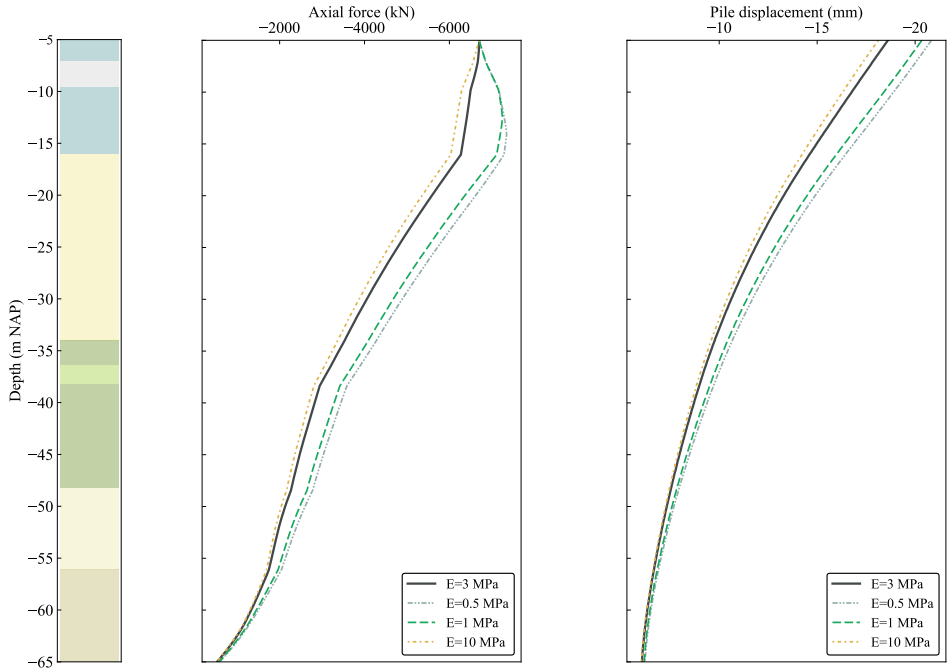

(a) Axial force vs depth

(b) Pile displacement vs depth

Figure 4.5: Short term sensitivity analyses of the stiffness of the Holocene clay layer.

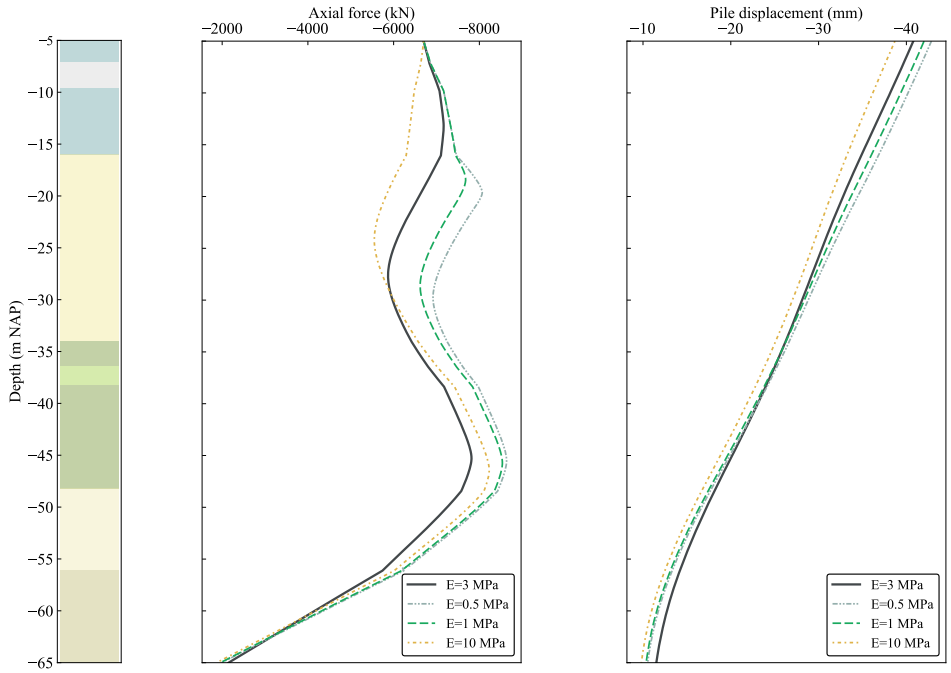

(a) Axial force vs depth

(b) Pile displacement vs depth

Figure 4.6: Long term sensitivity analyses of the stiffness of the Holocene clay layer.

Kedichem clay

Following, a sensitivity analysis was also carried out for the Kedichem clay stiffness, considering values of 10 MPa, 20 MPa, 30 MPa, 40 MPa, 60 MPa and 70 MPa, being 25 MPa the original reference value. SSI results are shown in Figure 4.7 for the short term and in Figure 4.8 for the long term (20,000 days after the construction is finalised). The results of the Kedichem clay show that variations in the stiffness lead to a wide span of variations of axial force and pile displacements. In Figure 4.7a it can be seen that in the short term when a large value of stiffness is chosen, the axial force displays an almost linear behaviour. For 30 MPa to 70 MPa, the results show an equivalent behaviour. However, when a smaller value is chosen (conservative design), the force contribution from the deep dense sand layers quickly becomes significant, as and the pile displacement increases (Figure 4.7b).

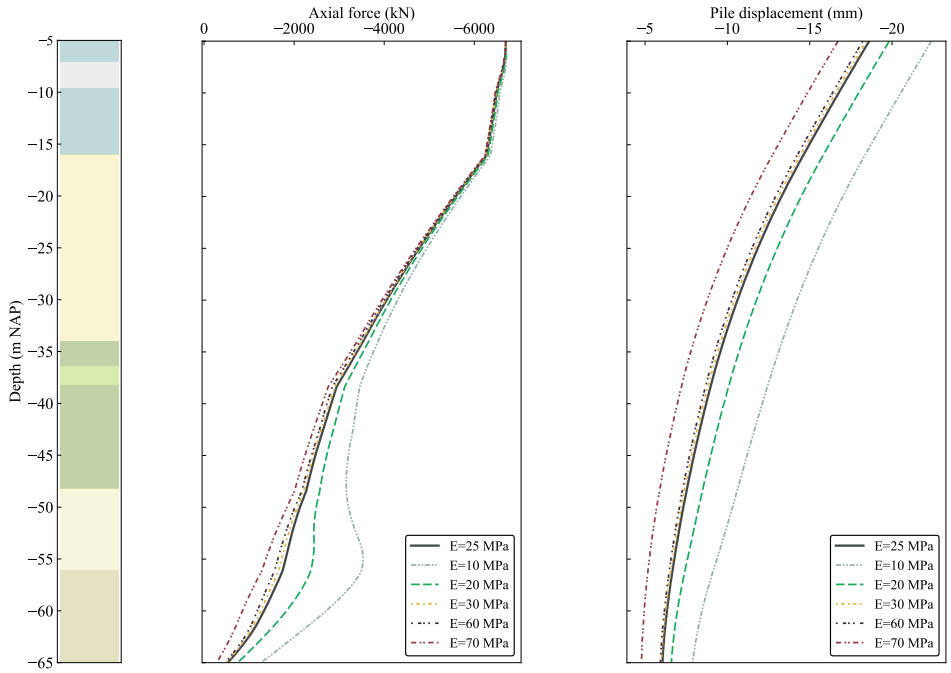

(a) Axial force vs depth **(b)** Pile displacement vs depth

Figure 4.7: Short term sensitivity analyses of the stiffness of the Kedichem clay layer.

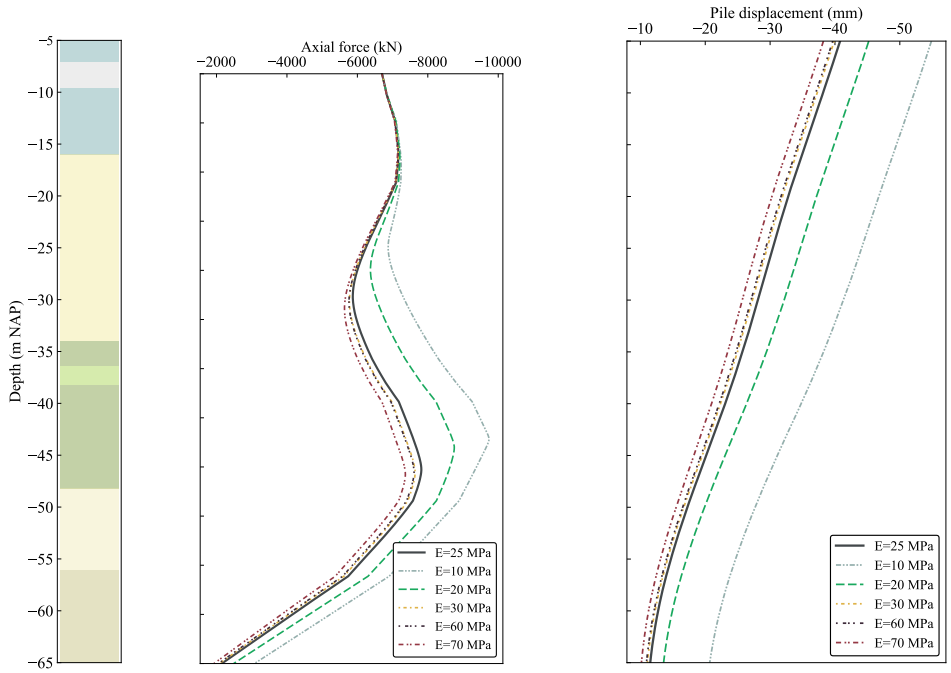

(a) Axial force vs depth **(b)** Pile displacement vs depth

Figure 4.8: Long term sensitivity analyses of the stiffness of the Kedichem clay layer.

A maximum reduction of 40% of the Young modulus, leads to an additional 22% of settlement, with respect to the standard model. A similar conclusion can be obtained from the

analyses in the long term (Figure 4.8b), where from 30 MPa to 70 MPa the behaviour is equivalent. Nonetheless, when considering a stiffness 40% smaller than the standard value, the pile displacement increases by 35%. The effect of different stiffnesses of the Kedichem clay will be further studied by means of Plaxis 3D.

4.6.2. Pile tip factors

An analysis was also made for the type of pile tip to be considered. Type 1 accounts for soil displacement piles, in which there is a stiff response of the foundation and therefore, the pile needs less displacement to mobilise full axial force. Parallelly, type 2 includes auger piles or relatively small soil displacement piles, where more displacement needs to occur in order to develop full bearing capacity. In this analysis, only the tip consideration was varied, for a load of 6700 kN in the short and long term. Results are shown in Figures 4.9 and 4.10 for the short and long term. It can be seen the type of pile tip influences the load distribution in the long term, more significantly than in the short term. The latter complies with the expected behaviour of this pile; as in the short term, most of the pile resistance comes from the shaft and the base resistance is not fully developed yet. The effects of pile tip factors can be disregarded for this load input.

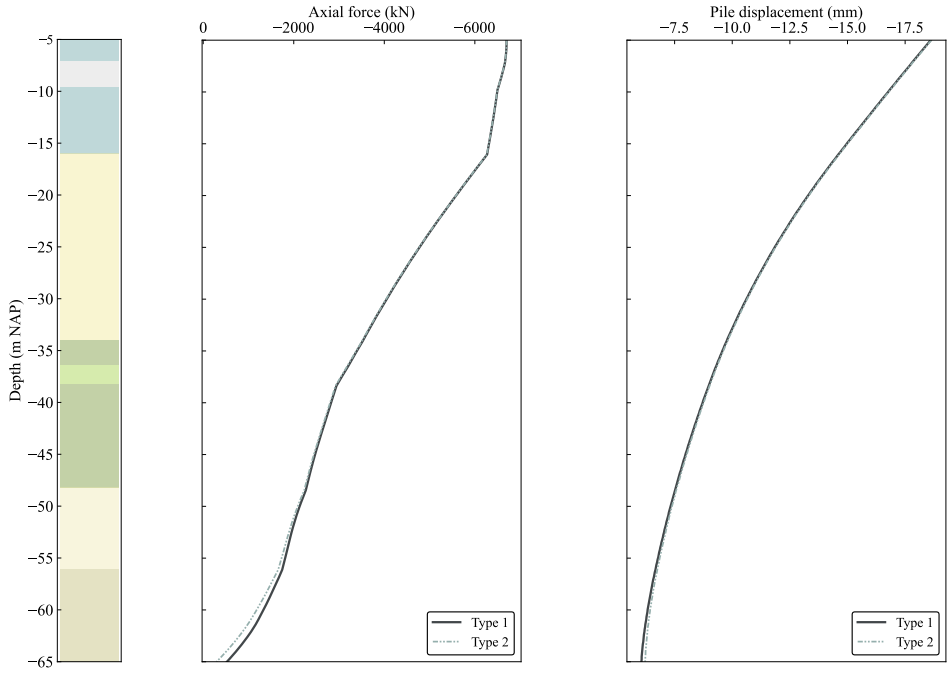

(a) Axial force vs depth **(b)** Pile displacement vs depth

Figure 4.9: Results of the short term sensitivity analyses of pile tip types.

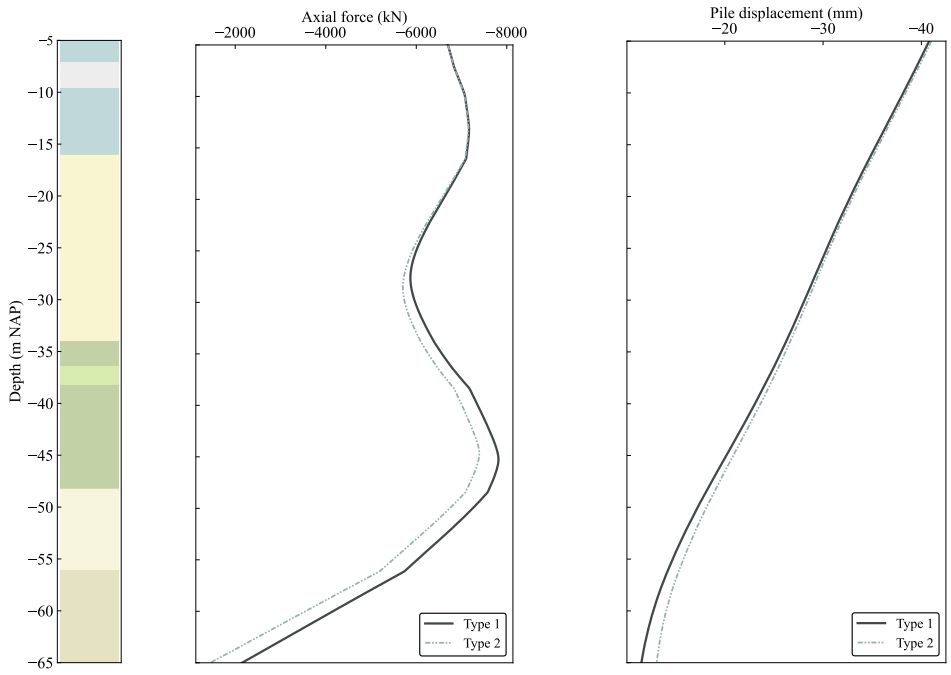

(a) Axial force vs depth **(b)** Pile displacement vs depth

Figure 4.10: Results of the long term sensitivity analyses of pile tip types.

4.6.3. Pile shaft factors

The effects of using different factors α_s for the calculation of the maximum mobilised shaft force for sand layers are explored, taking into account the calculation method established in NEN 9997-1 (2017).

The Pleistocene sand layer and the deep sand formation is evaluated independently, calculating their maximum mobilised shaft resistance with different α values. Since a type 1 pile is being considered, the standard value of alpha is 0.009, however, in this analysis, $\pm 30\%$ of this value will also be used, i.e. 0.0063 and 0.011. This percentage was chosen in accordance with the proposal of Ter Steege (2022).

Pleistocene sand layer
The maximum shaft resistance to be considered at the Pleistocene sand is shown in Table 4.5. The rest of the layers will remain with the specified values from Table 4.1.

Table 4.5: Maximum mobilised shaft resistance per layer considering different α_s values.

Layer	Depth (m NAP)		q_c (MPa)	Maximum mobilised shaft resistance (kN)		
				$\alpha_s = 0.009$	$\alpha_s = 0.0063$	$\alpha_s = 0.011$
Pleistocene sand	-16.0	-34.0	10	3878.11	2714.68	4739.91

Results are shown in the short term (Figure 4.11) and in the long term (Figure 4.12).

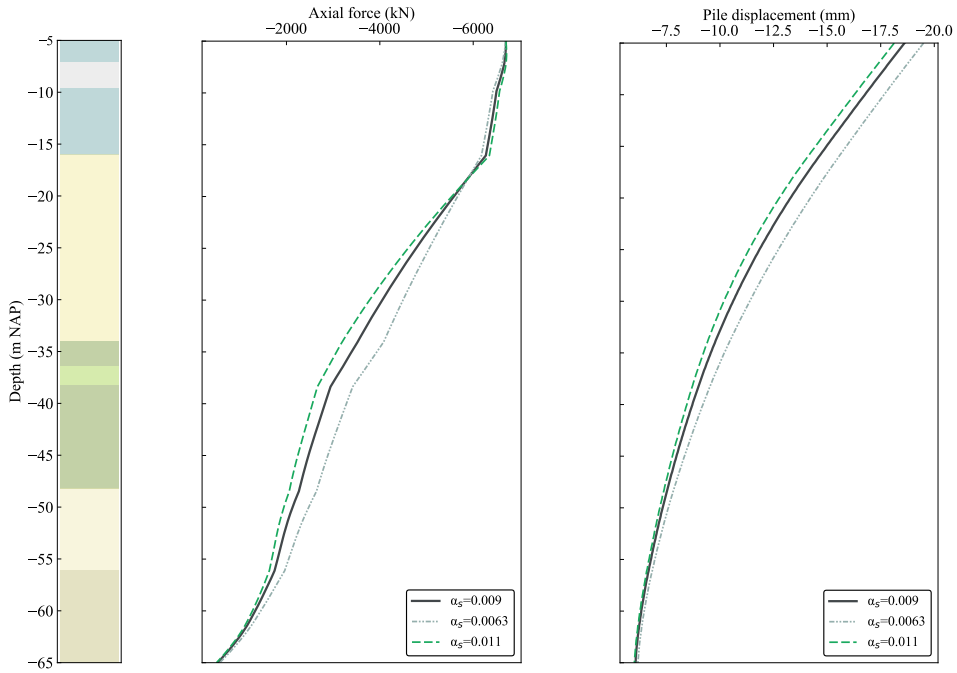

(a) Axial force vs depth **(b)** Pile displacement vs depth

Figure 4.11: Results of the sensitivity analyses of α_s for Pleistocene sand layer for 6700 kN in the short term.

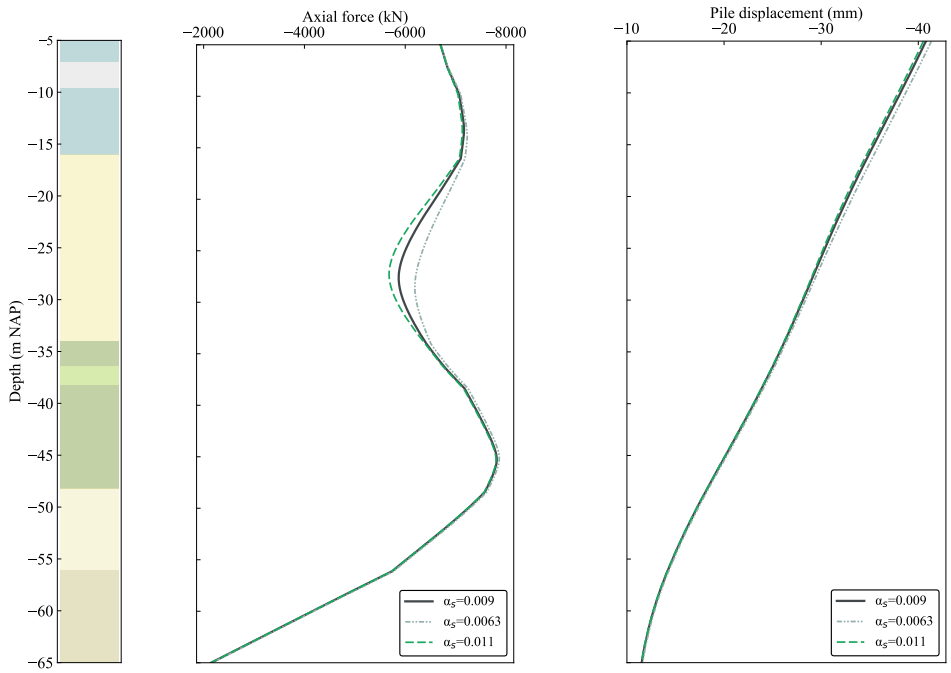

(a) Axial force vs depth **(b)** Pile displacement vs depth

Figure 4.12: Results of the sensitivity analyses of α_s for Pleistocene sand layer for 6700 kN in the long term.

By comparing these results, it can be seen that in the short term, decreasing the α_s value by 30% leads to 4.8% more displacement, whereas a 30% α_s increment decreases the pile

displacement by 2.5%. Moreover, in the long term, decreasing the α_s value by 30% leads to 1.3% more displacement, whereas a 30% α_s increment decreases the pile displacement by 2%. The variations in the Pleistocene sand resistance are more significant in the short term, as in the long term, the maximum mobilisation occurs at the pile end. However, variations are small.

Deep dense sand

The maximum shaft resistance to be considered for the deep dense sand analyses is shown in Table 4.6.

Table 4.6: Maximum mobilised shaft resistance per layer considering different α_s values.

Layer	Depth (m NAP)		q_c (MPa)	Maximum mobilised shaft resistance (kN)		
				$\alpha_s = 0.009$	$\alpha_s = 0.0063$	$\alpha_s = 0.011$
Dense silty sand	-48.0	-56.1	12	2042.47	1429.73	2496.35
Dense sand	-56.1	-65.0	20	3835.02	2684.51	4687.24

Results are shown in the short term (Figure 4.13) and in the long term (Figure 4.14) below. It can be seen that in the short term, decreasing and increasing the α_s value by 30% leads to 5% more and less displacement, respectively. Parallelly, in the long term, decreasing the α_s value by 30% leads to 1.2% more displacement, whereas a 30% α_s increment decreases the pile displacement by 0.9%. It can be seen that differences in the α_s value increase in the long term, however, as resistance is not fully mobilised yet, at 6700 kN effects are still not evident.

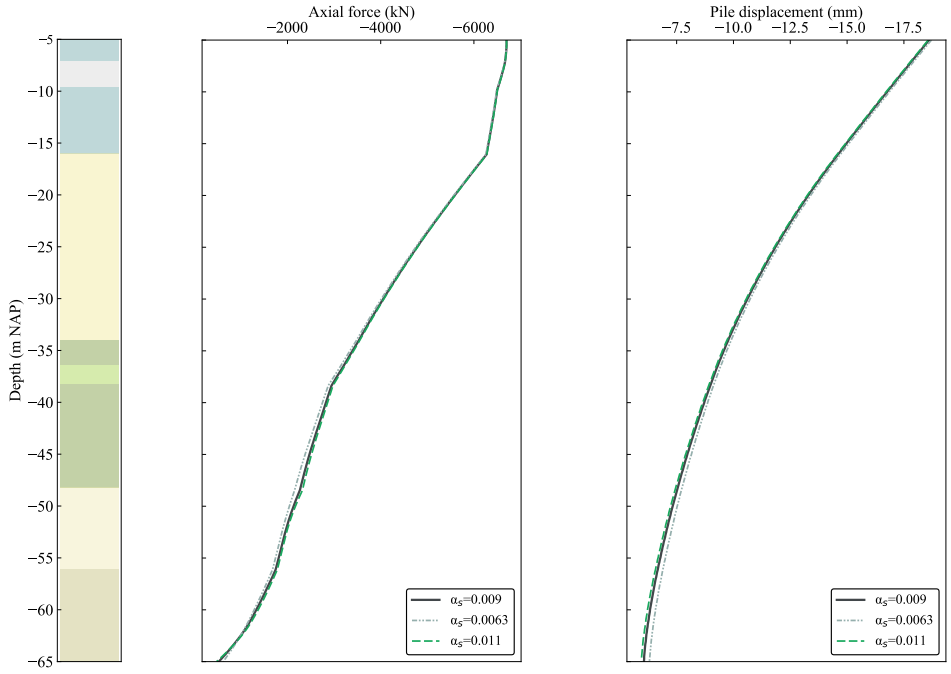

(a) Axial force vs depth **(b)** Pile displacement vs depth

Figure 4.13: Short term sensitivity analyses of α_s for the deeper dense sand layer for 6700 kN.

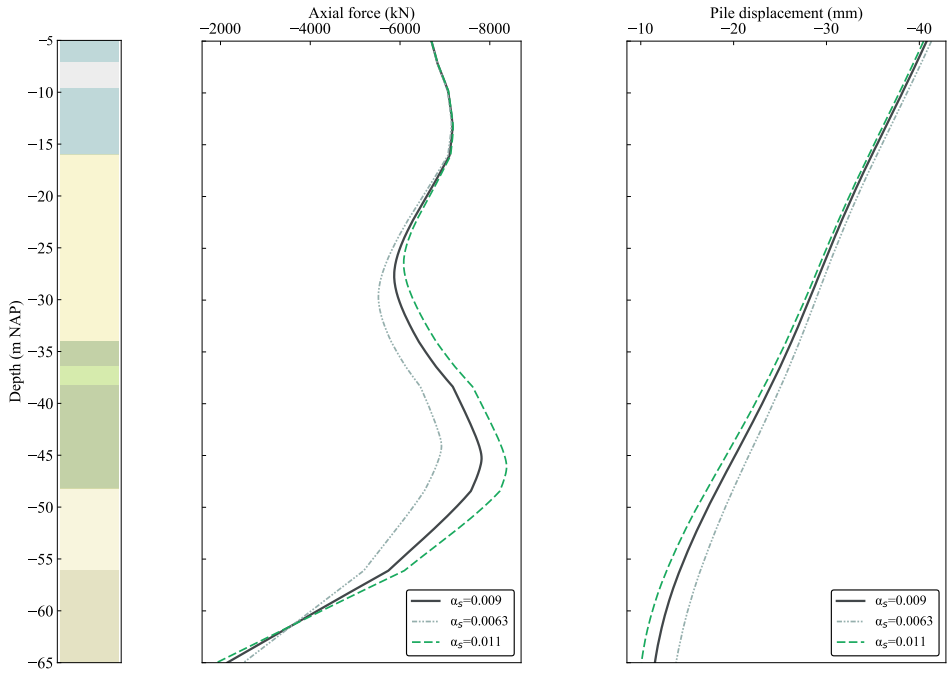

(a) Axial force vs depth **(b)** Pile displacement vs depth

Figure 4.14: Long term sensitivity analyses of α_s for the deeper dense sand layer for 6700 kN.

4.6.4. Pile diameter

The influence on the diameter of the pile was studied in four cases:

- The pile diameter is equal to the shaft of the Tubex pile (0.762 m) and it is constant throughout the whole pile.
- The pile tip diameter is considered for the sand layers (0.95 m) and the shaft diameter (0.762 m) for the clay layers.
- An average diameter between shaft and tip is considered for the pile segments surrounded by clay (0.85 m), and in the sand layers the tip diameter is used (0.95 m)[3].
- The whole pile length is considered equal to the pile tip diameter (0.95 m).

When calculating these piles in INTER, the effects of the diameter are taken into account in the stiffness input (EA) and the maximum mobilised shaft resistance. Results are shown in Figures 4.15 and 4.16 for the short and long term, respectively. It can be seen that the diameter influence in the short term is small, as the load distribution of all calculations is fairly equivalent and pile displacement maximum difference is 9%, between the results of diameters 0.762 m and 0.95 m. However, important differences are seen in the load distribution in the long term, mainly attributed to an increase in the tip bearing capacity. Nonetheless, pile displacement maximum difference is 7% when comparing results of calculations considering the tip diameter and shaft diameter.

It should be highlighted that diameter variations may be significant in the interpretation of

[3]This case was considered by Schippers and Broekens (2021) for bearing capacity calculations.

FO strain measurements once the final load has been reached.

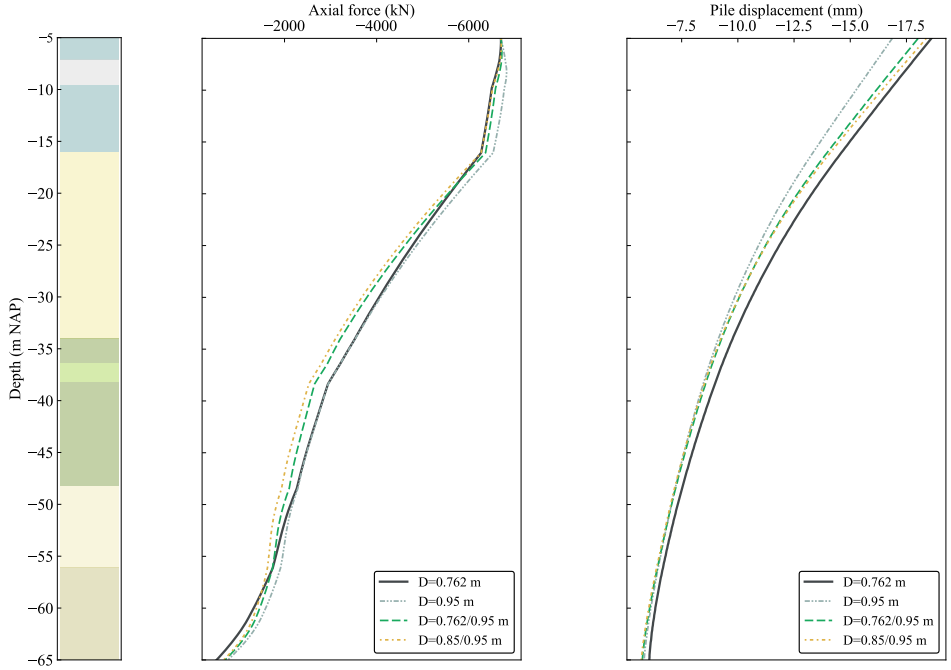

(a) Axial force vs depth **(b)** Pile displacement vs depth

Figure 4.15: Results of the short term sensitivity analyses of pile diameter.

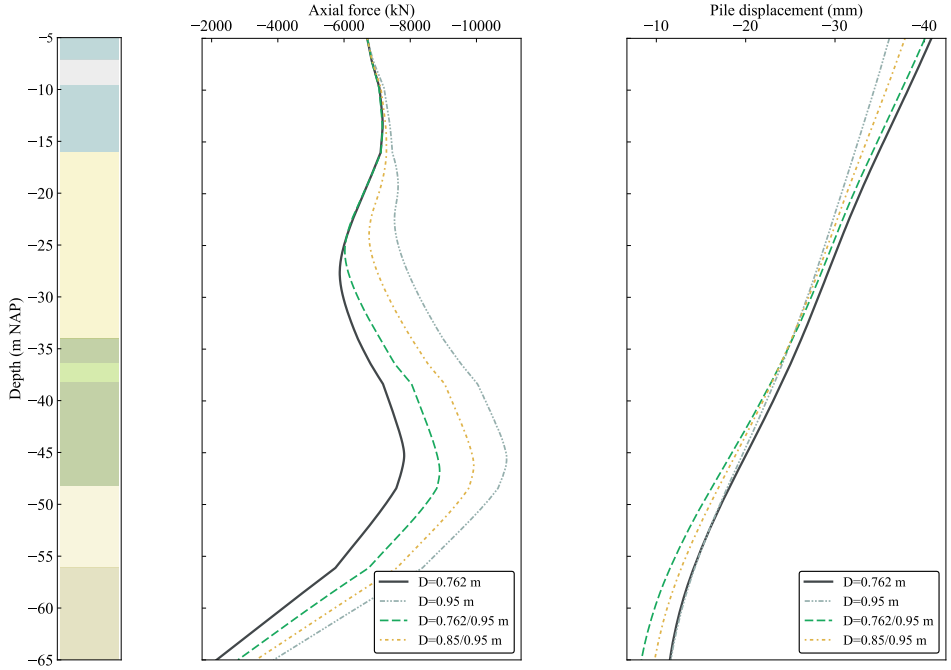

(a) Axial force vs depth **(b)** Pile displacement vs depth

Figure 4.16: Results of the long term sensitivity analyses of pile diameter.

4.6.5. Pile stiffness

The last sensitivity analysis was carried out considering ±20% of concrete average stiffness for the short and long term. While the Tubex pile is conformed by concrete, the steel case and grout with designed strength and stiffness values, it is possible that concrete's stiffness has slight variations. These values were used for the calculation of the whole pile stiffness and further used in the estimation of pile displacements and forces (as shown in Table 4.7).

Table 4.7: Pile stiffness calculation for different concrete stiffness values.

Term	Diameter	I (m^4)	A (m^2)	E_{concr} (GPa)	EA_{pile} (kN)
Short	0.744	0.015	0.435	25	1.52x10^7
				31	1.79x10^7
				37	2.06x10^7
Long	0.744	0.015	0.435	16	1.14x10^7
				20	1.31x10^7
				24	1.48x10^7

Results for the short-term stiffness are shown in Figure 4.17 immediately after a jump load of 6700 kN. At this load stage, the concrete stiffness variation does not have a significant impact on the SSI results.

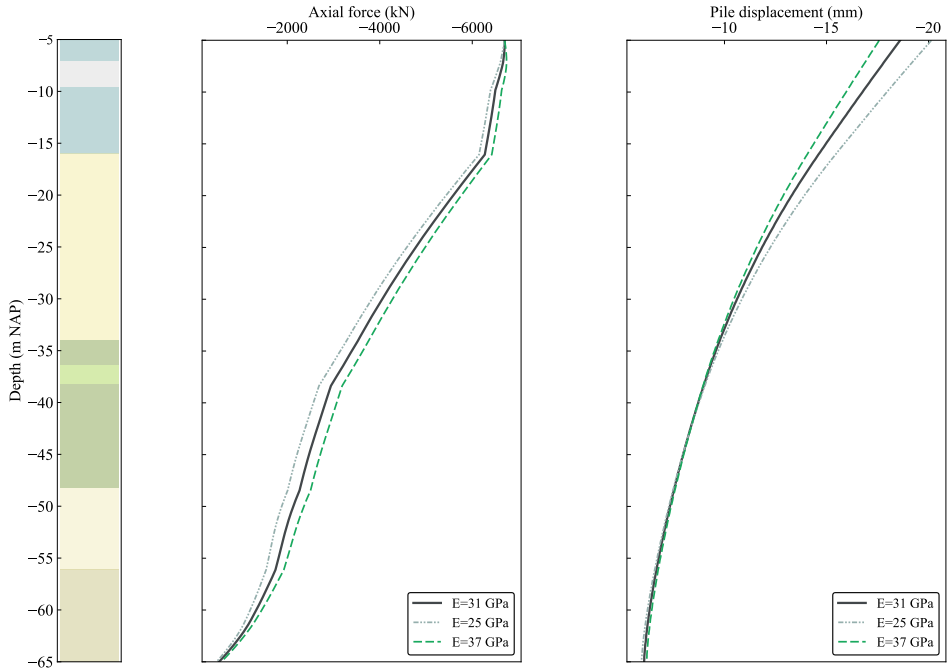

(a) Axial force vs depth. **(b)** Pile displacement vs depth.

Figure 4.17: Short term sensitivity analysis of concrete stiffness of the pile with no settlement profile.

Further, Figure 4.18 shows results of axial force and pile displacement on the long term. The concrete stiffness variation does not have a significant impact on the SSI results. However,

its effect is significant when interpreting the FO strain measurements (Equation 3.1).

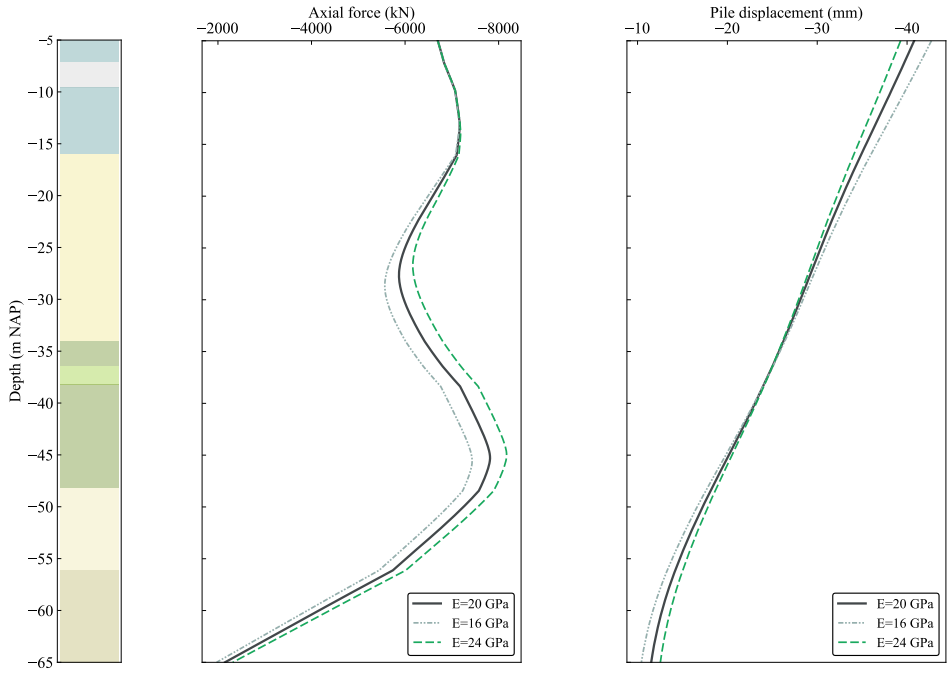

(a) Axial force vs depth. **(b)** Pile displacement vs depth.

Figure 4.18: Long term sensitivity analysis of concrete stiffness of the pile inwith no settlement profile.

Once the load distribution has been studied, and a sensitivity analysis has been carried out for all the involved parameters that may present uncertainty, more complex calculations can be developed and adjusted in accordance with these results.

4.7. Implications of sensitivity analyses for pile modelling

The outcomes of the sensitivity analyses have revealed practical implications for advanced pile modelling, which are discussed below.

First, the stiffness variations within the Holocene layer had a range from 0.5 MPa to 10 MPa. Results lead to a maximum difference of 9% in the final output in the long term, for values between 0.5 MPa and 3 MPa. Moreover, the stiffness of the Kedichem clay layer was varied from 10 MPa to 70 MPa. This parameter resulted pivotal since the analyses displayed maximum variations of 35% for stiffness values between 10 MPa and 25 MPa for the long term. As it clay consolidates, it leads to an important stress redistribution from the upper to the lower part of the pile. This will be further studied through Plaxis 3D modelling.

Next, changes in pile tip factors have more impact in the long term, leading to a shift in stress distribution where bottom pile resistance dominates. However, for gradual loading and short-term scenarios, the influence of pile tip type is minimal, as tip force is not mobilised in early load stages.

Then, α_s values were varied 30% for both existing sand layers. The effect of variations in the Pleistocene sand is more significant in the short term, while the alterations of said values in the deep dense sands are visible in the long term, which coincides with the shift of stresses the pile will undergo over time. While this effect is not as influential as the Kedichem clay stiffness for this case, variations in the α_s values may be considered for refining the models to fit FO site measurements, according to the propositions of Ter Steege, 2022.

After, when studying the pile diameter influence on SSI, important differences are seen in the load distribution in the long term, mainly attributed to an increase in the tip bearing capacity along with an increase of pile diameter. Nonetheless, pile displacement maximum difference is 7% when comparing results of calculations considering the tip diameter and shaft diameter. The consistent trend is that D=0.95 m results in the lowest displacements, while the other three cases show very similar behaviour within them. Further, it may be important to consider the diameter influence on the FO measurement interpretations.

Finally, pile stiffness may be significant for the interpretation of FO measurements.

These implications provide a foundation for the upcoming chapter on pile modelling in Plaxis 3D. They guide the exploration of load distribution in the context of very long piles.

5

Plaxis 3D modelling

5.1. General aspects

This section describes the procedure for developing the finite element (FE) modelling of the case study using the Plaxis 3D software. First, an overview of the modelling process is given. Then, the constitutive soil models selected for implementation will be described, considering their advantages and limitations. Subsequently, the soil parameters are presented. Next, an explanation of the process of creating various models of single piles using different elements is given; this includes volumetric piles and the simplified embedded beam row (EBR) tool, along with a thorough comparison of the obtained results. Finally, the modelling of the pile group using both techniques will be covered, including a comparative analysis of their respective outcomes.

5.2. Modelling process

The process of building a Plaxis 3D model is outlined in Figure 5.1. Geometric boundaries are first defined, followed by setting the soil profile by inputting material parameters and specifying the sequence of soil layers. Next, structures, structural loads, and structural material parameters are then defined. Subsequently, a mesh is generated with a specific mesh density. Following, initial water flow and boundary conditions are entered. Construction stages to be employed are specified. Numerical calculations are then conducted for all construction stages. Finally, analysis results are obtained in the form of charts or tables.

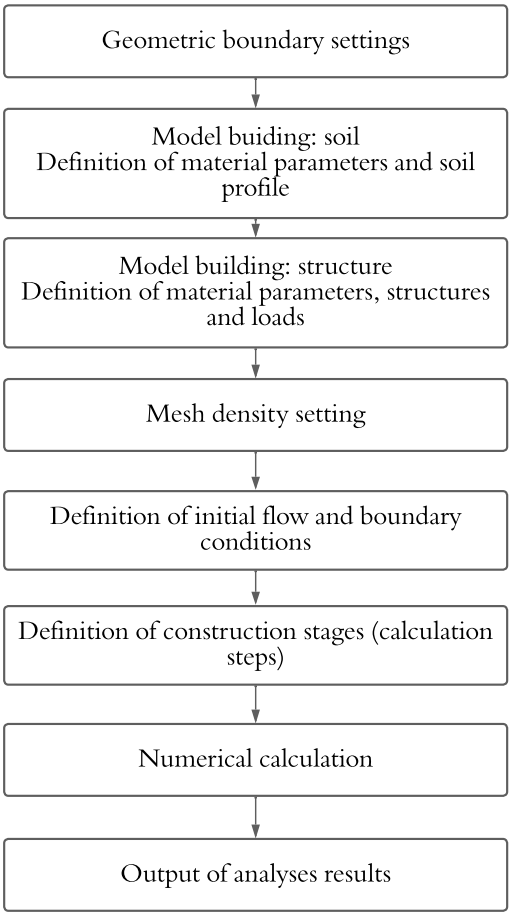

Figure 5.1: Flowchart of Plaxis 3D modelling process (adapted from Chen et al., 2023).

It was necessary to ensure the quality of the model set-up by doing a sensitivity analysis of the model geometric boundaries and mesh density, prior to the SSI analyses. The latter were carried out by considering different values of model limits and mesh sizes, and evaluating how different their results were, in comparison with the results obtained from the model with the finest mesh and the wider geometric boundaries. With this, it was possible to find the most efficient model set up, that gives accurate results with an optimal computation time. Since the geometrical model set-up is not part of the project scope, the aforementioned analyses are not included in this chapter. Nonetheless, in the following sections, the optimal model setup implemented for every different calculation will be briefly described.

5.3. Constitutive soil models

For this project, the Hardening Soil (HS) constitutive model was chosen to model all of the soil profile layers, except for the Kedichem clay layer, which was defined by means of Soft Soil Creep (SSC). In accordance with Schippers and Broekens (2021), as well as the analyses from Chapter 4, the Holocene clay layers are less relevant for the study case SSI results and therefore, are modelled with HS parameters like all sandy materials. Both are constitutive models that are commonly used in practice in the Netherlands due to the presence of soft soils and require parameters that are easy to calculate with the information currently available. Likewise,

there is plenty of experience with their implementation in other cases of high-rise building foundation models (Frissen, 2020; Schippers and Broekens, 2021; Schippers and Broekens, 2022; Hartman, 2023).

5.3.1. Hardening soil (HS)

In the HS model, the behaviour follows the Mohr-Coulomb failure criterion, but the soil considers changing stiffness during loading represented by a hyperbola. The model accounts for two types of hardening: shear hardening; which is the generation of plastic deviatoric strains by mobilization of the internal friction, and compaction hardening; the generation of plastic volumetric strains due to primary compression (Brinkgreve, 2020). Likewise, compression hardening includes the difference between loading and unloading stiffness and therefore accounts for the stress-dependency of all these stiffness moduli (Gouw, 2014). To consider these effects, the model needs four parameters additional to the Mohr-Coulomb criterion:

- Mohr-Coulomb strength parameters c', ϕ': cohesion (kPa) and friction angle (°).
- E_{ref50}: Secant stiffness in standard drained triaxial test (MPa).
- E_{refoed}: Oedometer stiffness (MPa).
- E_{refur}: Unloading/reloading stiffness (MPa).
- m: Power for stress-level dependency of stiffness (-).

This constitutive model presents the following advantages (Brinkgreve, 2020): It shows a good non-linear formulation of soil behaviour for soft and hard soils, it differentiates primary loading from unloading / reloading behaviour, it considers several stiffnesses for different stress paths and it memorizes pre-consolidation stress, making it better for overconsolidated soils. As limitations, Brinkgreve (2020) indicates that: Softening behaviour and creep are not included, there is no accumulation of strain or pore pressure in cyclic loading, the material is considered isotropic and it is not suitable for very soft soils.

5.3.2. Soft soil creep (SSC)

The SSC model is suitable for highly compressible soils. It is similar to the Soft Soil model (SSM) but considers time-dependent effects such as creep. In this model, elastic strains are calculated according to Hooke's law, plastic strains are considered by Mohr-Coulomb criteria and there is also generation of time-dependent deformations (creep or secondary compression) (Brinkgreve, 2020). The model will calculate creep as long as there is effective stress, which is generally dominated by initial stresses due to self-weight in foundation design (Hartman, 2023). The model parameters are mentioned below:

- Mohr-Coulomb strength parameters c', ϕ': cohesion (kPa) and friction angle (°).
- λ^*: Modified compression index (-).
- κ^*: Modified swelling index (-).
- μ^*: Modified creep index (-).
- ν_{ur}: Poisson's ratio for unloading/reloading (-).
- ψ: Dilatancy angle (°).

- K_0^{nc}: H/V stress ratio in normally consolidated 1D compression (-).

The advantages of the SSC model are that irreversible strains are formulated as viscoplastic instead of plastic, time-dependent behaviour is included in terms of creep, and considers compression-induced and shear-induced creep (Brinkgreve, 2020). Likewise, there is stress-dependency of stiffness, distinction between primary loading and unload/reload, and memory of preconsolidation stress.

The limitations are that anisotropy is not considered, as well as softening behaviour, and the parameters need careful calibration as it is a sensitive model; K_0^{nc} has a significant influence on the deformation behaviour, while the overconsolidated ratio (OCR) or pre-overburden pressure (POP) parameters impact the initial creep rate (Brinkgreve, 2020).

5.4. Soil parameters

This section develops the definition of soil parameters for the FE model. Table 5.1 presents the parameters of the entire soil profile (except the Kedichem clay). The HS parameter definition was done based on laboratory test results and available information on other projects in Rotterdam such as Zalmhaven (MOS GRONDMECHANICA BV, 2016), The Sax (GEOSONDA, 2018), and the A16 Noord (MOS GRONDMECHANICA B.V., 2022), as well as the site CPTs from POST (Schippers and Broekens, 2021). Derivation of parameters and the obtention of reference stiffnesses were done according to Lunne and Christoffersen (1983) and Brinkgreve (2022a).

Table 5.1: HS parameters for soil modelling.

Layer	Depth (m NAP)		q_c (MPa)	γ (kN/m^3)	γ_{sat} (kN/m^3)	$\sigma'v$ (kPa)	c' (kPa)	ϕ (°)	ψ (°)	$E'_{50;ref}$ (MPa)	$E'_{oed;ref}$ (MPa)	$E'_{ur;ref}$ (MPa)
Backfill sand (dry)	1.00	-1.00	5.0	18	20	18.00	0	30	0	10	10	40
Backfill sand	-1.00	-4.70	5.0	19	20	35.00	0	30	0	10	10	40
Sandy clay	-4.70	-7.10	0.8	15	15	40.45	0.6	22.5	0	5	5	20
Peat	-7.10	-9.60	0.8	11	11	41.94	1	15	0	3	2	8
Soft clay	-9.60	-16.00	0.7	14	14	55.35	2	17.5	0	4	4	16
Pleistocene sand	-16.00	-34.00	15.0	19	20	138.06	0	31	1.3	40	40	160
Kedichem clay I	-34.00	-36.40	4.0	19	20	149.08	13	22.5	0	-	-	-
Kedichem sand	-36.40	-38.20	12.0	19	20	157.36	0	26	0	27	27	108
Kedichem clay II	-38.20	-48.20	3.0	19	20	203.31	13	22.5	0	-	-	-
Dense silty sand	-48.20	-56.10	14.0	18	20	235.66	0	30	0	39	39	158
Dense sand	-56.10	-65.00	24.0	19	21	276.55	0	32	2	45	45	180

Note: q_c represents cone tip resistance, γ is soil unit weight, γ_{sat} is saturated unit weight, $\sigma'v$ is effective vertical stress at the middle of the layer, c' is cohesion, ϕ is friction angle, ψ is dilation angle, $E'_{50;ref}$ is reference secant stiffness modulus, $E'_{oed;ref}$ is reference stiffness oedometric modulus, and $E'_{ur;ref}$ is reference stiffness modulus at unload/reload.

Further, the SSC parameters from the Kedichem clay are shown in Table 5.2. The latter

were derived from laboratory testing of the aforementioned projects (MOS GRONDMECHANICA BV, 2016; GEOSONDA, 2018; MOS GRONDMECHANICA B.V., 2022), information from De Rotterdam subsoil conditions (Hoefsloot and Wiersema, 2020), and the oedometer tests database from the Municipality of Rotterdam (Gemeente Rotterdam, n.d.). It must be highlighted that the POP value was defined as 150 kPa in accordance with the oedometer tests from Gemeente Rotterdam (n.d.), and considering the geotechnical experience of the site, which takes into account the water levels being 15 m lower during the last ice age (LGM) 20,000 to 25,000 years ago.

Table 5.2: Plaxis 3D soil parameters for modelling of the Kedichem clay layer with SSC model.

Layers	Depth (m NAP)		$\kappa*$ (-)	$\lambda*$ (-)	$\mu*$ (-)	POP (kPa)
Kedichem clay I	-34.00	-36.40	0.01112	0.03331	0.00135	150
Kedichem clay II	-38.20	-48.20	0.01112	0.03331	0.00135	150

Note: κ^* is the modified swelling index, λ^* is the modified compression index and μ^* is the modified creep index.

5.5. Calculation stages

The calculation stages are presented in Figure 5.2.

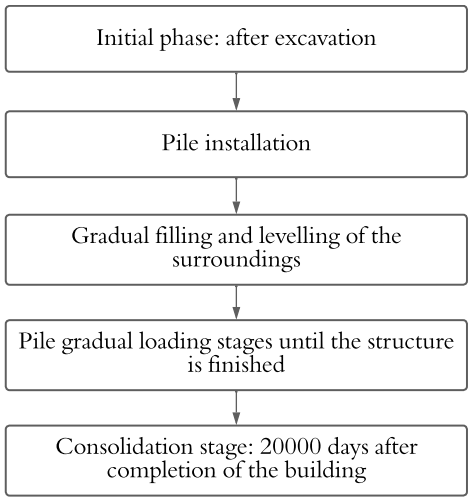

Figure 5.2: Flowchart of Plaxis 3D modelling of the construction stages.

The initial phase is taken after excavation to the basement level (-5 m NAP). The decision not to model excavation stages is rooted in the fact that the excavated material results in an overburden effective pressure of approximately 45 kPa, which is a small stress when compared to the load to which the piles are subjected due to the high-rise building. Notably, including the excavation process does not alter significantly the final outcomes of single pile modelling when studying the SSI at the completion of the building and further. However, it might become relevant when evaluating early loading stages.

Subsequently, the pile installation phase is defined. Then, the surface load stage simulates the gradual filling and levelling of the surroundings around the POST site. Next, diverse pile loading stages are included, up to the maximum static load per pile at 6700 kN (Schippers and Broekens, 2021). In each step, loads are applied as jump loads, with a duration of 0.1 days. Finally, the consolidation stage is defined, which lasts 20,000 days to allow for the gradual consolidation of clay layers.

5.6. Single pile modelling

This section describes the modelling process of a single pile in Plaxis 3D by considering a 3D solid pile and the EBR tool, including the same geometry and characteristics stated by the study project.

5.6.1. Solid 3D pile

The 3D solid pile is modelled as a finite volume inside the soil block and is the most realistic way of modelling the pile, soil and pile-soil interaction. Nonetheless, the challenges and limitations on their use are the following (Brinkgreve, 2022b): First, 3D solid piles may lead to an inefficient mesh, as there are too many elements that could be flawed in their shape. Second, there is a computational efficiency limitation that arises when modelling a large number of piles to be modelled. Third, the interaction between soil and structural elements may be restricted (locking of interfaces), leading to full bonding, or no relative displacement between them. Fourth, installation effects are not considered, although some features can be used in order to mimic them. Fifth, since the pile and soil elements have a large difference in stiffness, there is significant numerical instability (Frissen, 2020), which results in convergence problems and long computation time. A representation of the model is shown in Figure 5.3.

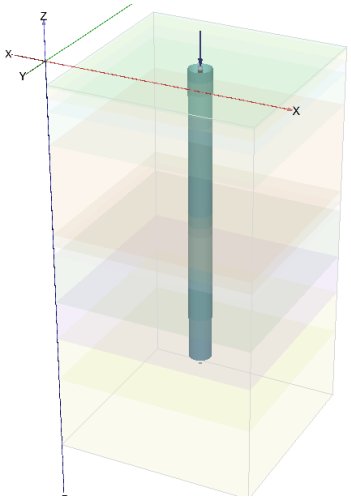

Figure 5.3: Scheme of a 3D solid single pile modelled in Plaxis 3D.

In order to build the Plaxis model, first, the pile must be defined. This can be done by either drawing a circle and then extruding it to create a volume, or importing a cylinder from CAD software. Next, an interface must be made at the pile shaft and the tip (bottom surface)

to model interaction properties. Following, the material set is defined, containing the pile properties (Table 5.3). Further, at the calculation phase, the pile must be enabled in the corresponding construction stage by assigning pile properties to the pile volume (replacing soil), and activating the interface responsible for the relative soil-structure displacement.

Table 5.3: Material set properties of 3D solid pile.

Constitutive model	Unit weight (kN/m^3)	Stiffness (GPa)
Linear elastic	24	29.7

It should also be noted that structural forces[1] result from the integration of stresses in volume elements, thus, they are not directly obtained from the cylinder. An alternative for getting results is to introduce an EBR (of equivalent pile length) inside the pile volume to obtain its output. This element may have its own material properties (Table 5.4) considering a slightly smaller diameter, and a much lower stiffness with respect to the 3D solid pile. Likewise, an elastic plate should also be considered, connecting both elements to avoid mesh-dependent results for the internal forces of the EBR (Brinkgreve, 2022a).

Table 5.4: Material set properties of the auxiliary EBR inside the 3D solid pile.

Constitutive model	Unit weight (kN/m^3)	Stiffness (GPa)	Diameter (m)
Linear elastic	24	0.001	0.7

In this case, axial skin resistance was set as layer-dependent and the tip force was defined with the same value obtained with the calculation from NEN 9997-1 (2017). However, Brinkgreve (2022a) states that when contained in a volume solid, the EBR will not follow the specified axial force distribution (i.e. linear, multilinear or layer-dependent), but will be influenced by the cylinder behaviour instead.

A summary of the modelling process of the solid 3D pile is shown in Figure 5.4.

[1] Axial force, shear force and bending moment.

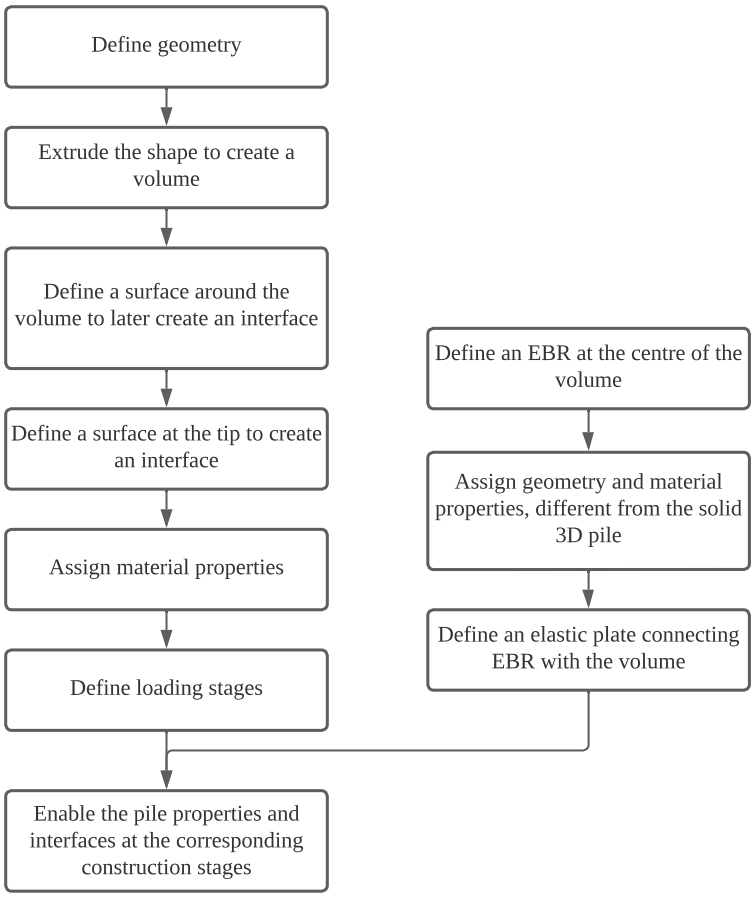

Figure 5.4: Flowchart of Plaxis 3D modelling process of a 3D solid pile.

5.6.2. Embedded beam row (EBR)

The EBR model was developed with the aim of reducing complexity and preventing numerical instability problems (Engin and Brinkgreve, 2009). It consists of beam elements connected to the existing soil block by introducing new interface nodes where the intersections between pile and soil occur; at the shaft and the tip. The beams are 3-node-line elements and six degrees of freedom per node, including three translational and three rotational degrees of freedom (Brinkgreve, 2022a). The element stiffness matrices are numerically integrated from four Gaussian integration points. These elements can account for beam deflections and changes in length when subjected to axial forces (Brinkgreve, 2022a). In this way, the interaction is given by the relative displacements between newly generated pile nodes and soil nodes (Engin and Brinkgreve, 2009). The shaft friction is defined as:

$$\Delta F_s = T_{skin} \Delta u_{rel} \tag{5.1}$$

where:
ΔF_s: shaft resistance increment at the integration points (kN)
T_{skin}: material stiffness matrix of the new skin interface (kN/m)

Δu_{rel}: relative displacement between the soil and the pile (m), obtained as

$$\Delta u_{rel} = \Delta u_p - \Delta s \tag{5.2}$$

where:
Δu: pile displacement increment (m)
Δs: soil displacement increment (m)

Likewise, the tip force is determined as:

$$\Delta F_b = D_b \Delta u_{rel,b} \tag{5.3}$$

where:
ΔF_b: base resistance increment (kN)
D_b: material stiffness matrix of the spring element at the pile tip (kN/n)
$\Delta u_{rel,b}$: relative displacement between the soil and the pile tip (m), obtained as

$$\Delta u_{rel,b} = \Delta u_b - \Delta u_{s,b} \tag{5.4}$$

where:
Δu_b: pile tip displacement increment (m)
$\Delta u_{s,b}$: soil displacement increment at the tip (m)

The EBR does not occupy a real volume inside the soil block, instead, an elastic region is created at the soil region within the pile, which has the size of the input pile diameter (Engin and Brinkgreve, 2009). This approach reduces the mesh-dependent effects (Engin and Brinkgreve, 2009). The interface properties for the EBR are obtained by using the R_{inter} parameter. The latter represents the relative stiffness between the modelled pile and the adjacent soil (Brinkgreve, 2022a), and is implemented to determine their interaction as follows:

- $R_{inter} = 0$: No bonding, there is no pile-soil interaction or load transfer.
- $R_{inter} = 1$: Full bonding, there is no relative pile-soil displacement.
- $0 < R_{inter} < 1$: Partial bonding, depending on the input value.

The interface strength properties are then calculated as:

$$\tau = c_{inter} + \sigma'_v tan(\phi_{inter}) \tag{5.5}$$

where:
τ: shear strength (kPa)
c_{inter}: cohesion of the interface (kPa)

σ'_v: effective stress (kPa)
ϕ_{inter}: internal friction angle of the interface (°)

c_{inter} and ϕ_{inter} are obtained as:

$$c_{inter} = R_{inter} c' \tag{5.6}$$

$$tan(\phi_{inter}) = R_{inter} tan\phi \tag{5.7}$$

where:
c': soil cohesion (kPa)
ϕ: soil internal friction angle (°)

Furthermore, the bearing capacity of the EBR must be an input. The tip resistance maximum value is defined by the user, and the shaft resistance can be defined as linear, multilinear, or layer-dependent. The linear distribution interpolates between defined top and bottom values, while the multilinear interpolates between several defined skin friction values along the shaft. Likewise, the layer-dependent distribution relates the skin friction to the strength of each adjacent soil layer (Engin and Brinkgreve, 2009).

The EBR model has the following advantages against 3D solid piles (Brinkgreve, 2020): it has a more efficient computation time, it presents accurate results for axial loading, it is possible to consider a large number of piles and structural forces and pile displacements are a direct element output. A representation of the model is shown in Figure 5.5.

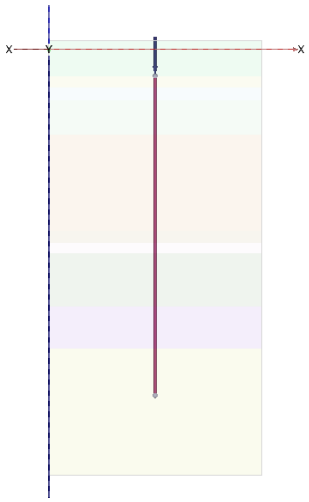

Figure 5.5: Scheme of an EBR as a solid single pile modelled in Plaxis 3D.

Nonetheless, it has the following limitations: First, installation effects are not included (Brinkgreve, 2020) and therefore are suitable for piles that cause a limited disturbance of the surrounding soil during installation. Second, it presents limitations when applied to lateral loading, due to full bonding (Brinkgreve, 2020). Third, the elastic region approach has reduced

the mesh-dependent effects, but they are not completely mitigated (Frissen, 2020). Fourth, the pile tip calculations may present singularities, as the tip force is only calculated with one spring (Frissen, 2020) and it has a relatively soft response (Brinkgreve, 2020). In order to overcome the latter, a new formulation was developed by Smulders et al. (2019) in which the SSI interaction is evaluated at the pile circumference, instead of the centreline. With this, the mesh sensitivity is reduced and the behaviour at the base is calculated as stress, instead of a single-point force.

The model build-up works as follows. First, a line must be created and transformed into an EBR element. Second, pile material properties, as well as interface properties, are defined as shown in Table 5.5 and assigned to the respective geometry.

Table 5.5: Material set properties of the EBR pile model.

Constitutive model	Unit weight (kN/m^3)	Stiffness (GPa)	Diameter (m)	R_{inter}(-)
Linear elastic	6	29.7	0.762	0.7

It should be noted the EBR does not occupy a volume inside the soil block but overlaps it. Thus, the pile unit weight to be input must be the difference between the soil unit weight and the real pile unit weight, to compensate for overlap (Brinkgreve, 2022a). A summary of the modelling process of an EBR pile is shown in Figure 5.6.

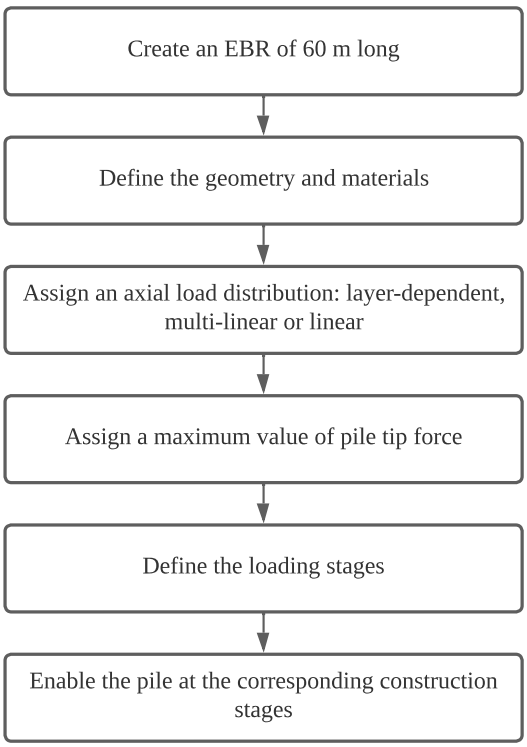

Figure 5.6: Flowchart of Plaxis 3D modelling process of an EBR pile.

Two EBR models were calculated; one was built considering a layer-dependent axial resistance calculation, and a fixed tip force of 6000 kN (calculated according to NEN 9997-

1 (2017)), and another one considering a multi-layer distribution calculated with the alpha method from NEN 9997-1 (2017). In both cases, the optimal model consisted of a medium size element mesh (in accordance with Frissen (2020) and Hartman (2023)) and a 40x40 m Plaxis 3D model.

5.7. Comparison of results of single pile models

In this section, the results obtained from single pile models, in terms of axial force and pile displacement, are shown. For comparison, results were taken into account in the short term, after inducing a jump load of 6700 kN (Figure 5.7), and in the long term, 20,000 days after the construction is finalised (Figure 5.8).

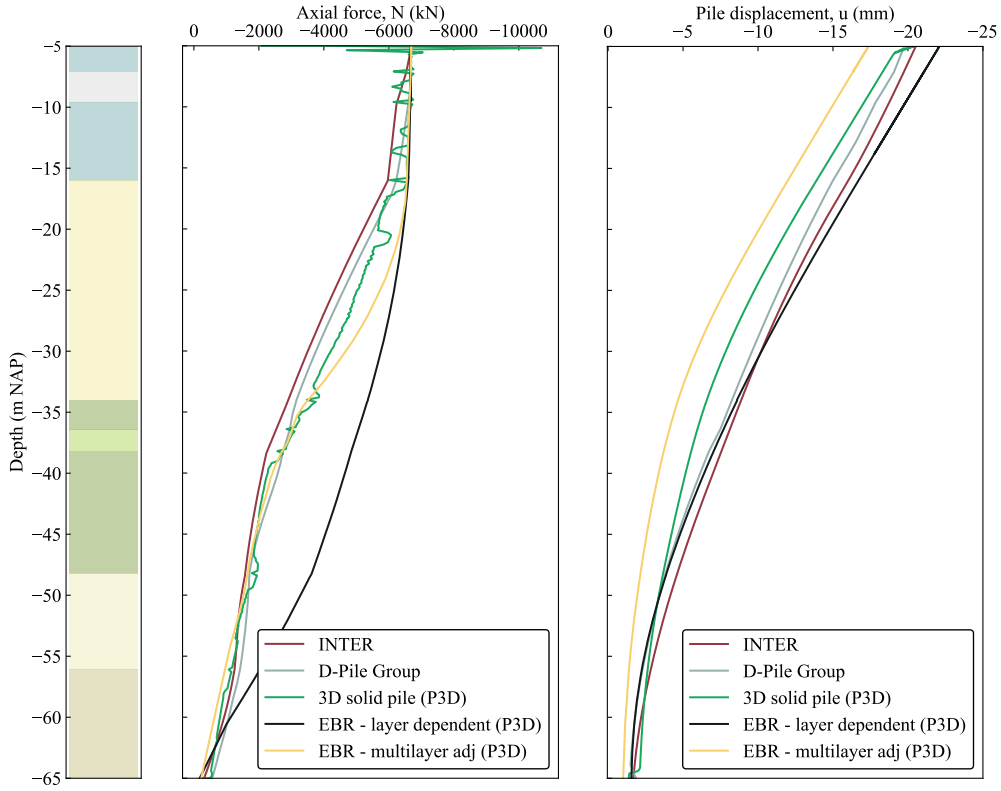

(a) Axial force vs depth **(b)** Pile displacement vs depth

Figure 5.7: Results of single pile calculations in the short term by several modelling elements.

Figure 5.7a and Figure 5.7b show the results in the short term of axial force and pile displacements, respectively. First, the results of INTER and D-Pile Group are included, which are in accordance with the standards specified by the NEN 9997-1 (2017) and correspond to the traditional Dutch pile design. In both programs, 20 mm of pile displacement was calculated for a jumpload of 6700 kN. Next, the volumetric pile is defined, which is the most realistic way of modelling in FE, but due to its complexity, it shows some numerical instability in the results and its computation time was significantly larger. The SSI shows a similar load distribution to D-Pile Group or INTER, and a pile displacement of 19 mm. Nonetheless, it can be seen that solid 3D pile mobilised more resistance in the Pleistocene sand than the NEN 9997-1 (2017)

models. Further, the EBR results with a layer-dependent distribution show a softer response; there is less force development in the Pleistocene sand, and more in the deeper dense sand. It also has a higher pile displacement than the other models, 21 mm. Finally, the EBR model that implements the multilayer distribution adjusted according to the NEN 9997-1 (2017) presents an axial distribution similar to the 3D solid pile, but also a displacement of 16.5 mm, smaller than the rest of the models.

Following, Figure 5.8a and Figure 5.8b show the results in the long term of axial force and pile displacements, respectively. In all the results it is evident a force shift towards the bottom of the pile, as well as the presence of negative skin friction. This phenomenon occurs as a consequence of the Kedichem clay consolidation (Schippers and Broekens, 2022), which also leads to the settlement of the Pleistocene sand and Holocene pack.

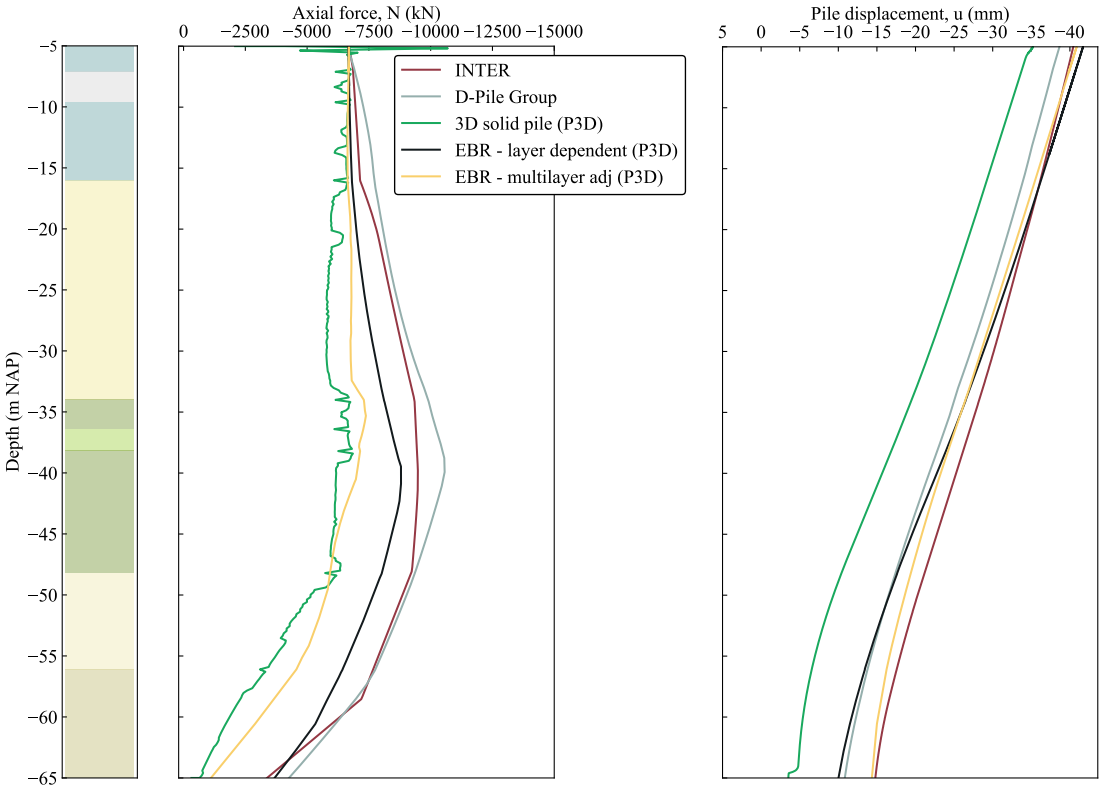

(a) Axial force vs depth **(b)** Pile displacement vs depth

Figure 5.8: Results of single pile calculations in the long term by several calculation means.

First, it is observed that the calculation performed with single spring models presents a final pile displacement of 40 mm for INTER and 38 mm for D-Pile Group, whose differences are attributed to the hysteresis modelled in INTER's code (van Dalen et al., 2014). Then, the 3D solid pile shows a stiffer response than the D-Pile Group in which most of the axial force develops in the deeper dense sand. It also presents a tip resistance of 2000 kN, i.e. almost half of the value presented by D-Pile Group or INTER. Likewise, the 3D solid pile had a displacement of 35 mm, being the smallest value of all models. However, the volumetric pile results still show numerical instability in the long term, and it was the model with most computation time. Further, the EBR with a layer-dependent axial distribution showed a soft

response in which significant force is developed at the tip and end of the shaft, as well as a displacement of 43 mm. Finally, the EBR with a multi-layer force adjustment presents a stiffer axial force, similar to 3D solid pile and DPile Group results, with a displacement equal to 40 mm.

5.8. Pile group modelling

Pile group models corresponding to the corners of the construction site are built, as each group contains an instrumented pile that will be used to verify the accuracy of the modelling. The groups are shown in Figure 5.9. Since the project is symmetrical, only two groups are considered. Group 1 considers eight piles in a trapezoidal arrangement; first, there is a row of three piles adjacent to the sheet pile wall, with a centre-to-centre (c-c) separation of 2.1 m. Next, there is another row of three piles with a c-c separation of 1.45 m between them and a c-c distance of 1.398 m from the first pile row. Finally, the group contains another row of two piles with a c-c distance of 1.463 m between them, and a separation of 1.382 from the second pile row. Similarly, Group 2 is composed of six piles organized in three rows and two columns, forming a rectangle. The average c-c distance between rows is 1.435 m, and between columns is 1.4 m. All the piles considered in this project have the same geometry.

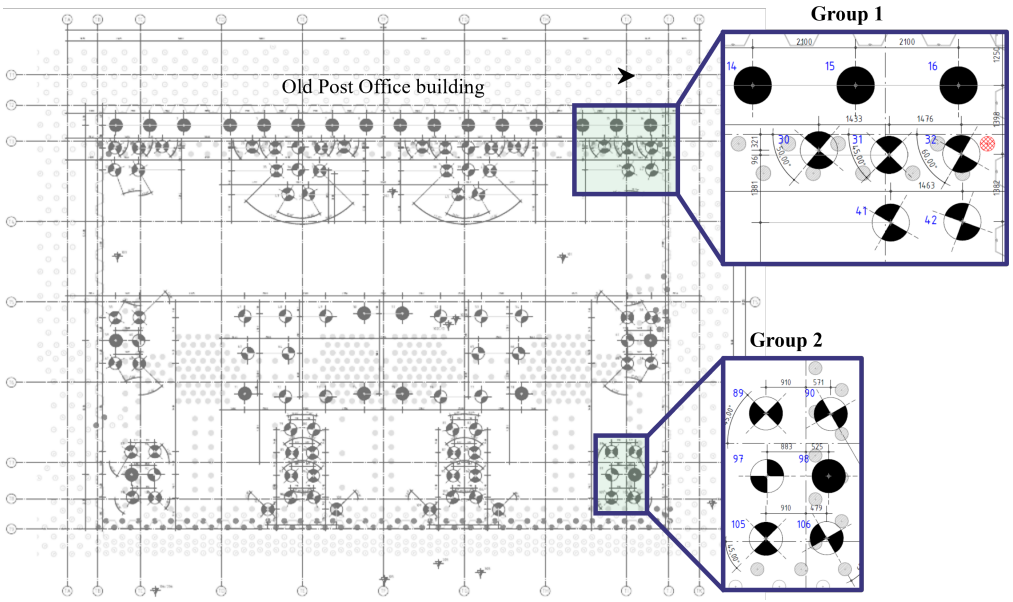

Figure 5.9: Modelled pile groups (adapted from Pieters Bouwtechniek, 2021).

The models were created by means of 3D solid piles and EBR. Likewise, loads of 6700 kN were considered for each pile, equivalent to the average final static load from the high-rise building per pile. The results of these models are shown in the following sections and will be compared with the FO measurements and adjusted as needed to match the real-site scenario in Chapter 7.

5.8.1. Group 1

Results of the middle pile of group 1 are presented in this section, as it is the instrumented pile on site. The short term behaviour is evaluated in Figure 5.10, where the single pile behaviour is also included for ease of comparison. It can be seen that all the group models display an equivalent load distribution (Figure 5.10a). Nonetheless, the pile displacement plot (Figure 5.10b) shows important differences: The volumetric pile has a total displacement of 30 mm, and only mobilises 2 mm in the tip, presenting a very stiff behaviour. Further, the model created with EBR and a layer-dependent force distribution has a middle pile displacement of 30 mm, and 11 m on the tip. Likewise, the EBR pile group, considering a multilayer load distribution has the same tip displacement as the former model (11 mm) but presents a softer response with a total displacement of 43 mm. In both plots, the group effect is evident when compared to the single pile behaviour, as there is a significantly less mobilised force in the Pleistocene sand from the groups, and consequently a higher displacement (Bowles, 1997).

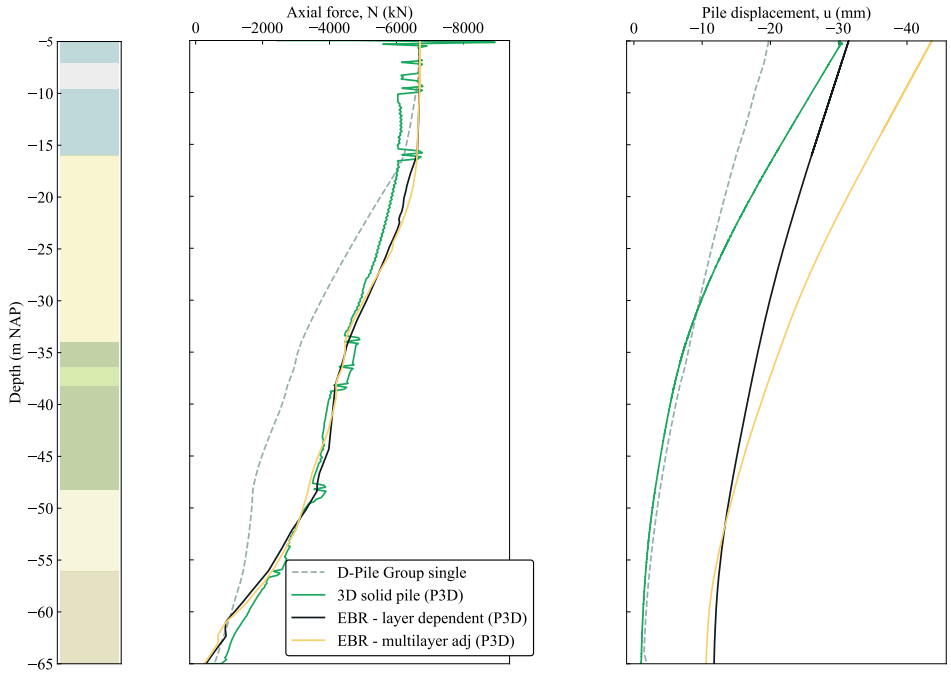

(a) Axial force vs depth **(b)** Pile displacement vs depth

Figure 5.10: Results of pile group 1 calculations in the short term by several modelling elements.

The long term behaviour is shown in Figure 5.11 for the middle pile in group 2, where it can be seen results are similar to the short term. While load distribution is equivalent between the three models, there are important differences in the pile displacement; The volumetric pile shows 46 mm throughout its entire length, but only 2 mm on its tip. Further, the model created with EBR and a layer-dependent force distribution has a middle pile displacement of 44 mm, and 19 m on the tip. Likewise, the EBR pile group, considering a multilayer load distribution has the same tip displacement as the layer-dependent model but its total displacement is 59 mm. When compared to the single pile results, it can be seen that the group limits the normal force the middle pile could potentially develop, in comparison with a single pile.

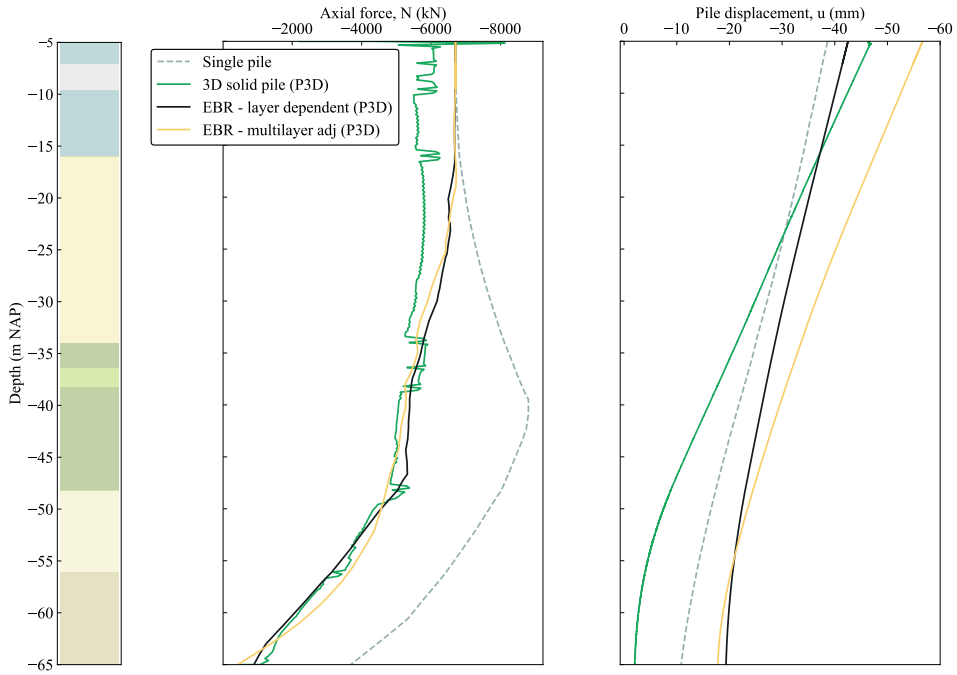

(a) Axial force vs depth

(b) Pile displacement vs depth

Figure 5.11: Results of pile group 1 calculations in the long term by several modelling elements.

5.8.2. Group 2

The results of the middle pile of group 2 are presented in this section. Figure 5.12 includes the short term behaviour. In this group, the volumetric pile shows considerable numerical instability in the axial force results (Figure 5.12a), but the EBR layer calculations prove to be stable and similar to the results of pile group 1 (Figure 5.10). Moreover, the pile displacement plot (Figure 5.10b) shows the volumetric pile model has a total displacement of 36 mm, and a tip displacement of 17 mm, which is larger than the tip displacement of group 1 model displayed. Further, the model created with EBR and a layer-dependent force distribution has a middle pile displacement of 31 mm, while the EBR model considering a multilayer load distribution displaces 42 mm, showing the softest response of all models. In both plots, the group effect is evident when compared to the single pile behaviour, as there is a significantly less mobilised force in the Pleistocene sand from the groups, and consequently the displacement is 1.5 to 2 times higher.

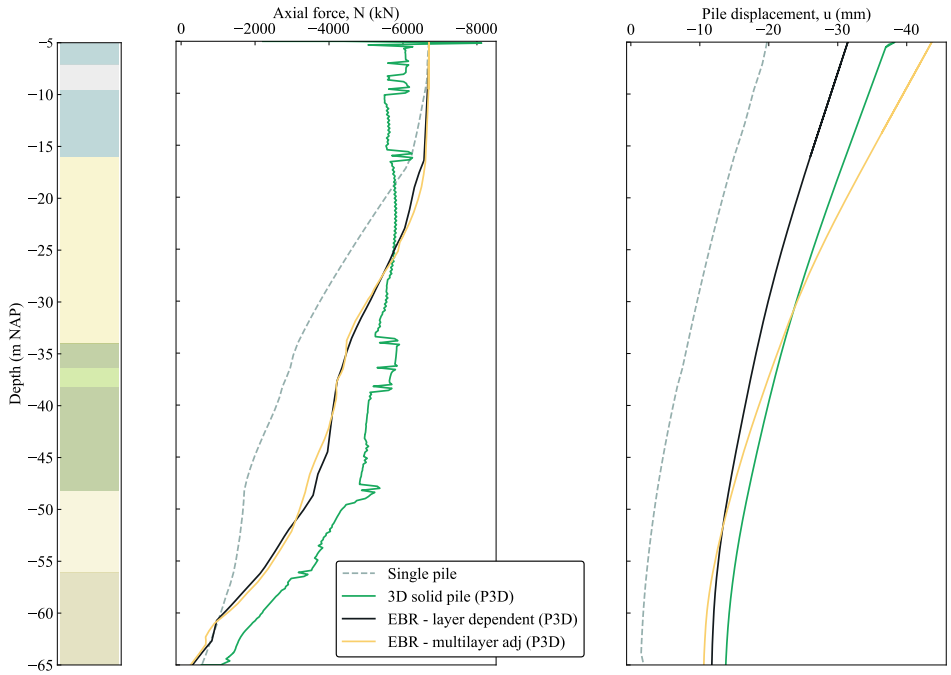

(a) Axial force vs depth **(b)** Pile displacement vs depth

Figure 5.12: Results of pile group 2 calculations in the short term by several modelling elements.

The long term behaviour is shown in Figure 5.13 for the middle pile in group 2.

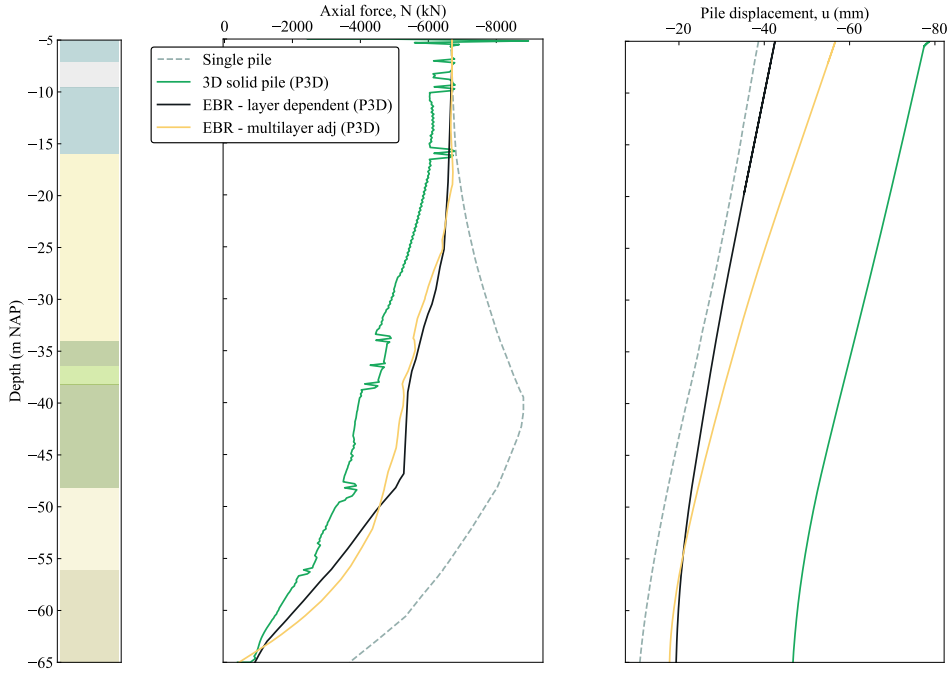

(a) Axial force vs depth **(b)** Pile displacement vs depth

Figure 5.13: Results of pile group 2 calculations in the long term by several modelling elements.

The three models follow their respective displayed behaviour from the short term anal-

yses. The axial force distributions (Figure 5.13a) are equivalent, with the volumetric pile model showing important numerical instability. The group effects are evident. Further, in the pile displacement plot (Figure 5.13b) all models show significant differences: the EBR layer-dependent pile has a similar total displacement to the single pile model (41 mm), but at the tip the displacement is 2 times larger than the latter. Likewise, the EBR pile group, considering a multilayer load distribution has the same tip displacement as the layer-dependent model but its total displacement is 59 mm. The volumetric pile shows a very large displacement of 79 mm, which suggests it is a product of numerical instability and should not be considered in further analyses of group 2.

6

Results of site measurements

6.1. General aspects

This chapter presents the FO strain measurements results upon gradual loading, as well as the axial force calculated from Equation 3.1. The baseline measurement was taken in the four piles on September 30th 2022 when there was no load on top of the foundation yet. The piles were installed and cast 28 days before the readings, thus the concrete had already reached its design strength.

Further, measurement 2[1] was carried out on July 4th 2023 for three piles: 97, 31 and 18, as pile 92 was inaccessible on-site at that moment. The fourth level of the high-rise building was being built, and therefore the site load was composed of the basement, the initial slab together with the load-bearing walls and columns, and two levels, as shown in Figure 6.1.

Figure 6.1: Construction progress (July 4th, 2023).

[1]This data set is further referred to as *measurement 2*, as in January there was a failed attempt to measure pile 97. While the latter is not considered in this interpretation explanation, it still produced (incorrect) results.

The baseline and measurement 2 are considered for the axial force calculation hereby presented, for piles 97, 31 and 18. This chapter presents only the results of FO measurements upon gradual loading, a detailed explanation of the interpretation process of the FO measurements is included in Appendix C.

6.2. Estimation of the current load on site

The assumptions and calculations to determine the load at the site at the time of the measurements are presented below. According to the structural information of the POST Rotterdam, the basement slab has a thickness of 0.5 m, and the aforementioned concrete base box (load-bearing walls and columns) has an average height of 5.3 m. Further, the piles located in the west of the site have a 2 m thick cap on top of them. With this information, a stress of 187.2 kPa is obtained for pile group 1, and 139.2 kPa for pile group 2.

Following, according to the structural plan, group 1 is subjected to an additional 7728 kPa, while pile group 2 carries 6231 kPa, which accounts for the total static load of the high-rise building, respectively. Considering that the structure has 43 floors at the time of the analysis (according to the latest information from Habitat and Urban (2023)), means group 1 will carry 179.2 kPa per floor, while group 2 will be subjected to 144.9 kPa per floor. On July 4th, 2023, when strain measurement 2 was obtained, only two levels were constructed and therefore, a surface load of 545.6 kPa is assumed for pile group 1, and 429.0 kPa for pile group 2.

It must be noted that this is an educated estimation with the limited available information, as it is a real-time measurement and not a controlled load test. It is possible that the actual load is slightly smaller since at that date, the concrete structure was built without details. However, this information is sufficient to be able to perform the FO interpretation work from data on-site.

6.3. FO measurements (upon gradual loading)

6.3.1. Pile 97

Figure 6.2 shows the results of strain and force for pile 97, which corresponds to the middle pile of group 2. The FO has demonstrated robust performance by surviving installation and manipulation on site. In Figure 6.2a, strain measurements indicated a continuous compressive behaviour from -11 m NAP to the pile's end, whereas at the top, readings indicate tension jumps. The axial force (Figure 6.2b) analysis revealed variations in accordance with the existing soil profile. Major axial force contribution occurred between -15 m NAP and -37 m NAP, corresponding to the Pleistocene sand layer depth. From -40 m NAP to -55 m NAP, the graph displayed a concave curve with negligible force, as expected for Kedichem clay under small loads. At the pile bottom, between the dense silty sand and dense sand, some uniform force developed, though less significant than in the Pleistocene sand layer.

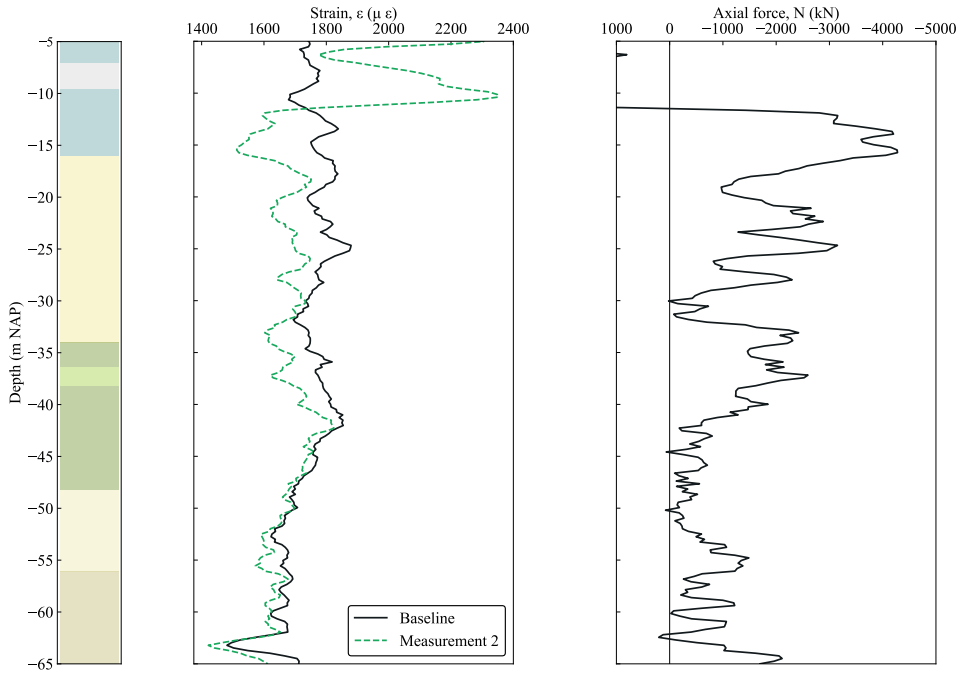

(a) Strain measurements vs depth. **(b)** Axial force results vs depth.

Figure 6.2: Strain and axial force results of pile 97.

While the strain measurements of pile 97 follow a similar trend to the site stratigraphy, there is high uncertainty on the results at early load stages. In the first place, from 0 to -11 m NAP, there are high jumps in the readings suggesting tension. While the reason is uncertain, hypotheses include the following:

- Tension readings are a consequence of some construction procedure, i.e. the curing effects during the casting of the basement slab, non-uniform concrete curing of the pile throughout its entire length, or uplift of the basement slab after pumping stopped.
- The FO could be misaligned from the centre of the pile and thus bending strains are introduced in the readings.
- It is possible that the piles are undergoing tension at the top due to the unloading from the excavation since the structural load at the moment is very small.
- Structure load is small and therefore is currently being carried by the slab.

Second, Figure 6.2b shows resistance from the bottom of the pile equivalent to the Pleistocene sand layer contribution, whereas, at this stage, axial force at the deep dense sand layer is expected to be negligible.

Third, the cable of this pile is only reachable per one end, thus, readings were carried out by using the BOTDR interrogation method. Therefore, the measurements have a resolution of 50 $\mu\varepsilon$, which indicates that the cable struggles to measure strain changes smaller than the aforementioned, resulting in unclear or noisy data (Güemes et al., 2014). This might stem from factors like sensor sensitivity or reading equipment accuracy, leading to widely spaced readings and data noise.

6.3.2. Pile 31

Pile 31 corresponds to the middle pile of group 1, and thus may be comparable to the results of pile 18. It is the only pile that has a full FO cable loop, which means every measurement takes two mirrored readings, for redundancy. Likewise, the full cable loop allows to implement the BOTDA interrrogation method for taking measurements, and thus the readings' resolution is 6 $\mu\varepsilon$, which is higher than in BOTDR (50 $\mu\varepsilon$). Figure 6.3 includes the strain results of pile 31, referred to as measurements a (Figure 6.3a) and b (Figure 6.3b), since the cable has a full loop. It should be noted that there is a shift between the readings of each side of the loop and therefore the results shown below fall into two different ranges; Measurement (a) exhibits results from -1000 $\mu\varepsilon$ to -600 $\mu\varepsilon$, while measurement (b) range is from -200 $\mu\varepsilon$ to 200 $\mu\varepsilon$. Nonetheless, in both cases, the strain increment between measurement 0 and measurement 2 is equivalent.

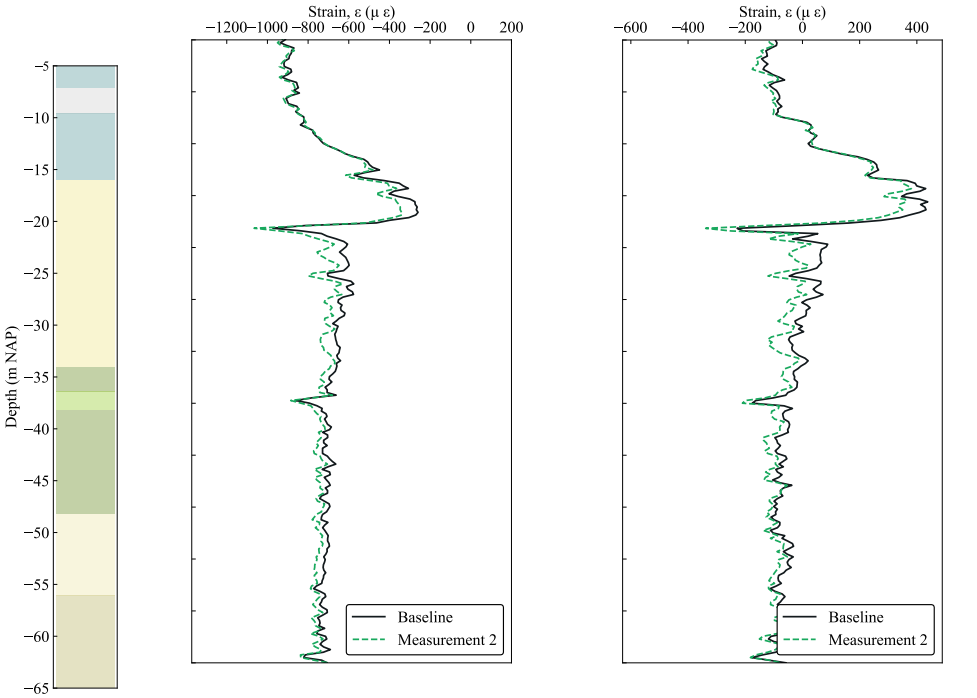

(a) Strain measurements vs depth: Measurement (a).

(b) Strain measurements vs depth: Measurement (bb).

Figure 6.3: Strain results of pile 31.

Further, Figure 6.4 shows axial force for both mirrored data sets. The results show a stable force behaviour from -16 m NAP to the pile's end. Just like pile 97, axial force patterns align with the site soil profile (Figure 6.2), but less noise is introduced, as the cable of pile 31 has a better resolution. It should be observed that there is an axial force *bulge* of approximately 2000 kN, between -16 m NAP and -32 m NAP, corresponding to the Pleistocene sand layer depth. Likewise, under this loading scheme, the contribution of the underlying layers (Kedichem clay, dense silty sand and deeper dense sand) is almost zero, as most of the resistance comes from the Pleistocene sand.

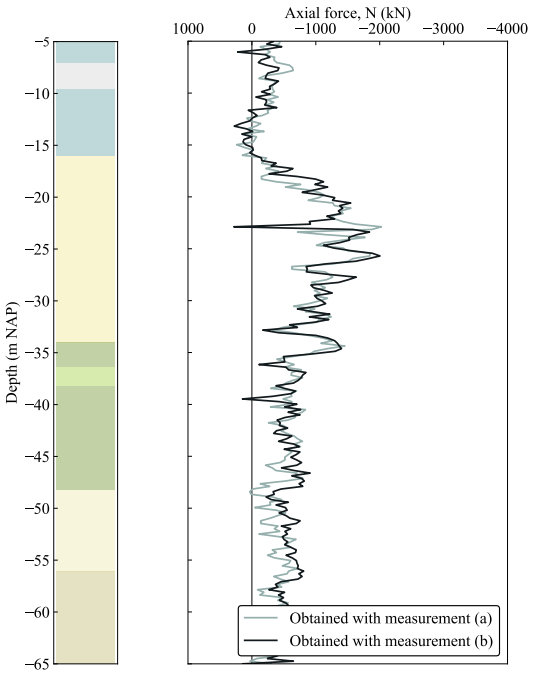

Figure 6.4: Axial force results of pile 31.

However, some discrepancies appear in the measurements. For instance, the site strain measurements exhibit a particular trend from 0 to -23 m NAP, with a tension jump at -23 m NAP (Figure 6.3a). This region shows less strain increment compared to the depth range from -23 m NAP to -65 m NAP, which contradicts the expected behaviour for a small load in the short term. Under this loading stage, it is expected to see more axial force developed on the top of the pile instead of at the bottom. Similarly, the axial force plot indicates nearly negligible force between -5 m NAP and -16 m NAP, which corresponds to the Holocene pack depth. While the contribution of this layer is expected to be small, the force should be consistent with the Pleistocene sand force results.

In order to study this effect, further investigation is needed over time. However, since the scope of this project is to study the soil-structure interaction while the high-rise building is being built, the gradual loading limits the pace of data collection, necessitating several years to validate any changes over time. Nevertheless, some hypotheses are included to help understand the latter, which also applied to pile 97.

- Tension readings may be a consequence of some construction procedure, i.e. excavation, the curing effects during the casting of the basement slab, uplift of the slab after the pumping stopped, or non-uniform concrete curing of the pile throughout its entire length.
- It is possible that there is a misalignment of the FO cable from the central axis, which could introduce bending strains into the measurements.
- The installation of adjacent piles might influence the radial stresses acting on this zone.
- Given the pile's considerable length, variations in curing time, especially in the upper part, could have led to an improper baseline measurement, which should have been taken

afterwards.

- Different hydrodynamic and radial stress conditions could be present within the Pleistocene sand, which could impact the grout cover of the pile, resulting in different cross-sectional geometries compared to the surrounding clay layers, influencing the force bulge size and altering measurements in the upper clay layers.
- Negative skin friction in the Holocene clay layers could be transferring load to the Pleistocene sand faster than expected.
- Since the structure load is currently small, it is possible that the piles are undergoing tension at the top due to the unloading from the excavation. The present load may not be large enough to counteract the excavated material.
- Structure load is small and therefore is currently being carried by the slab.

6.3.3. Pile 18

Figure 6.5 includes the results of strain and force for pile 18. Results present similar inconsistencies to pile 97. First, contrary to the anticipated behaviour during the initial load stages of the pile, a larger strain increment is shown from -35 m NAP to the bottom of the pile (6.5a), in comparison with the measurements from 0 to -35 m NAP. This leads to unexpected trend results in the force profile (Figure 6.5b), as it presents a higher force development at the bottom than at the top. Moreover, pile 18 was also measured by means of BOTDR and consequently, readings are noisy and widely spaced.

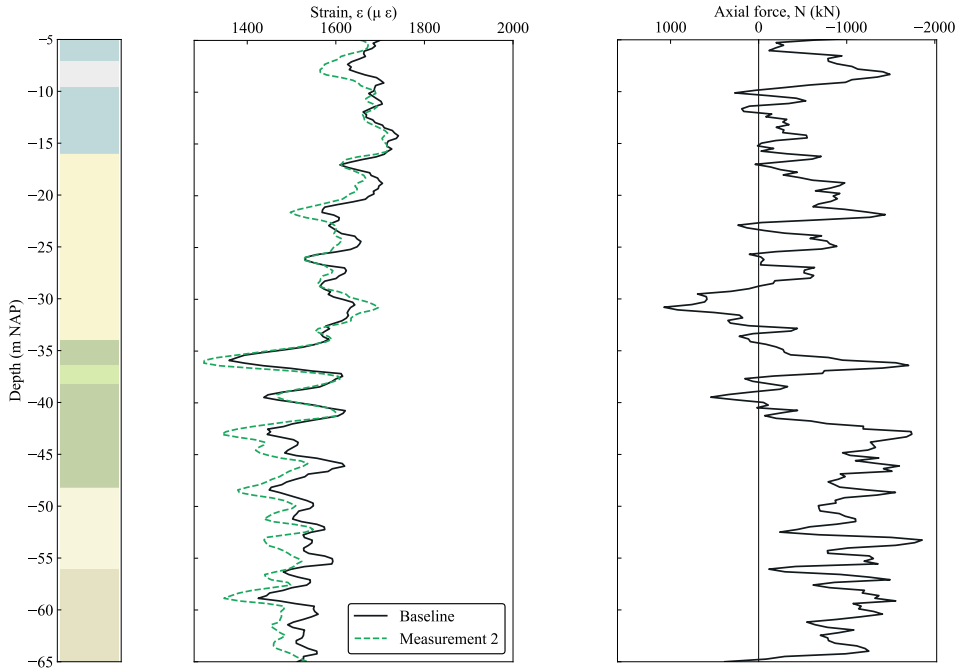

(a) Strain measurements vs depth. **(b)** Axial force results vs depth.

Figure 6.5: Strain and axial force results of pile 18.

The reason for this unusual behaviour remains unclear, and no concrete explanation has been established to explain the discrepancy. The possibility of inaccurate results cannot be

ruled out at the moment, as further measurements are required to ascertain the accuracy of these readings and identify any potential sources of error. Nonetheless, hypotheses formulated for pile 97 and pile 31 also apply for this case: First, tension readings are a consequence of some construction procedure; second, the FO could be misaligned from the centre of the pile and thus bending strains are introduced in the readings; third, as the structure load is currently small, it is possible that the piles are undergoing tension due to unloading from the excavation; finally, the structure load is small and therefore it could be currently carried by the slab.

6.4. Comparison of models to FO measurements in the short term

In this section, the middle pile of the previously calculated group models is compared with the force obtained from the site.

6.4.1. Group 1

The behaviour of the middle pile of group 1 is analysed. Figure 6.6 includes the axial force results obtained by means of Plaxis 3D modelling (modelled as a 3D solid pile and as an EBR), and the force calculated from the strain measurements of pile 31 (equivalent to the middle pile of group 1). The decision to exclude the results of pile 18 relies on the analyses presented in section 6.3. Results from pile 31 are expected to be more reliable than those from pile 18, as they were taken with the BOTDA method.

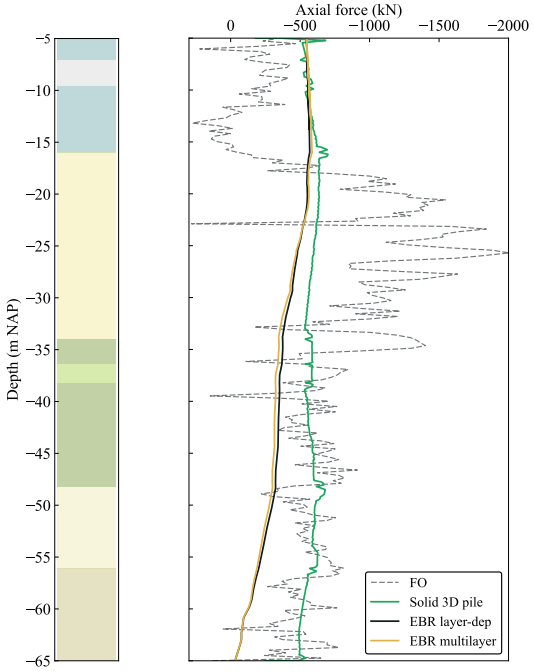

Figure 6.6: Comparison of axial force results of middle pile by several calculation means against FO results (of pile 31).

Pile 31's trend aligns with the adjacent soil profile. Despite noisy data, an evident axial force bulge is identifiable at the Pleistocene sand depth. At the underlying layers, relatively constant uniform measurements are shown, indicating lower axial force in the lower pile section. However, some inconsistencies are present; First, measurements display tension at the pile's top from -5 m NAP to -17 m NAP. Second, the readings from -33 m NAP until the end of the pile do not behave as expected from the analyses in Chapter 5. Calculations showed that for the short term, there is no significant force mobilisation from the layers under the Pleistocene sand, while the FO results show an approximately constant reading of 500 kN. With the information available at the moment, it is not possible to make conclusions regarding the latter.

Due to the above, when comparing the FO force results to the model calculations (Figure 6.6) it is not possible to choose which is the best way to model this foundation. Nonetheless, it can be observed that the 3D solid pile results have a good match with pile 31 measurements from -33 m NAP to -65 m NAP and thus, this model can explain that at this loading stage, the middle pile of group 1 is undergoing a large group effect in which force is barely mobilised.

6.4.2. Group 2

The axial force obtained from the middle pile's Plaxis 3D models is compared against the axial force results of pile 97 and shown in Figure 6.7.

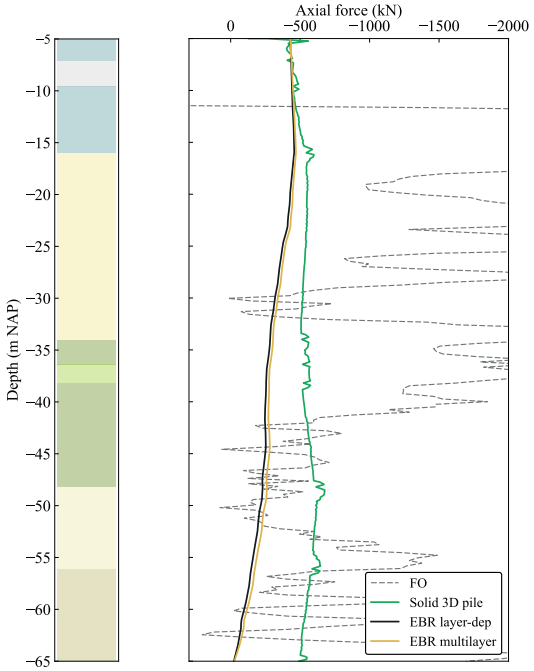

Figure 6.7: Comparison of axial force results of the middle pile by several calculation means against FO results (of pile 97).

As mentioned in section 6.3, pile 97 presents noisy readings and current unreliable measurement. Although at the moment it is not possible to validate the modelled piles, the mea-

surements show a trend that is consistent with the site soil profile; most of the axial force can be seen to develop in the Pleistocene sand depth, while the force is negligible at the depth of the second Kedichem clay. Moreover, pile 97 exhibits unusual behaviour at the part in contact with the deep dense sand, as measurements show resistance developed at that point, which is not expected during this loading stage. Inconsistencies also emerge at the top part of the pile (from -5 m NAP to -17 m NAP), implying tension at the pile's top.

At the moment, it is not possible to determine which is the best way to model these 60 m long piles from the FO data, since the measurement results differ widely from the models, and in order to analyse them, or to determine if there was any error in the instrumentation, it will be necessary to continue measuring on site over time. Nonetheless, when comparing the results of group 1 models against group 2, it can be seen that both groups have equivalent behaviours, and thus it could be stated that they can be modelled using the same elements.

6.5. Implications of FO measurements on pile modelling

Initially, it was proposed to carry out some adjustments to the pile models in order to have a better fit to the output results of the FO measurements. However, as mentioned above, at this loading stage it is not possible to determine which is the best way to model these 60 m long piles, since the measurement results differ widely from the models. In order to analyse them, or to determine if there was any error in the instrumentation, it will be necessary to continue measuring on site over time.

Previous hypotheses (section 6.3) explore potential factors such as instrumentation, work-site activity, and geotechnical effects influencing these deviations. Noisy readings are common at low load levels, and were also anticipated during this project's development. To comprehensively study this effect, more site measurements under varied load schemes are essential. Yet, since this is not a load test in which time and load (or displacement) variables are controlled, obtaining additional measurements will require substantial time, as the construction works of the high-rise building need to progress to have more load on the foundation.

As for selecting the EBR layer-dependent model, a provisional choice based on the current understanding of both pile groups is made. The building's future heavier loads will offer insights into model performance. Notably, volumetric piles provide the most realistic models, and as shown in 6.4.1, they could even explain inconsistencies in the force behaviour. Nonetheless, they also present numerical instability and inefficient computation time, leading to the present adoption of the EBR approach with a layer-dependent force distribution. For future analysis, a short-term model comparison is recommended within a few years with the aforementioned modelling tools. In future evaluations, volumetric pile models are expected to be the most accurate, but would also represent higher computational costs.

Due to the latter, and since both pile groups appear to behave similarly, EBR layer-dependent is implemented to model the high-rise building foundation, in order to predict the SSI of the whole foundation in the long term in Chapter 7.

7

Results of models and implications on design

7.1. General aspects

A model was developed considering the entire foundation of the POST Rotterdam high-rise building, in order to study the impact of the SSI of the POST building on the final design and its surroundings. First, the construction of the final models is described. Then, the spring stiffnesses of the piles corresponding to groups 1 and 2, obtained in the final model, are calculated. A comparison is made with respect to the spring stiffness of a single pile model (obtained from previous chapters). Further, the 50-year settlement curve of the area caused by the construction of POST Rotterdam is obtained, and the differential settlement implications for the surrounding buildings are described. Next, a simplified model is built and its results are discussed and compared to the ones obtained with the final detailed model. Finally, a sensitivity analysis is carried out considering variations in the stiffness of the Kedichem clay layer for the whole model, as discussed in Chapter 4.

7.2. Plaxis 3D model of POST Rotterdam

A detailed structure was elaborated according to the actual specifications of the study project, as shown in Figure 7.1. Hereby, the complete box containing the basement slab and the ground floor is represented, which includes the structural walls and columns that connect the building to its foundation and are responsible for transmitting the load to it.

The structure (Figure 7.1a), adapted from the model in Schippers and Broekens (2021) has a surface of 34 x 26 m, in which the basement slab is located at -5 m NAP, with a thickness of 0.5 m. Underlying, 2 m thick blocks are locally modelled on top of the pile groups. Subsequently, all the piles were modelled as a series of EBR with a layer-dependent load distribution (Figure 7.1b), as mentioned in Chapter 6. In addition, distributed loads are applied to the top of the structural box to represent the permanent structural loads, which deviate slightly from the average point load of 6700 kN per pile.

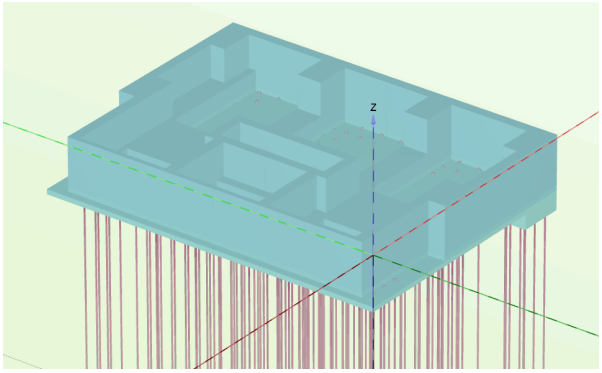

(a) Structure.

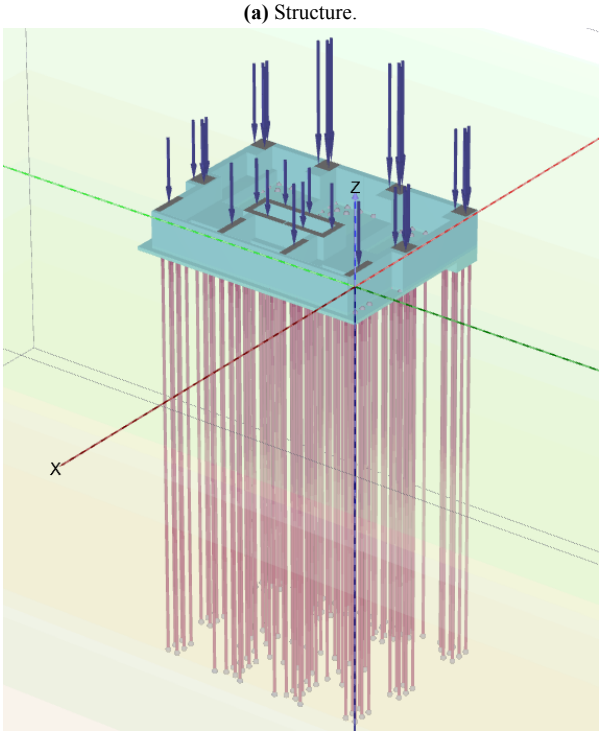

(b) Geotechnical model.

Figure 7.1: Plaxis 3D model of POST Rotterdam.

7.3. Calculation of spring stiffness of various piles

This section presents the pile displacement calculated for all the piles of groups 1 and 2. With this, the spring stiffness of each pile is calculated in the short and long term, and compared with the one calculated with a single pile. Following, the group effects are evaluated, as well as the structural implications of the pile displacement.

It must be noted that in practice, this comparison is not often done. Piles are generally incorporated into the structural model as single springs (Hartman, 2023), and the difference in displacement between the single spring models and the foundation of the whole building is dealt with in the structural design. Nonetheless, the calculations hereby presented had the purpose of analysing the SSI behaviour of different piles within the same pile groups, which could be further verified by monitoring measurements.

7.3.1. Single pile model

In the previous chapters, a series of single piles were modelled using various methods. The average pile displacement was 21 mm for a jump load of 6700 kN (plus an estimated 300 kN of negative friction according to Schippers and Broekens (2021)) in the short term, and 39 mm in the long term (20,000 days after the termination of the high-rise building). The spring stiffness calculated for a single pile is equal to:

- 333.3 MN/m in the short term.
- 179.48 MN/m in the long term.

Due to the particular conditions of these foundations, the spring stiffness changes over time. Although the long-term displacement of the piles is not only due to the load but also from negative skin friction, consolidation and creep, it is important to specify it for structural and future monitoring purposes.

7.3.2. Pile group 1

The pile displacements of the two pile group types at the corners of the high-rise building were evaluated to understand the group effect in this foundation and to verify if the short and long-term spring stiffness is comparable with that of single pile models. In this section, the results of group 1 are discussed. Table 7.1 presents the displacements and spring stiffness of group 1. In all cases, a load of 6700 kN plus an estimated 300 kN of negative friction (according to Schippers and Broekens (2021)) was considered.

Table 7.1: Calculation of spring stiffnesses of the piles of group 1 using a detailed structure model.

Pile	Displacement (mm)		Springs (MN/m)	
	Short term	Long term	Short term	Long term
Pile 14	59.90	63.03	116.86	111.06
Pile 15	59.69	62.87	117.27	111.34
Pile 16	59.38	62.62	117.88	111.79
Pile 30	58.43	61.55	119.80	113.73
Pile 31	58.31	61.46	120.05	113.90
Pile 32	58.08	61.27	120.52	114.25
Pile 41	57.06	60.17	122.68	116.34
Pile 42	56.82	59.97	123.20	116.73

Piles situated along the building's edges exhibit greater stiffness compared to those located at the centre of the group or nearer the building's core. The pile group, as a whole, demonstrates more substantial displacement when contrasted with individual piles. While the SSI behaviour follows the same trend as the single pile behaviour, the spring stiffness results are three times lower than the results of the single pile in the short term, while in the long term, the results are approximately 70% higher than those of the single pile.

7.3.3. Pile group 2

Results for group 2 are shown in Table 7.2. The group effect is also evident in this case, since according to the results, the piles with the greatest displacement are those closest to the centre of the building, while those in contact with the edge of the site have a stiffer response. This group presents smaller displacements in both terms than group 1.

Table 7.2: Calculation of spring stiffnesses of the piles of group 2 using a detailed structure model.

Pile	Displacement (mm)		Springs (MN/m)	
	Short term	Long term	Short term	Long term
Pile 89	47.10	50.01	148.62	139.97
Pile 90	46.11	49.09	151.81	142.60
Pile 97	46.03	48.98	152.07	142.92
Pile 98	44.96	47.98	155.69	145.89
Pile 105	45.00	48.00	155.56	145.83
Pile 106	45.00	48.00	155.56	145.83

7.3.4. Comparison with the design calcuations

The study conducted by Schippers and Broekens (2021) develops a model of half the building, a valid approach given the building's symmetry. In this model, results show that the spring stiffness of a single pile is applicable to represent all the piles within the building. However, the analyses presented here reveal different results. The latter indicates that while single pile models provide a good representation of SSI behaviour for the study case, piles modelled as a complete group exhibit a softer response compared to a single pile. It is important to carry on a single pile and pile group verification since the different responses can lead to discrepancies. Moreover, differences in the models can be partly attributed to their respective geometries. In this analysis, the Plaxis 3D models were extended to -80 m NAP, which is equivalent to 19 times the diameter of the design pile. This depth is greater than the 4 times the diameter (4D) recommended by the NEN 9997-1 (2017) and therefore, boundary effects may be present in the results.

7.4. Settlement in the surroundings

The settlement of the area is determined in order to study the effect that the high-rise building will have on the area in 50 years (20,000 days), in terms of differential settlement, which may represent important damage to the Old Post Office. The settlement profile follows section A-A', traced in Figure 7.2. Plaxis 3D results are shown in Figure 7.3.

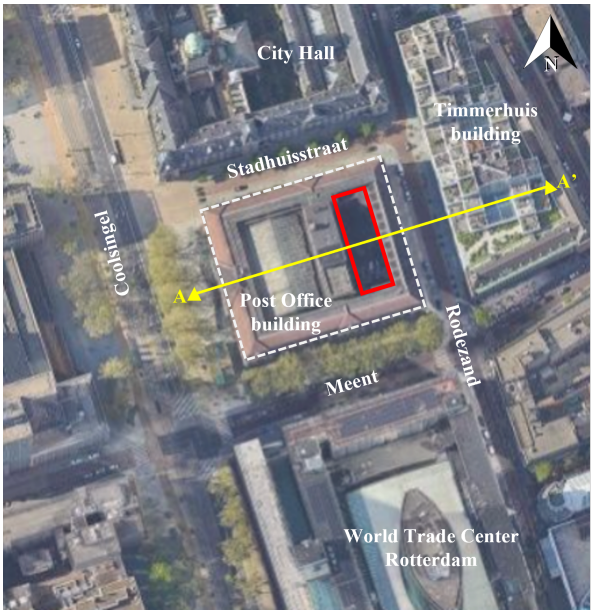

Figure 7.2: Location of A-A' section.

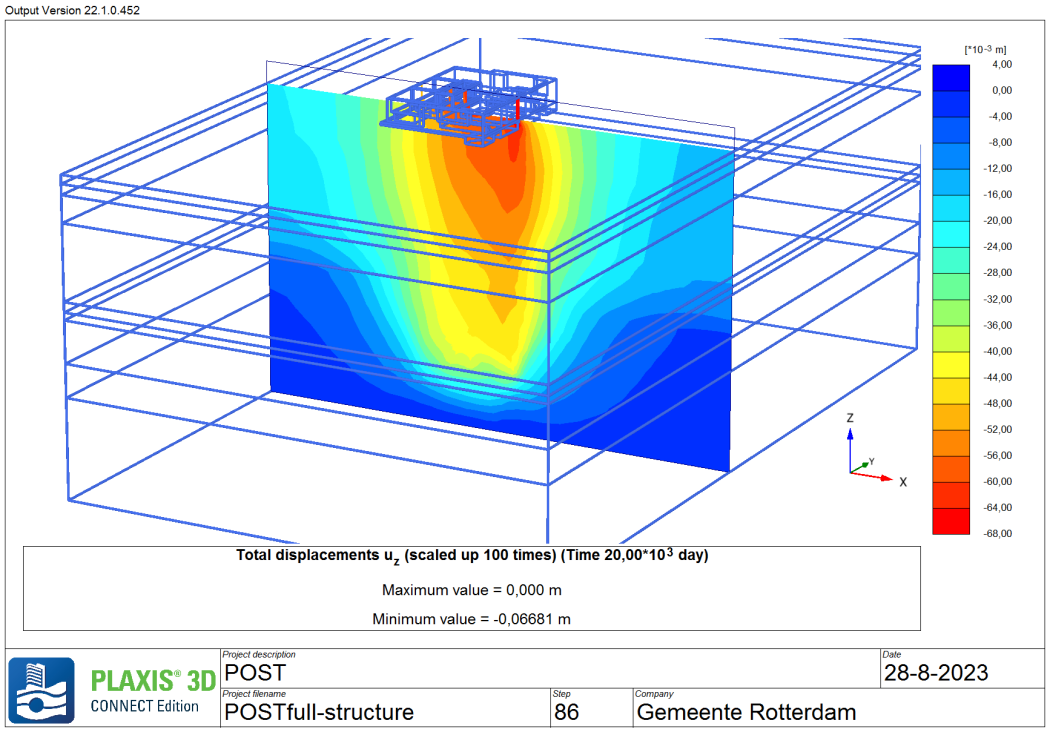

Figure 7.3: Settlement profile of Plaxis 3D detailed model of POST Rotterdam.

Figure 7.4 shows the calculated settlement profile of the area. The model presents a maximum settlement of 6.4 cm in 50 years. At the Old Post Office side, a maximum differential settlement of 18 mm over 10 m is calculated (1/555), while the Timmerhuis building shows a maximum differential settlement of 7 mm in 10 m (1/1428). The assessment and prediction of

damage generally involves differential settlement, rotation, relative rotation, deflection ratio, tilt and induced strains in the building (Prosperi et al., 2023). Moreover, NEN 9997-1 (2017) describes various limits of angular distortion depending on the settlement profile, that range from 1/2000 to 1/200 (Prosperi et al., 2023), being 1/500 for this case, a slight damage.

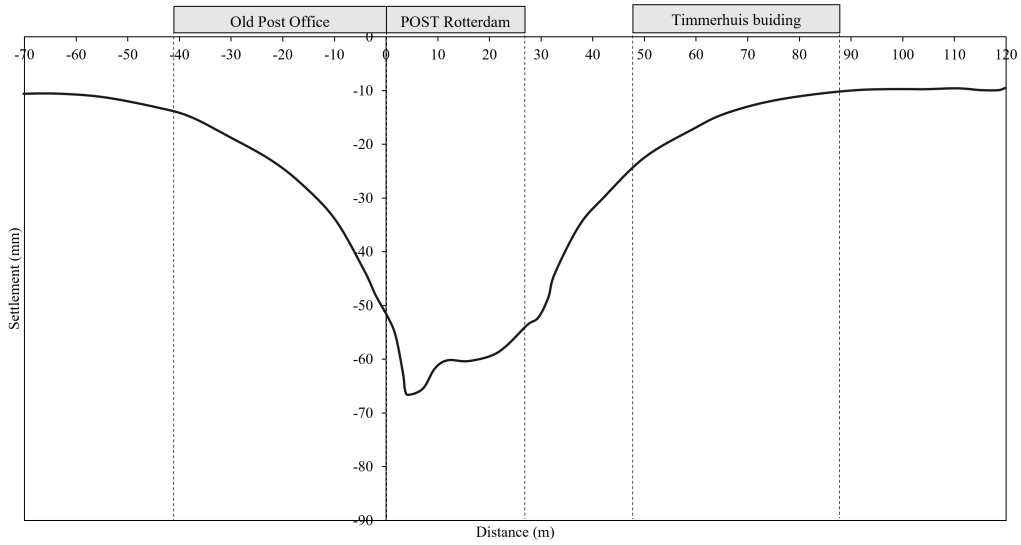

Figure 7.4: Settlement profile of the POST site 20,000 days after completion of POST building.

It should be noted that the adjacent buildings were modelled using surface loads, and their stiffness was not taken into account in the calculations. Like most old historic buildings in the Netherlands, the Old Post Office has a masonry structure which is capable of reducing stress changes by creep and relaxation of the material (Prosperi et al., 2023), and thus, it can hold differential settlements at some degree. In addition, it is supported by wooden piles, which have relatively low spring stiffness, making them flexible and capable of absorbing tension from the structure. Consequently, the results presented above may be considered conservative and represent the maximum potential angular distortion.

Nevertheless, given the historical significance of the Old Post Office and the economic loss rate from building damage (Prosperi et al., 2023), it is important to continue the structural monitoring (Quattro Expertise BV, 2021) to prevent significant damage arising from differential settlements, which could either be traditional instrumentation or by means of air-borne methods (Prosperi et al., 2023). The damage assessment will be dependent on the availability of measurements and monitoring information (Prosperi et al., 2023). In addition, the model shows a small differential settlement for the Timmerhuis building, whose effect is not detrimental to the structure.

7.5. Simplified model

A second model was developed in which the structure is represented with simplified loads, instead of the building stiffness (Figure 7.5). The basement slab was defined as a plate with concrete properties, and the total building load was taken as static uniform point loads of 6700

kN on top of the slab at the head of each pile. Further, the foundation was input as a series of EBR with a layer-dependent load distribution, as described in Chapter 5. This simplification was done to help the calculations run faster and verify how these considerations differ from a model with a detailed structure, as in Schippers et al. (2021).

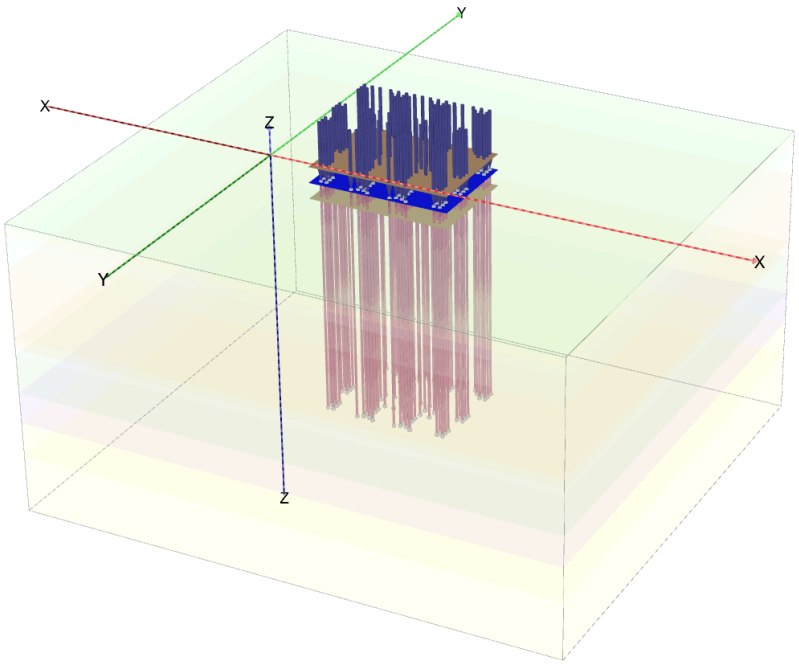

Figure 7.5: Plaxis 3D simplified model of POST Rotterdam.

Spring stiffnesses were also calculated for the piles conforming groups 1 and 2, as shown in Tables 7.3 and 7.4, respectively.

Table 7.3: Calculation of spring stiffnesses of the piles of group 1 using a simplified model.

Pile	Displacement (mm)		Spring stiffness (MN/m)	
	Short term	Long term	Short term	Long term
Pile 14	70.21	74.36	99.70	94.14
Pile 15	67.17	71.36	104.21	98.09
Pile 16	63.82	68.25	109.68	102.56
Pile 30	69.33	73.34	100.97	95.45
Pile 31	67.15	71.23	104.24	98.27
Pile 32	67.90	71.95	103.09	97.29
Pile 41	67.90	71.95	103.09	97.29
Pile 42	65.94	70.14	106.16	99.80

Table 7.4: Calculation of spring stiffnesses of the piles of group 2 using a simplified model.

Pile	Displacement (mm)		Springs (MN/m)	
	Short term	Long term	Short term	Long term
Pile 89	66.92	70.67	104.60	99.05
Pile 90	65.56	69.42	106.77	100.84
Pile 97	66.92	70.67	104.60	99.05
Pile 98	64.14	68.11	109.14	102.77
Pile 105	63.87	67.94	109.60	103.03
Pile 106	62.60	66.77	111.82	104.84

In the simplified model, the loads are directly transferred to the foundation without affecting the surrounding soil, resulting in more pronounced displacement. Likewise, in the model that includes the entire structure, the loads are distributed throughout it, requiring less pile displacement to mobilise forces. In either case, both models show smaller spring stiffness values than those calculated with a single pile, suggesting a higher overall pile displacement.

The settlement profile of the area was also obtained with the simplified model, as presented in Figure 7.6.

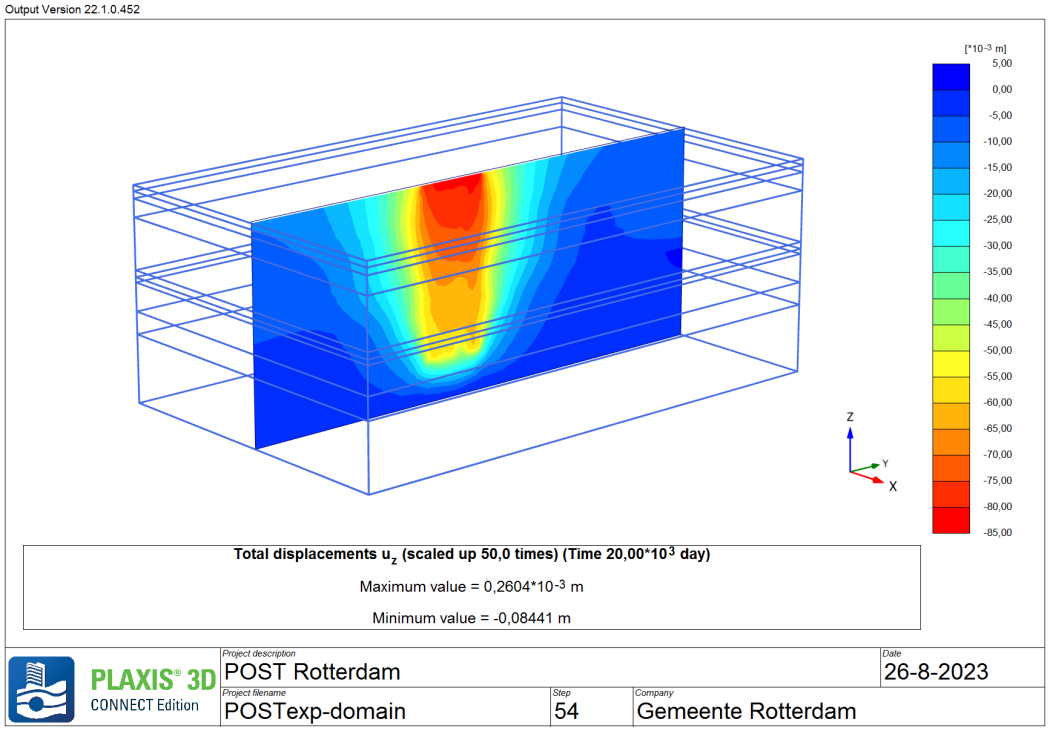

Figure 7.6: Settlement profile of Plaxis 3D simplified model of POST Rotterdam.

According to the latter, a maximum settlement of 8.4 cm in 50 years is calculated, which is higher than the 6.4 cm obtained with the detailed model. At the location of the Old Post Office, a maximum differential settlement of 35 mm over 10 m is expected. With this estimation, an angular distortion of 1/285 is obtained. Likewise, for the Timmerhuis building a

differential settlement of 12 mm over 10 m was calculated (angular distortion of 1/800). A stiffer foundation results in less settlements of a high-rise building structure.

As aforementioned, in practice calculations are not reported this way; the building stiffness is not commonly included in the geotechnical model, as it tends to be assessed by structural engineering. However, new methods have been investigated to model the building as an infinitely stiff plate, effectively integrating geotechnical and structural models into a unified calculation (Hartman, 2023). The calculations hereby presented have the purpose of analysing the SSI behaviour of different piles within the same pile groups, which could be further verified by monitoring measurements, even if in practice it is not commonly reported in this way.

7.6. Sensitivity of the stiffness of the Kedichem clay layers

From Chapter 4, it was seen that the Kedichem clay stiffness is the uncertain parameter that has a higher influence on the SSI of a single pile. In this section, the stiffness and creep parameters are varied in the whole model, considering $\pm$ 30% of the chosen values, with the aim of evaluating their effect in the area surrounding the POST Rotterdam. The different parameters are presented in Table 7.5.

Table 7.5: Variations of the stiffness and creep parameters of the Kedichem clay.

Stiffness	κ^* (-)	λ^* (-)	μ^* (-)
Standard	0.01112	0.03331	0.00135
Higher	0.00778	0.02332	0.00094
Lower	0.01445	0.04330	0.00175

The effects of settlements in 50 years are evaluated at -18 m NAP, since that is the pile tip level of the adjacent structures (Schippers and Broekens, 2021) that will be affected by the high-rise building. Results are shown in Figures 7.7, 7.8 and 7.9 for the standard, higher, and lower stiffness parameters, respectively. When comparing Figure 7.7 and Figure 7.8, it can be seen the maximum soil settlement reduces by 0.7% if a stiffer clay is considered. Likewise, the maximum settlement increases by 5% if a softer material is input. With this, it is possible to observe that for the complete model, the stiffness variations of the Kedichem clay do not have as much impact on the settlement calculation of the building area, as they do for the single pile analysis, and that an adequate parameter choice was made for the development of this study.

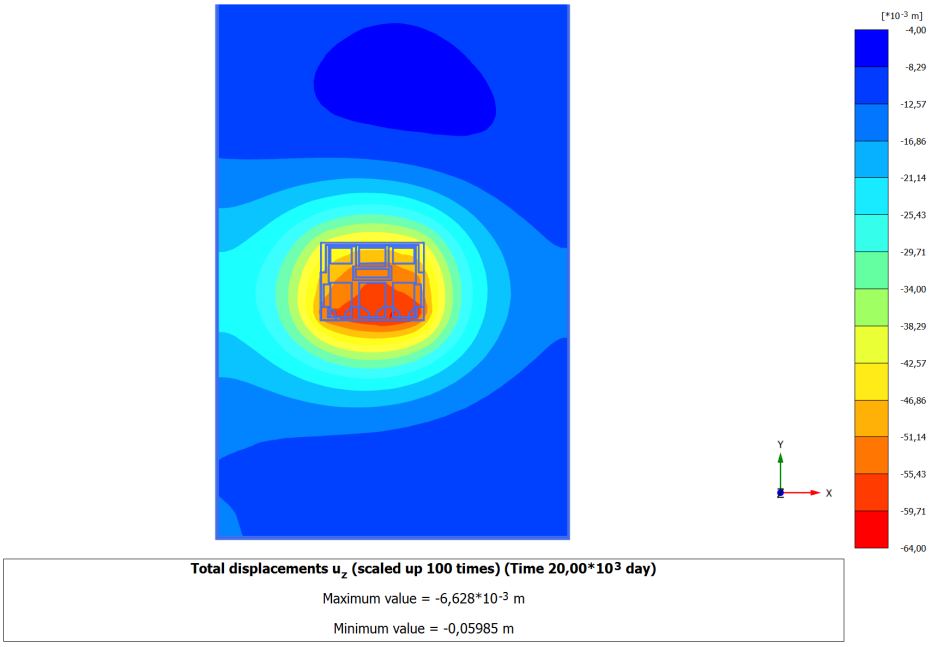

Figure 7.7: Settlement profile of Plaxis 3D detailed model of POST Rotterdam, with standard stiffness.

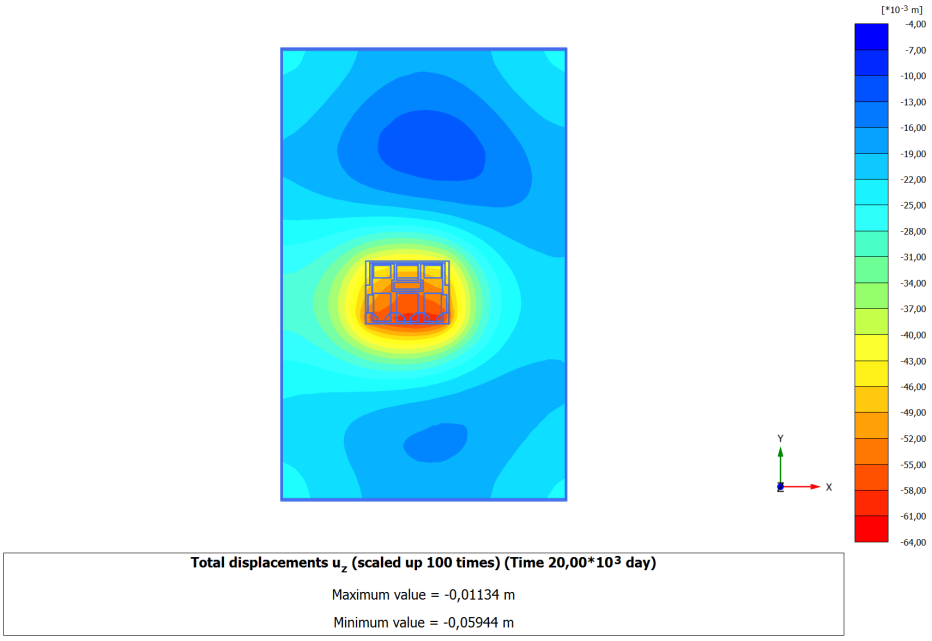

Figure 7.8: Settlement profile of Plaxis 3D detailed model of POST Rotterdam, with higher stiffness.

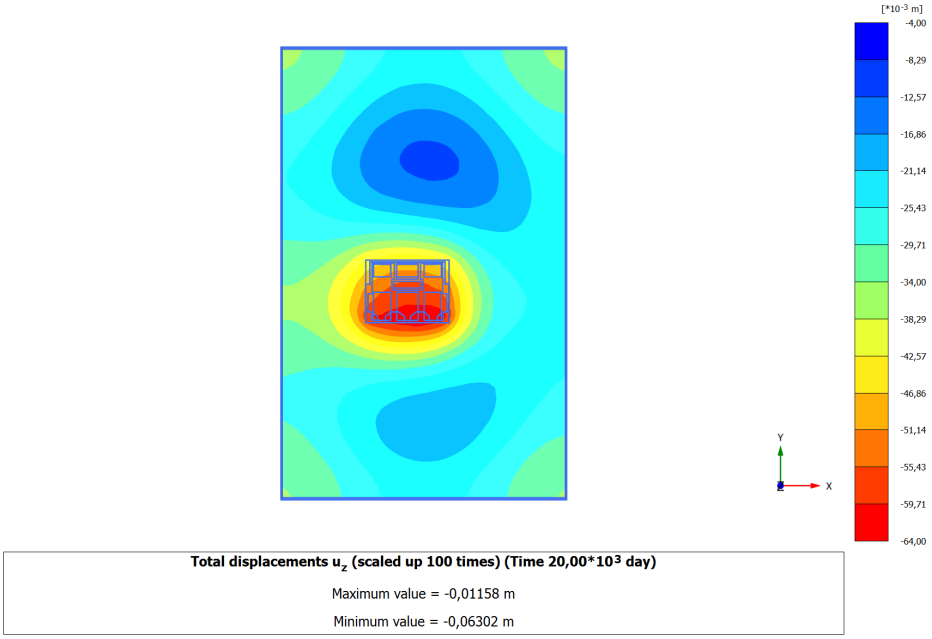

Figure 7.9: Settlement profile of Plaxis 3D detailed model of POST Rotterdam, with lower stiffness.

8

Conclusions and recommendations

8.1. Conclusions

This thesis addressed the SSI behaviour of foundation engineering for high-rise buildings. The main focus was to study load distribution along 60 m long piles subjected to gradual loading, considering the construction of the POST Rotterdam high-rise building as the study project. The key findings can be summarized as follows:

First, during the initial phases, most of the resistance contribution comes from the shaft, particularly evident at the Pleistocene sand layer, while the deeper dense sands barely mobilise any shaft and tip force. Gradual loading observations from the POST construction site corroborate this behaviour, demonstrating the shaft's dominance during this stage. However, as loading progresses and the Kedichem clay layer consolidates, a noticeable shift in load distribution appears, in which significant resistance quickly mobilises at the bottom of the pile. This occurs because, when the Kedichem clay layer starts consolidating, settlements occur in all the layers on top of it. Therefore, when the Pleistocene sand layer settles, its capability to mobilise shaft resistance is limited and resistance has to be developed at the deeper sands, as stated by Schippers et al. (2021) and Schippers and Broekens (2021). The latter answers the first research question, on how soil is distributed in very long piles, in the short and long term, considering Rotterdam's soil profile.

Second, uncertain parameters impacting SSI modelling include Kedichem clay stiffness and creep, affecting axial force distribution and pile displacement. Additional parameters, including the stiffness of the Holocene clay layer, shaft α_s factors for sand layers, pile diameter, and pile stiffness, exert secondary influences on the results.

Third, FO strain measurements were taken from POST Rotterdam foundation piles. Readings indicated cable resilience despite manipulation and work activities. While the strain measurements follow a similar trend to the site stratigraphy, there is high uncertainty about the results at early load stages. For instance, readings exhibit high tension jumps, and axial force development at the bottom of the pile shows, which was expected to be negligible at this stage.

While the reason is currently uncertain, hypotheses include the following:

- Tension readings are a consequence of some construction procedure, i.e. the curing effects during the casting of the basement slab, non-uniform concrete curing of the pile throughout its entire length, or uplift of the basement slab after pumping stopped.
- Misalignment from the centre of the pile and thus bending strains are introduced in the readings.
- Pile tension at the top due to the unloading from the excavation since the structural load at the moment is very small.
- Structure load is small and therefore is currently being carried by the slab.

Opportunities for site enhancement are given as future recommendations.

Fourth, EBR layer-dependent piles were provisionally chosen to model the foundation of the entire POST building. The analyses of corner pile group spring stiffness reveal the significance of the group effect in both cases. In practice, piles are generally incorporated into the structural model as single springs (Hartman, 2023), and the difference in displacement between the single spring models and the foundation of the whole building is dealt with in the structural design. Nevertheless, the calculations hereby presented have the purpose of being further verified by monitoring measurements.

Fifth, the impacts of POST loads on neighbouring structures were evaluated over 20,000 days. At the Old Post Office side, a maximum differential settlement of 18 mm over 10 m is calculated (1/555), while the Timmerhuis building shows a maximum differential settlement of 7 mm in 10 m (1/1428). For this case, this angular distortion indicates slight damage in the structure, however, these calculations may be taken as a lower limit of differential settlements, as the stiffness of the surrounding buildings (Schippers and Broekens, 2021; Prosperi et al., 2023; Hartman, 2023) was not considered in the model.

Moreover, modelling a stiffer foundation results in fewer settlements of the high-rise building structure. Although in practice, the building stiffness is not included in the geotechnical model but is incorporated in the structural model, new methods have been investigated to integrate geotechnical and structural models into a unified calculation (Hartman, 2023). Opportunities for model verification are given as future recommendations.

Nevertheless, the calculations hereby presented have the purpose of being further verified by monitoring measurements. Opportunities for model verification are given as future recommendations.

Finally, the stiffness and creep variations of the Kedichem clay do not have as much impact on the settlement calculation of the building area, as they do for the single pile analysis. An adequate parameter choice was made for the development of this study.

8.2. Recommendations

A list of recommendations for modelling, instrumentation practice and future research is shown below.

Modelling

1. Single pile and pile group verification: As highlighted by this research, variations between single pile and pile group behaviour underscore the need to validate both scenarios independently. The different responses can lead to discrepancies if not considered appropriately.
2. Model bottom boundary: In this analysis, the Plaxis 3D models extended to 15 m below the pile tip level, which is equivalent to 19D of the design pile. This length is considerably longer than the 4D specified by the NEN 9997-1 (2017), however, there is still uncertainty about the effect of this distance on the pile displacement and soil settlement results.
3. Alternative modelling approaches: Exploring other software tools and modelling methodologies other than Plaxis 3D, could provide alternative insights into the load distribution of very long piles.
4. Block foundation: In this research, the possibility of modelling the foundation as an infinitely rigid block, instead of individual piles, was not explored. While this approach cannot be verified by means of the instrumented piles on site, it could define an upper limit on the expected SSI behaviour in the future. It must be noted that for this analysis results are essential to carry out a sensitivity analysis on the model background, as mentioned above.

Site instrumentation and data processing

1. Instrumentation quality: Ensuring the acquisition of high-quality FO measurements onsite is important for accurate data interpretation. As the FO cables are susceptible to site activities, careful handling and minimal interference are vital. Likewise, having the possibility of measuring temperature with the FO cables could provide more accurate data and insights into behaviour.
2. Additional instruments: In this case study, only load-transfer instrumentation was available. Furthermore, installing strain gauges on the piles would provide valuable information about the pile displacement.
3. Site measurements: Areas of improvement include more control of the site schedule. A real project is harder to coordinate as it is highly dependent on the site construction schedule. Better coordination would have led to acquiring more quality data, significant to this investigation. Likewise, the possibility of accessing remotely to FO readings in the future will ease the measuring/schedule conflicts.
4. For future instrumentation of high-rise buildings with FO, it would be beneficial to consider the installation of FO both in the middle pile and the edge pile in order to further study the group effects and the springs of different piles.

Future research

1. To expand the scope of this work beyond static loads, dynamic wind loads could be integrated into the analysis, providing insights into the influence of high-rise building dynamics on pile behaviour. For the latter, it is recommended to wait until the high-rise building construction is finalised.
2. Further FO readings could resolve uncertainties and validate observations related to the current anomalies in measurements. At the moment, the gradual loading limits the pace of data collection, necessitating several years to validate any changes over time.
3. This case study may offer the possibility of verifying the newly integrated geotechnical and structural model (mattress model) in the future, by means of the site instrumentation. For the latter, waiting until the high-rise building construction is finalised is recommended.
4. A deeper understanding of the behaviour of Kedichem clay could be attained through a more extensive testing campaign and laboratory results.
5. With the Old Post Office's historical value in mind, as well as the cost of building damage, continued structural monitoring, either traditional or new air-borne methods, is essential to prevent significant damage from differential settlements.

8.3. Contributions and future impact

This study addresses gaps in understanding load distribution within very long piles, proposing a practical modelling approach and extending valuable recommendations and avenues for prospective investigation. As the use of very long piles becomes more prevalent in Rotterdam, this research contributes to the optimization of the design and enhancement of safety protocols. In summation, it contributes to the comprehension of load distribution in very long piles.

By implementing modern sensing techniques, such as FO, the stress distribution along the piles can be studied more accurately. In the future, along with extensive validation research, this study may contribute to the optimization and standardisation of the design of long-piled foundations in Rotterdam. Current approaches can be adjusted in order to make a less conservative design and more uniform criteria. This will result in a positive economic impact in the construction costs and safety of the high-rise building and the surroundings.

References

Arch Daily. (2023). Construction progress of POST Rotterdam. https://www.archdaily.com/981826/new-images-reveal-construction-progress-of-odas-post-rotterdam/627cd1773e4b31acb2000047-new-images-reveal-construction-progress-of-odas-post-rotterdam-photo?ad%7B%5C_%7Dmedium=widget%7B%5C&%7Dad%7B%5C_%7Dname=navigation-prev

Bica, A. V., Prezzi, M., Seo, H., Salgado, R., & Kim, D. (2014). Instrumentation and axial load testing of displacement piles. *Proceedings of the Institution of Civil Engineers: Geotechnical Engineering*, *167*(3), 238–252. https://doi.org/10.1680/geng.12.00080

Bilgen, M., & Günday, A. (2021). Phase BOTDR based Distributed Acoustic Sensing. *13th International Conference on Electrical and Electronics Engineering, ELECO 2021*, (December), 345–349. https://doi.org/10.23919/ELECO54474.2021.9677862

Bowles, J. (1997). *Foundation analysis and design* (5th ed.).

Brinkgreve, R. (2022a). *PLAXIS Manual (V22) [Software]*. (Plaxis BV). https://communities.bentley.com/products/geotech-analysis/w/wiki/46137/manuals---plaxis.

Brinkgreve, R. (2020). *Reader of MSc course CIE4361 Behaviour of Soils & Rocks [Reader]*. (tech. rep.). Delft University of Technology (TU Delft).

Brinkgreve, R. (2022b). Modelling piles and pile groups in FEM.

Chen, S. L., Chang, S. W., Qiu, Z. Y., Tang, C. W., Zhang, X. L., & Chen, Y. (2023). Numerical Model for Rectangular Pedestrian Underpass Excavations with Pipe-Roof Preconstruction Method: A Case Study. *Applied Sciences (Switzerland)*, *13*(5952). https://doi.org/10.3390/app13105952

de Battista, N., Kechavarzi, C., & Soga, K. (2016). Distributed fiber optic sensors for monitoring reinforced concrete piles using Brillouin scattering. *Sixth European Workshop on Optical Fibre Sensors*, *9916*, 1–4. https://doi.org/10.1117/12.2236633

Deltares. (2020). *D-Pile Group User Manual*.

Duffy, K., Gavin, K., Askarinejad, A., Korff, M., Lange, D. D., & Roubos, A. (2022). Field testing of axially loaded piles in dense sand. *Proceedings of the 20th International Conference on Soil Mechanics and Geotechnical Engineering*, 3253–3258.

Duffy, K., Gavin, K., Lange, D. D., & Korff, M. (2022). Residual stress measurement of driven precast piles using distributed fibre optic sensors. *11th International Stress Wave Conference*, 1–6. https://doi.org/10.5281/zenodo.7146663

Engin, H. K., & Brinkgreve, R. (2009). Investigation of pile behaviour using embedded piles. *Proceedings of the 17th International Conference on Soil Mechanics and Geotechnical Engineering: The Academia and Practice of Geotechnical Engineering*, *2*, 1189–1192. https://doi.org/10.3233/978-1-60750-031-5-1189

Frissen, M. (2020). *Determination of differential settlements of high-rise building foundations in soft soil conditions* (Doctoral dissertation). TU Delft.

Fundex Verstraeten BV. (2021). FUNDEX Expertise. http://www.fundex.nl/expertise/

Gavin, K., Kovacevic, M. S., & Igoe, D. (2021). A review of CPT based axial pile design in the Netherlands. *Underground Space*, *6*(1), 85–99. https://doi.org/10.1016/j.undsp.2019.09.004

Gemeente Rotterdam. (n.d.). *Oedometric tests performed in Rotterdam: Data base* (tech. rep.).

GEOSONDA. (2018). *Sax, Rotterdam* (tech. rep.).

Gilbert, R. I. (2013). Time-dependent stiffness of cracked reinforced and composite concrete slabs. *Procedia Engineering*, *57*, 19–34. https://doi.org/10.1016/j.proeng.2013.04.006

Gouw, T. L. (2014). Common mistakes on the application of plaxis 2D in analyzing excavation problems. *International Journal of Applied Engineering Research*, *9*(21), 8291–8311.

Güemes, A., Fernandez-Lopez, A., & Lozano, A. (2014). Fiber Optic Distributed Sensing. *STO-EN-AVT-220 Lecture Series*, 1–16.

Habitat, C. o. T. B., & Urban. (2023). Postkantoor Rotterdam. https://www.skyscrapercenter.com/building/postkantoor/8716

Hartman, I. (2023). *Soil-Structure Interaction Modelling of High-Rise Building Settlements due to Compressible Soil Layers below Foundation Level* (Doctoral dissertation). TU Delft. http://repository.tudelft.nl/.

Hoefsloot, F. J. M., & Wiersema, R. W. (2020). Evaluation and prediction of high-rise building settlements based on satellite data. *Geo Monitoring*, *24*(1), 79–91. https://doi.org/10.15488/9342

Hoogvliet, M., van de Ven, F., Buma, J., van Oostrom, N., Brolsma, R., Filatova, T., Verheijen, J., & Bosch, P. (2012). *Quick scan van beschikbaarheid schadegetallen en mogelijkheden om schades te bepalen* (tech. rep.). Deltares.

Ismail, A., Binti Siat Sirat, Q. A., Kassim, A. B., & Mohamad, H. B. (2019). Strain and temperature calibration of Brillouin Optical Time Domain Analysis (BOTDA) sensing system. *IOP Conference Series: Materials Science and Engineering*, *527*(1). https://doi.org/10.1088/1757-899X/527/1/012028

Kania, J., & Sorensen, K. K. (2020). Application of distributed fibre optic cables in piles. *Geotechnical Engineering Journal of the SEAGS & AGSSEA*, *51*(3), 1–9. https://www.researchgate.net/publication/339051388

Kausel, E. (2010). Early history of soil-structure interaction. *Soil Dynamics and Earthquake Engineering*, *30*(9), 822–832. https://doi.org/10.1016/j.soildyn.2009.11.001

Kechavarzi, C., Pelecanos, L., de Battista, N., & Soga, K. (2019). Distributed fibre optic sensing for monitoring reinforced concrete piles. *Geotechnical Engineering*, *50*(2), 43–51.

Kok, S., & Angelova, L. (2020). Impact droogte op funderingen. *Deltares rapport*. https://www.verzekeraars.nl/media/7875/20200930-rapport-impact-droogte-op-funderingen.pdf

Lunne, T., & Christoffersen, H. P. (1983). Interpretation of cone penetrometer data for offshore sands. *Proceedings of the 15th Annual Offshore Technology Conference*, 181–192. https://doi.org/10.4043/4464-ms

Matic, I., de Nijs, R., de Vos, M., & Roubos, A. A. (2019). Full-scale load testing on long prefabricated concrete piles in the Port of Rotterdam. *Proceedings of the XVII ECSMGE-2019: Geotechnical Engineering foundation of the future*.

Monsberger, C. M., Lienhart, W., & Hayden, M. (2020). Distributed fiber optic sensing along driven ductile piles: Design, sensor installation and monitoring benefits. *Journal of Civil Structural Health Monitoring*, *10*(4), 627–637. https://doi.org/10.1007/s13349-020-00406-3

MOS GRONDMECHANICA BV. (2016). *Grondonderzoek Zalmhaven te Rotterdam* (tech. rep. No. 0).

MOS GRONDMECHANICA B.V. (2022). A16 Noord: Laboratory tests.

NEN 9997-1. (2017). *Eurocode 7: Geotechnisch ontwerp van constructies - Deel 1: Algemene regels.*

Pieters Bouwtechniek. (2021). *Post Rotterdam High-rise: Palenplan op wekniveau* (tech. rep.).

POST. (2021). POST ROTTERDAM. https://www.postrotterdam.nl/

Poulos, H. G. (1968). Analysis of the settlement of pile groups. *Geotechnique*, *18*(4), 449–471. https://doi.org/10.1680/geot.1968.18.4.449

Prosperi, A., Korswagen, P. A., Korff, M., Schipper, R., & Rots, J. G. (2023). Empirical fragility and ROC curves for masonry buildings subjected to settlements. *Journal of Building Engineering*, *68*(January), 106094. https://doi.org/10.1016/j.jobe.2023.106094

Quattro Expertise BV. (2021). *Monitoring omgeving: Post Rotterdam* (tech. rep.). Quattro Expertise.

Rajapakse, R. (2016). 15 - Negative skin friction (downdrag). In *Pile design and construction rules of thumb (second edition)* (pp. 213–223). https://www.sciencedirect.com/science/article/pii/B9780128042021000152

Robbemont, A. J., & Janssen, B. (2018). *Post Rotterdam: CC3 toets definitief ontwerp* (tech. rep. september). https://www.postrotterdam.nl/

Schippers, R. J., Bijnagte, J., & van Tol em., A. F. (2021). Geotechnisch ontwerp van de Zalmhaven te Rotterdam (Deel 1). *GEOTECHNIEK SPECIAL 10 JAAR GEOBEST*, (September), 26–31.

Schippers, R. J., & Broekens, R. R. (2021). *Renovatie voormalig Postkantoor Rotterdam. Funderingadvies, zettingsbeschouwingen en bouwkuipadvies.* (tech. rep. november).

Schippers, R. J., & Broekens, R. R. (2022). Geotechnisch ontwerp van de Zalmhaven te Rotterdam (Deel 2). *GEOTECHNIEK*, (augustus 2021), 10–15.

Smulders, C. M., Hosseini, S., & Brinkgreve, R. (2019). Improved embedded beam with interaction surface. *17th European Conference on Soil Mechanics and Geotechnical Engineering, ECSMGE 2019*, *2019-Septe*. https://doi.org/10.32075/17ECSMGE-2019-0193

Ter Steege, F. B. (2022). *Screw and screw-injection piles: Classification of the load-settlement response and improving the design process* (Doctoral dissertation).

The POST Bouw. (2023). The POST construction news. https://www.thepostbouw.nl/nieuws/

Van den Born, G., Kragt, F., Henkens, D., Rijken, B., Van Bemmel, B., & Van der Sluis, S. (2016). Dalende bodems, stijgende kosten. *Planbureau voor de Leefomgeving: Rapportnummer 1064*, 96. https://www.pbl.nl/sites/default/files/downloads/pbl-2016-dalende-bodems-stijgende-kosten-1064.pdf

van Overstraten Kruijsse, F. C. M. (2019). *The installation effects of screwed displacement piles* (Doctoral dissertation). TU Delft. Delft. http://repository.tudelft.nl/.

van Dalen, J. H., van Dee, R. C., & Spruit, R. (2014). Interactieberekeningen Funderingselementen met het programma 'INTER'. *Geotechniek*, 28–33. www.ballast-nedam.nl

van Ravenzwaaij, J., Iten, M., Spruit, R., & de Boer, A. (2018). Geotechnical and structural applications of fiber-optic sensing. *High Tech Concrete: Where Technology and Engineering Meet - Proceedings of the 2017 fib Symposium*, *1*, 1287–1298. https://doi.org/10.1007/978-3-319-59471-2

Woestenburg, G. P. (2020). *High-Rise buildings on compressible soil* (Doctoral dissertation). TU Delft.

Zhang, D., Shi, B., Gui, H. L., & Xu, H. Z. (2004). Improvement of spatial resolution of Brillouin optical time domain reflectometer using spectral decomposition. *Optica Applicata*, *34*(2), 291–301.

A

Site investigation

Sondering 101

Opdracht	: 1703818	Conus nummer	: S15-CFII-1651	NEN-EN-ISO-22476-1	
Plaats	: Rotterdam	Soort conus	: Elektrisch	Klasse 3, type TE1	
Datum	: 26-02-2018	Opp. conuspunt	: 1500 mm^2	Sondeerunit	: SR2
Project	: Voormalig postkantoor			Blad	: 1 van 3

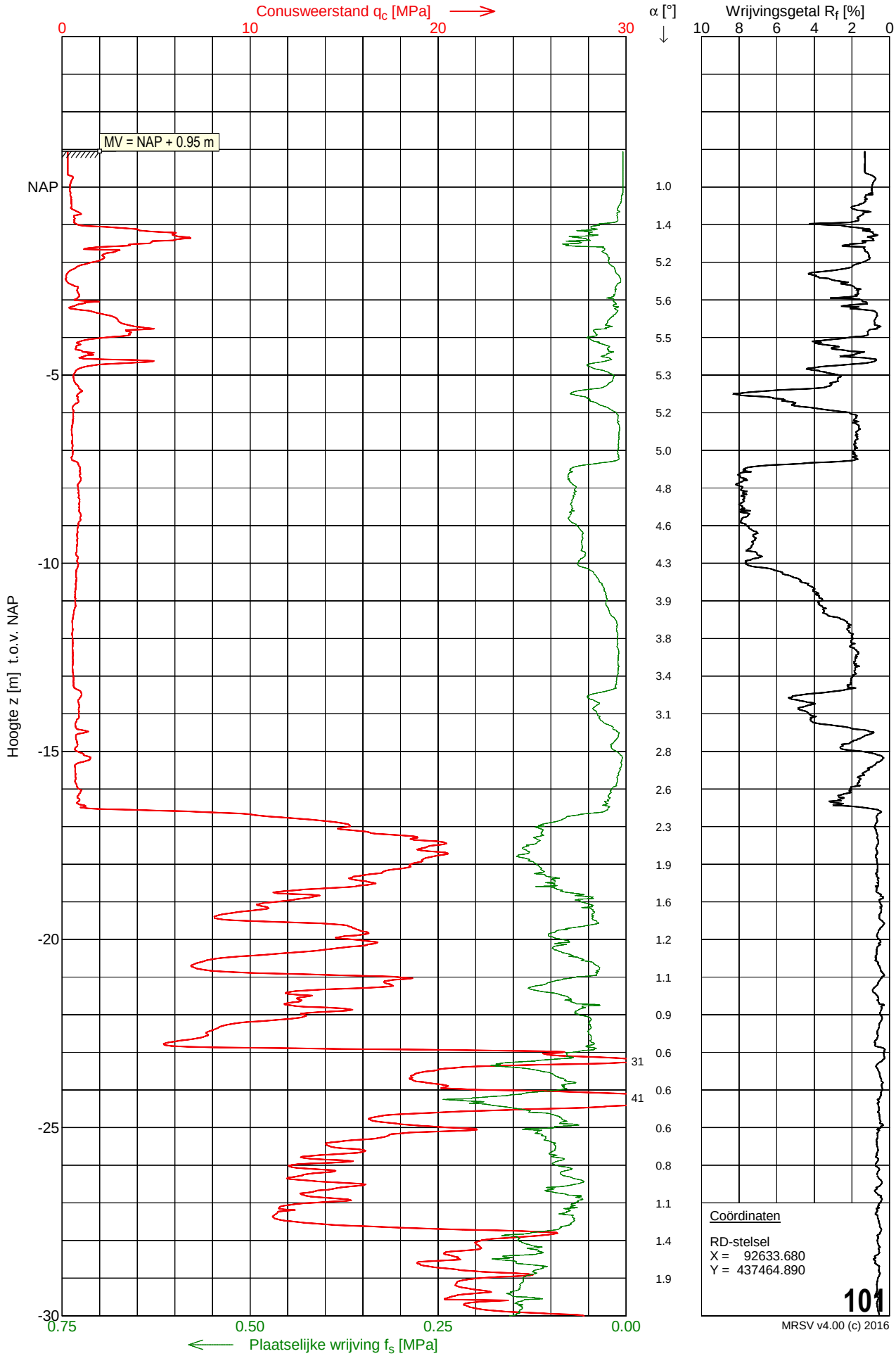

Sondering 101

Opdracht	: 1703818	Conus nummer	: S15-CFII-1651	NEN-EN-ISO-22476-1	
Plaats	: Rotterdam	Soort conus	: Elektrisch	Klasse 3, type TE1	
Datum	: 26-02-2018	Opp. conuspunt	: 1500 mm^2	Sondeerunit	: SR2
Project	: Voormalig postkantoor			Blad	: 2 van 3

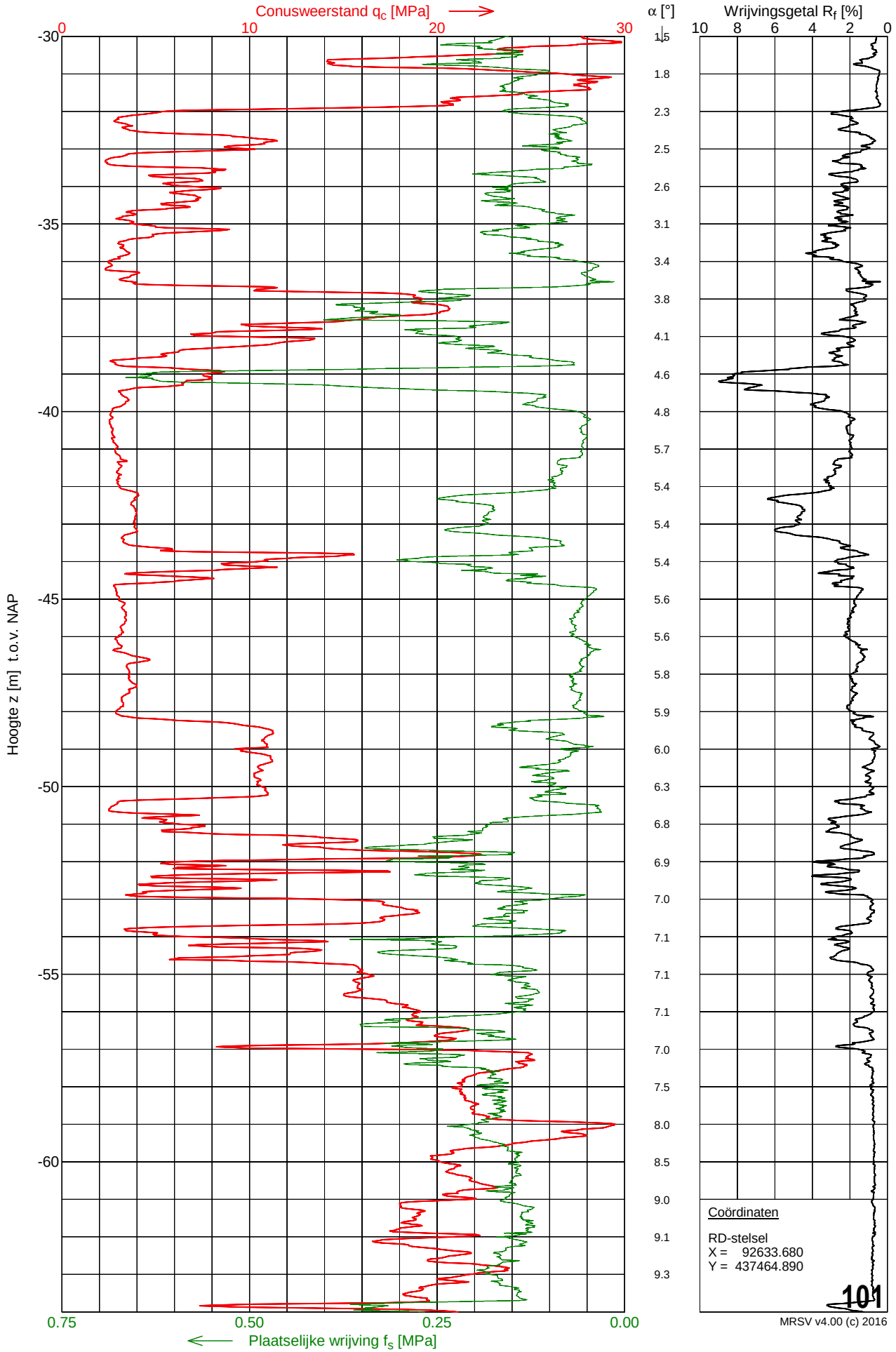

MRSV v4.00 (c) 2016

Sondering 101

Opdracht	: 1703818	Conus nummer	: S15-CFII-1651	NEN-EN-ISO-22476-1	
Plaats	: Rotterdam	Soort conus	: Elektrisch	Klasse 3, type TE1	
Datum	: 26-02-2018	Opp. conuspunt	: 1500 mm^2	Sondeerunit	: SR2
Project	: Voormalig postkantoor			Blad	: 3 van 3

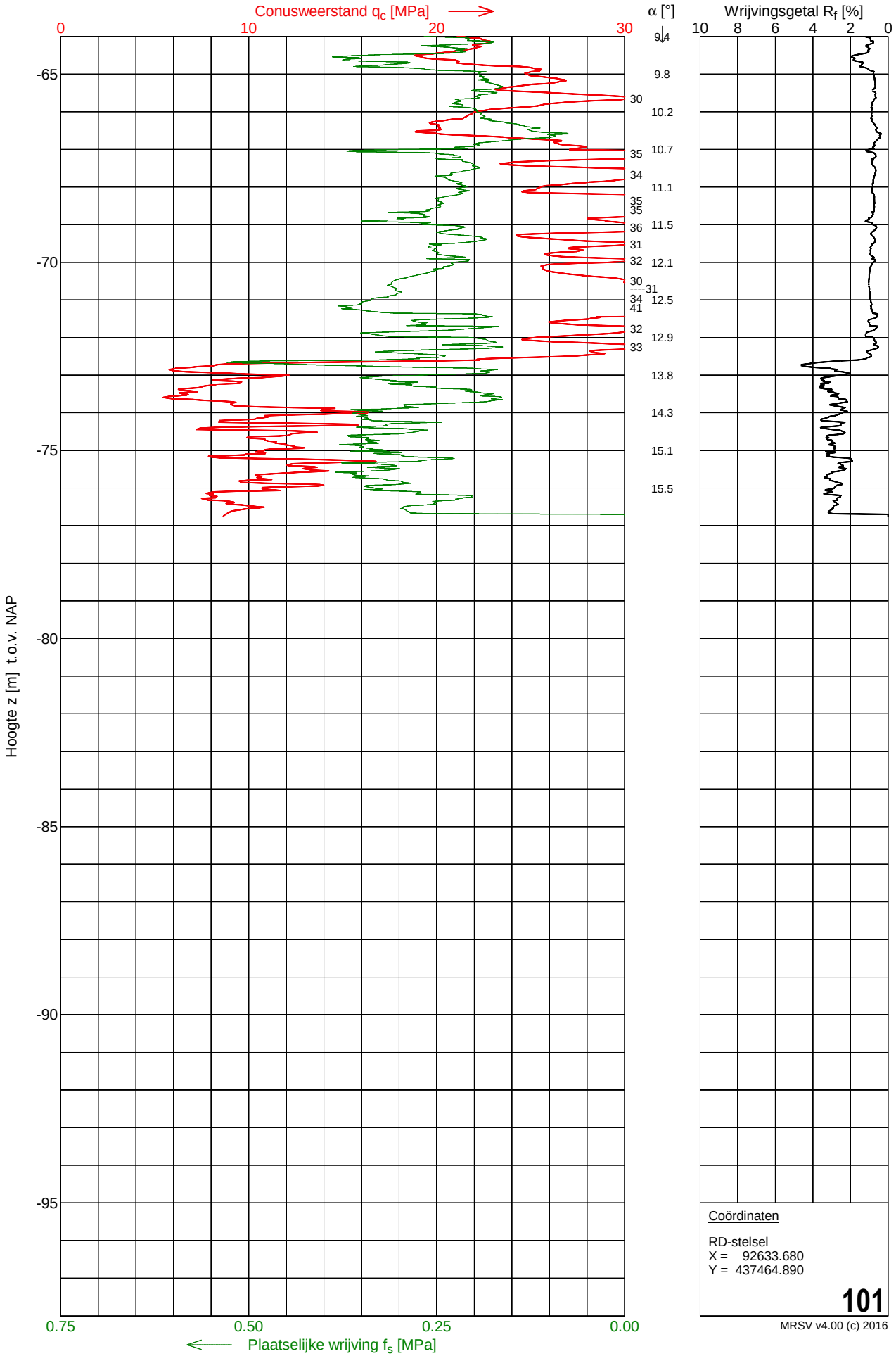

Sondering 102D

Opdracht	: 2100886	Conus nummer	: S15-CFII.1759	NEN-EN-ISO-22476-1	
Plaats	: Rotterdam	Soort conus	: Elektrisch	Klasse 3, type TE1	
Datum	: 08-09-2021	Opp. conuspunt	: 1500 mm^2	Sondeerunit	: SR2
Project	: Postoffice			Blad	: 1 van 3

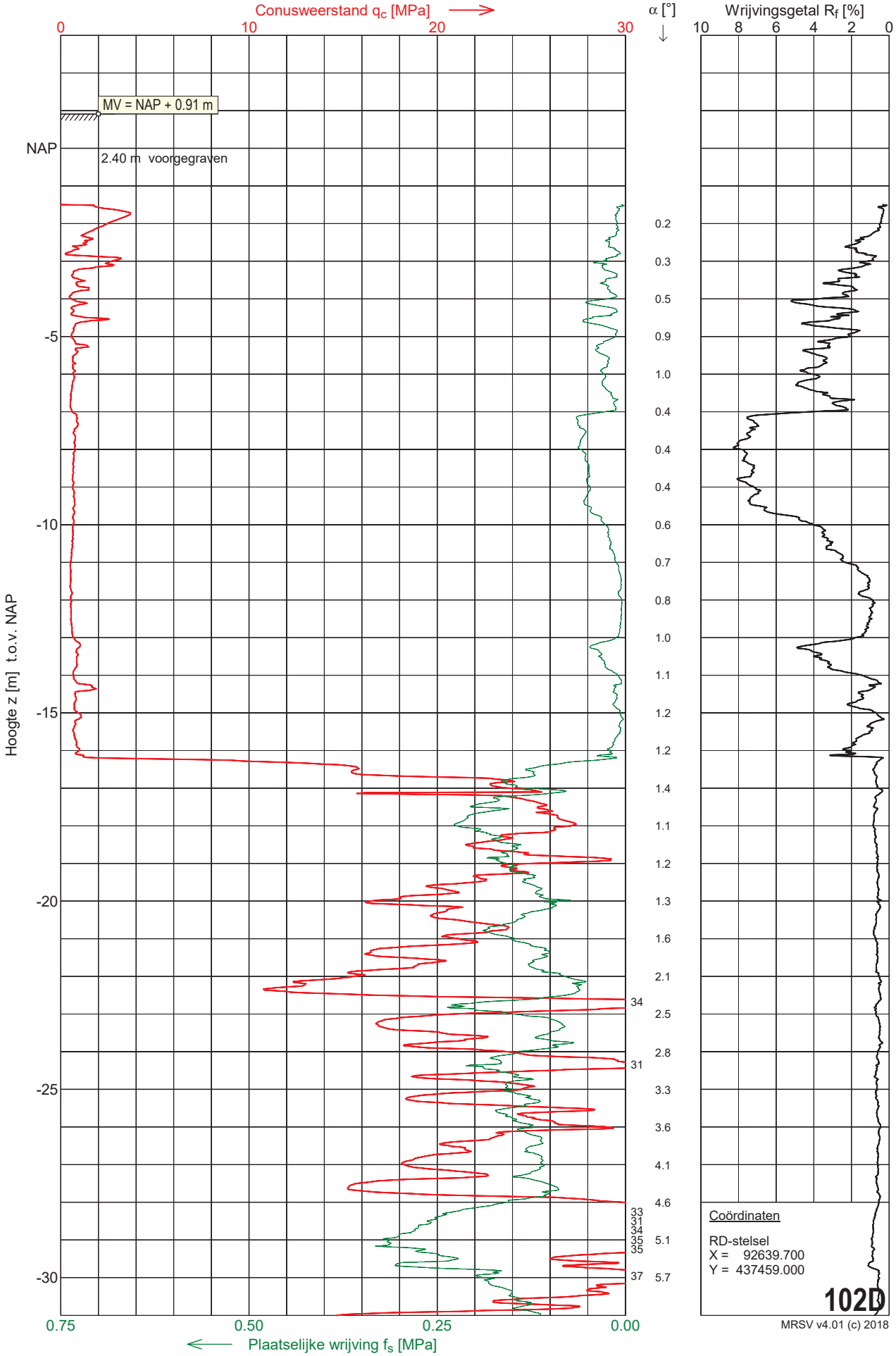

Sondering 102D

Opdracht	: 2100886	Conus nummer	: S15-CFII.1759	NEN-EN-ISO-22476-1	
Plaats	: Rotterdam	Soort conus	: Elektrisch	Klasse 3, type TE1	
Datum	: 08-09-2021	Opp. conuspunt	: 1500 mm^2	Sondeerunit	: SR2
Project	: Postoffice			Blad	: 2 van 3

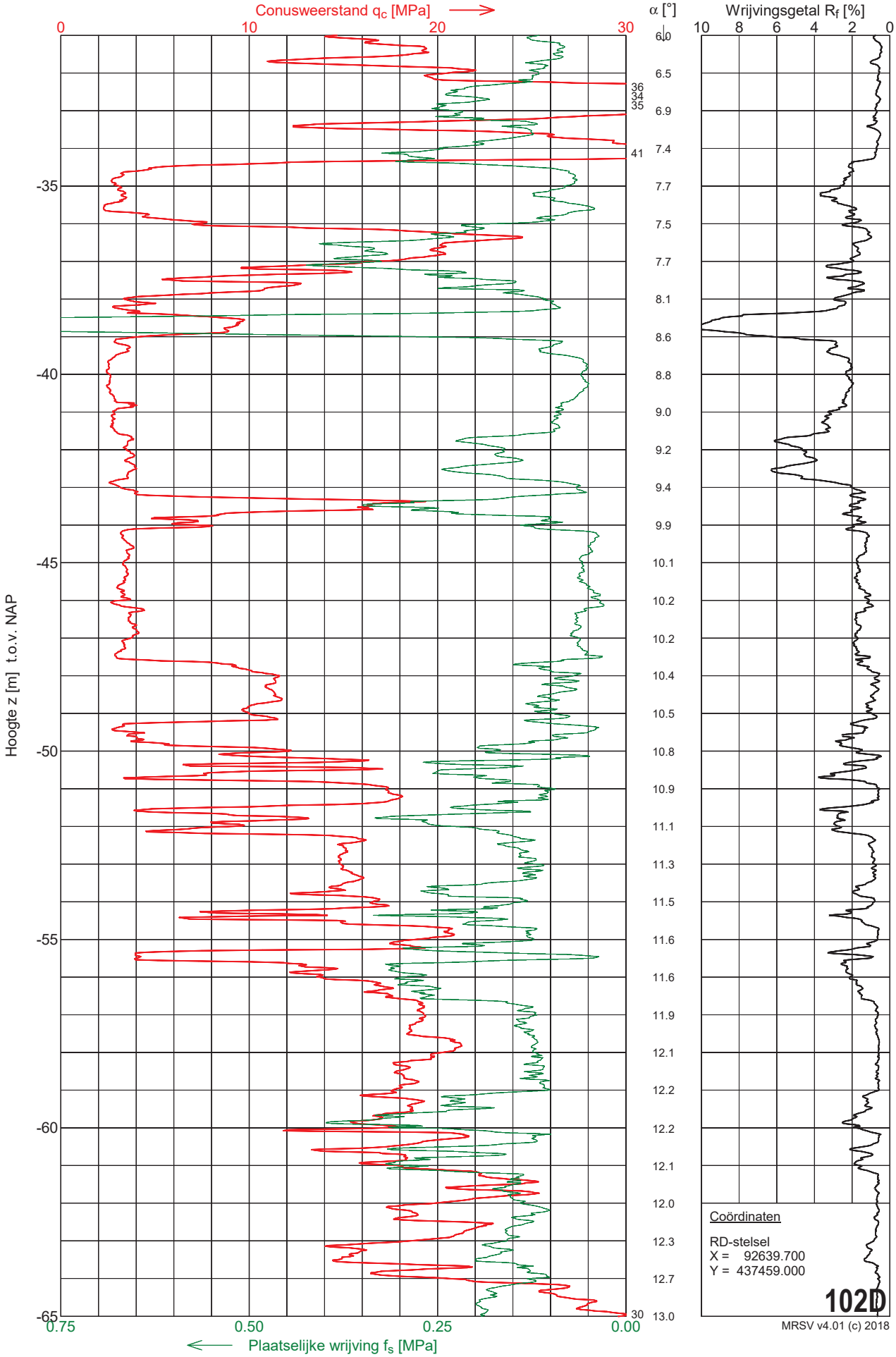

MOS GRONDMECHANICA

Sondering 102D

Opdracht	: 2100886	Conus nummer	: S15-CFII.1759	NEN-EN-ISO-22476-1	
Plaats	: Rotterdam	Soort conus	: Elektrisch	Klasse 3, type TE1	
Datum	: 08-09-2021	Opp. conuspunt	: 1500 mm^2	Sondeerunit	: SR2
Project	: Postoffice			Blad	: 3 van 3

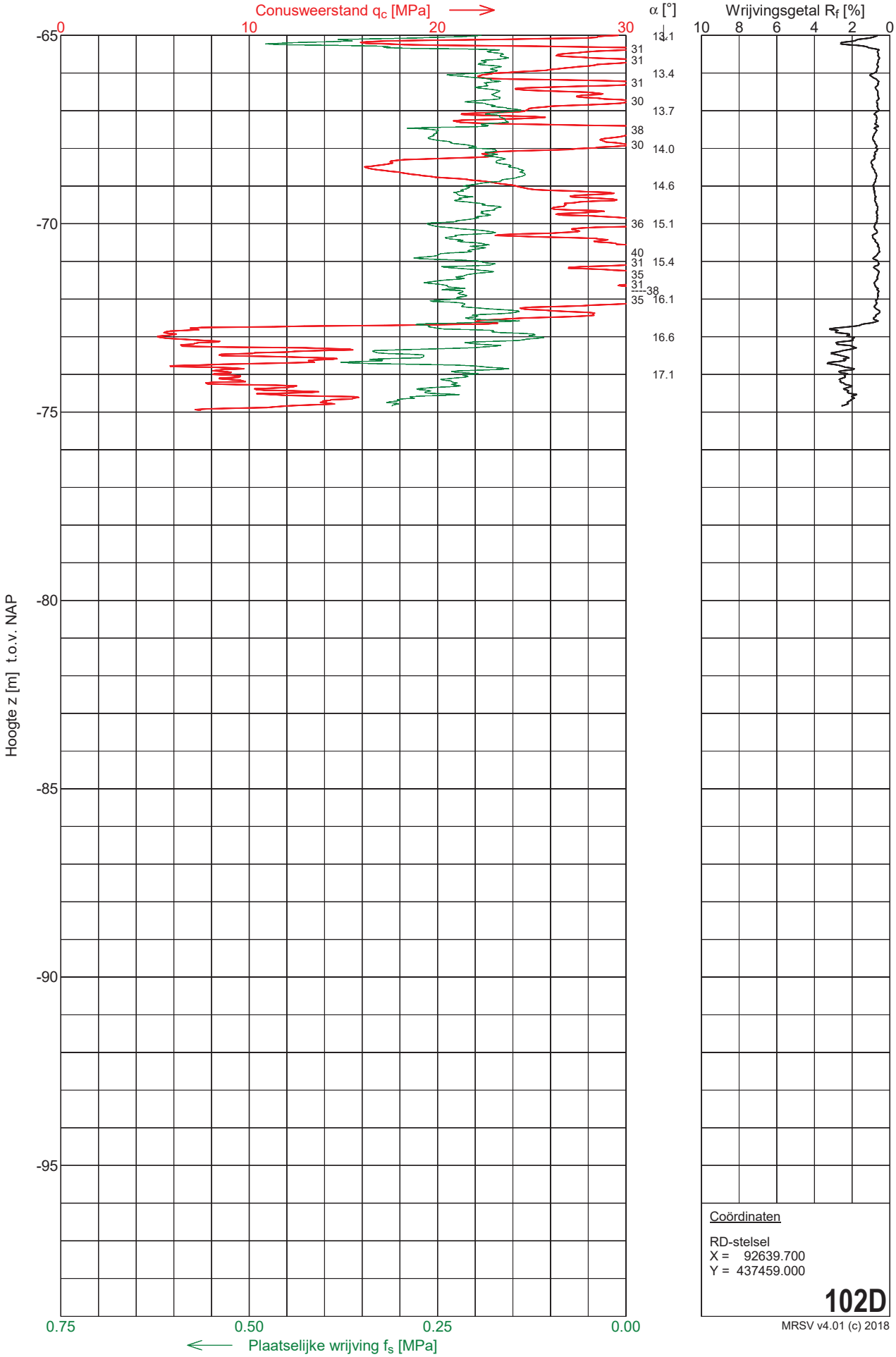

Coördinaten

RD-stelsel
X = 92639.700
Y = 437459.000

102D

MRSV v4.01 (c) 2018

Sondering 103

Opdracht	: 1703818	Conus nummer	: S15-CFII.1325	NEN-EN-ISO-22476-1	
Plaats	: Rotterdam	Soort conus	: Elektrisch	Klasse 3, type TE1	
Datum	: 27-02-2018	Opp. conuspunt	: 1500 mm^2	Sondeerunit	: SR2
Project	: Voormalig postkantoor			Blad	: 1 van 3

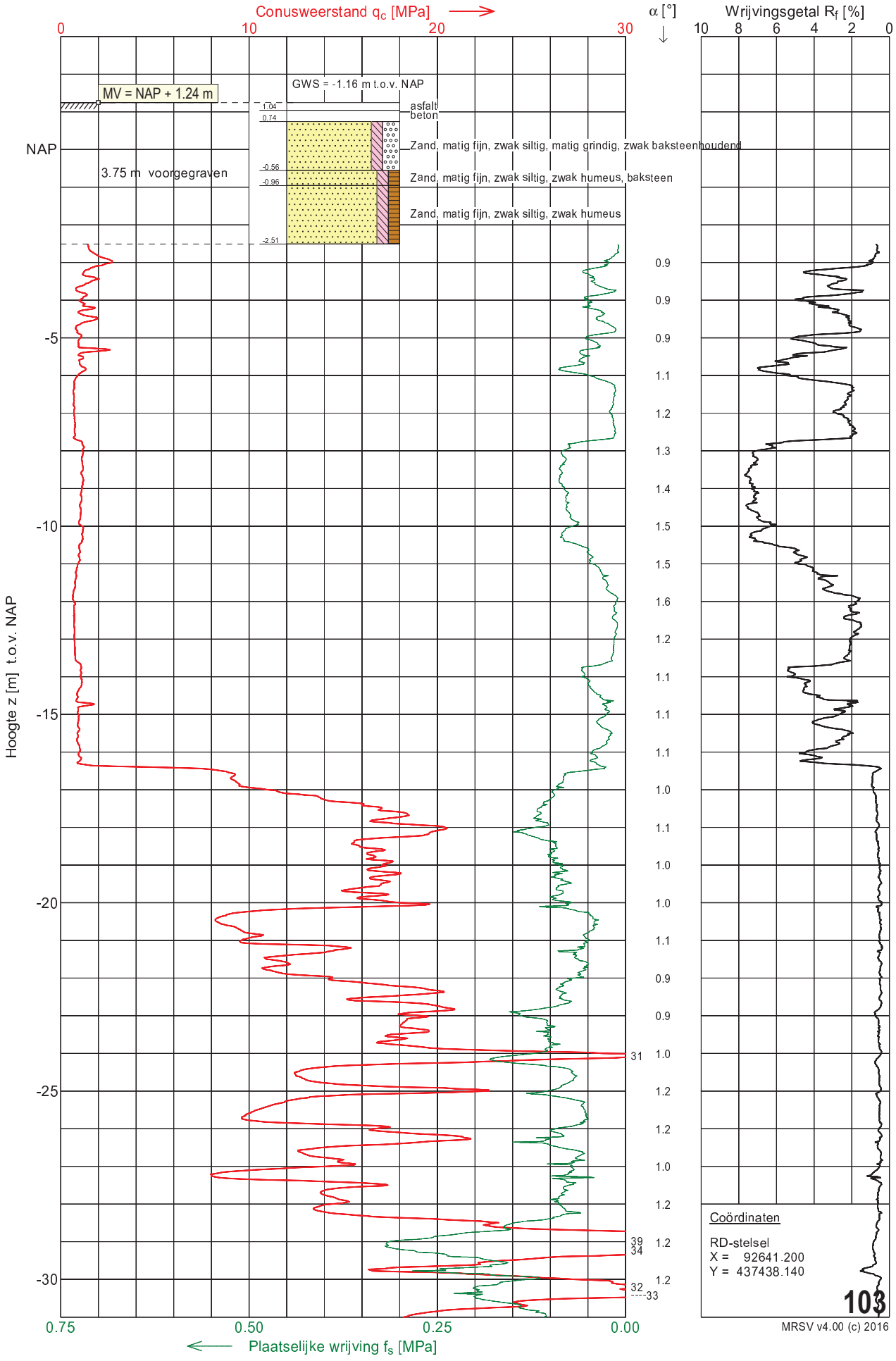

Sondering 103

Opdracht	: 1703818	Conus nummer	: S15-CFII.1325	NEN-EN-ISO-22476-1	
Plaats	: Rotterdam	Soort conus	: Elektrisch	Klasse 3, type TE1	
Datum	: 27-02-2018	Opp. conuspunt	: 1500 mm^2	Sondeerunit	: SR2
Project	: Voormalig postkantoor			Blad	: 2 van 3

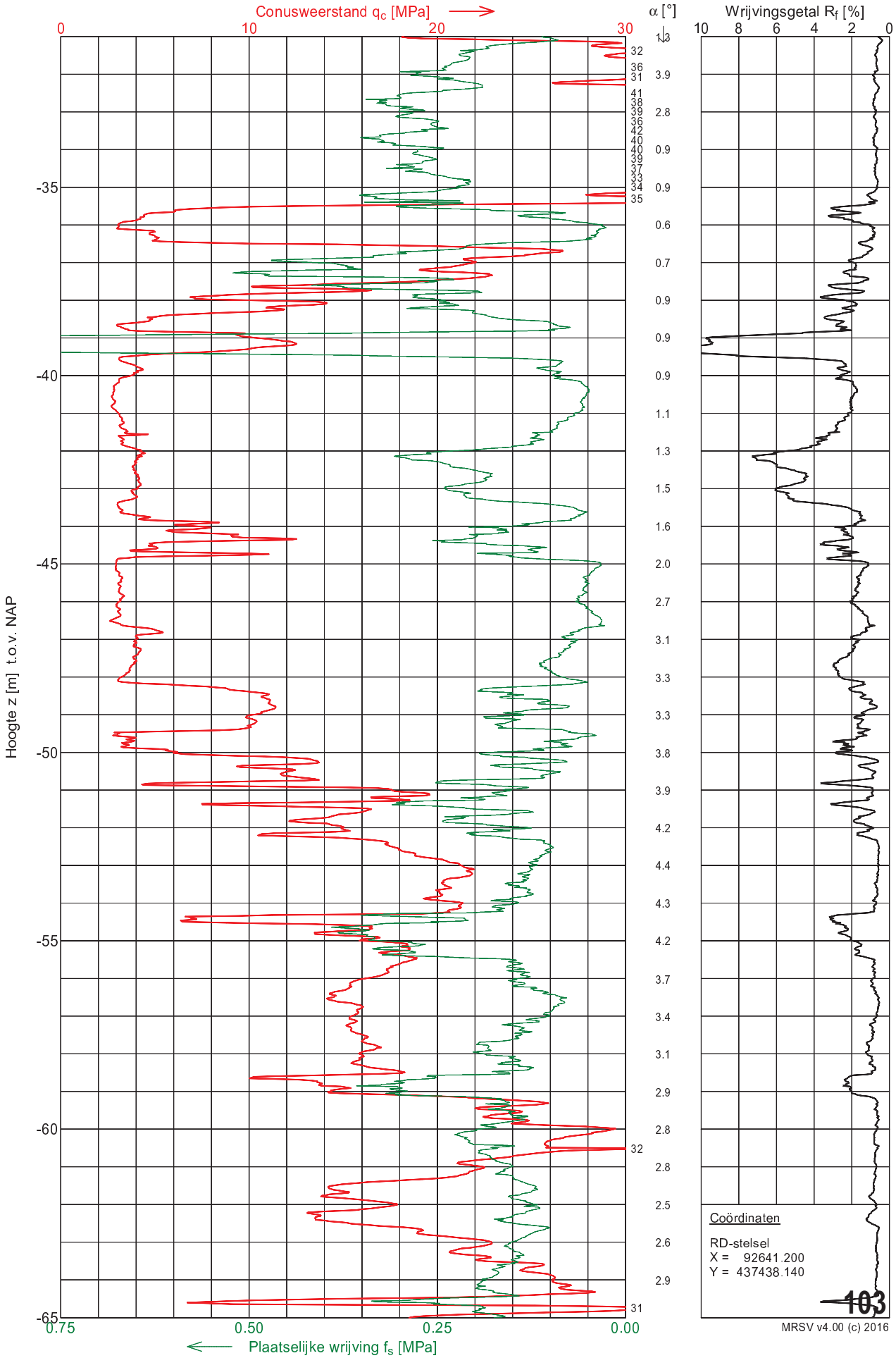

Sondering 103

Opdracht	: 1703818	Conus nummer	: S15-CFII.1325	NEN-EN-ISO-22476-1	
Plaats	: Rotterdam	Soort conus	: Elektrisch	Klasse 3, type TE1	
Datum	: 27-02-2018	Opp. conuspunt	: 1500 mm^2	Sondeerunit	: SR2
Project	: Voormalig postkantoor			Blad	: 3 van 3

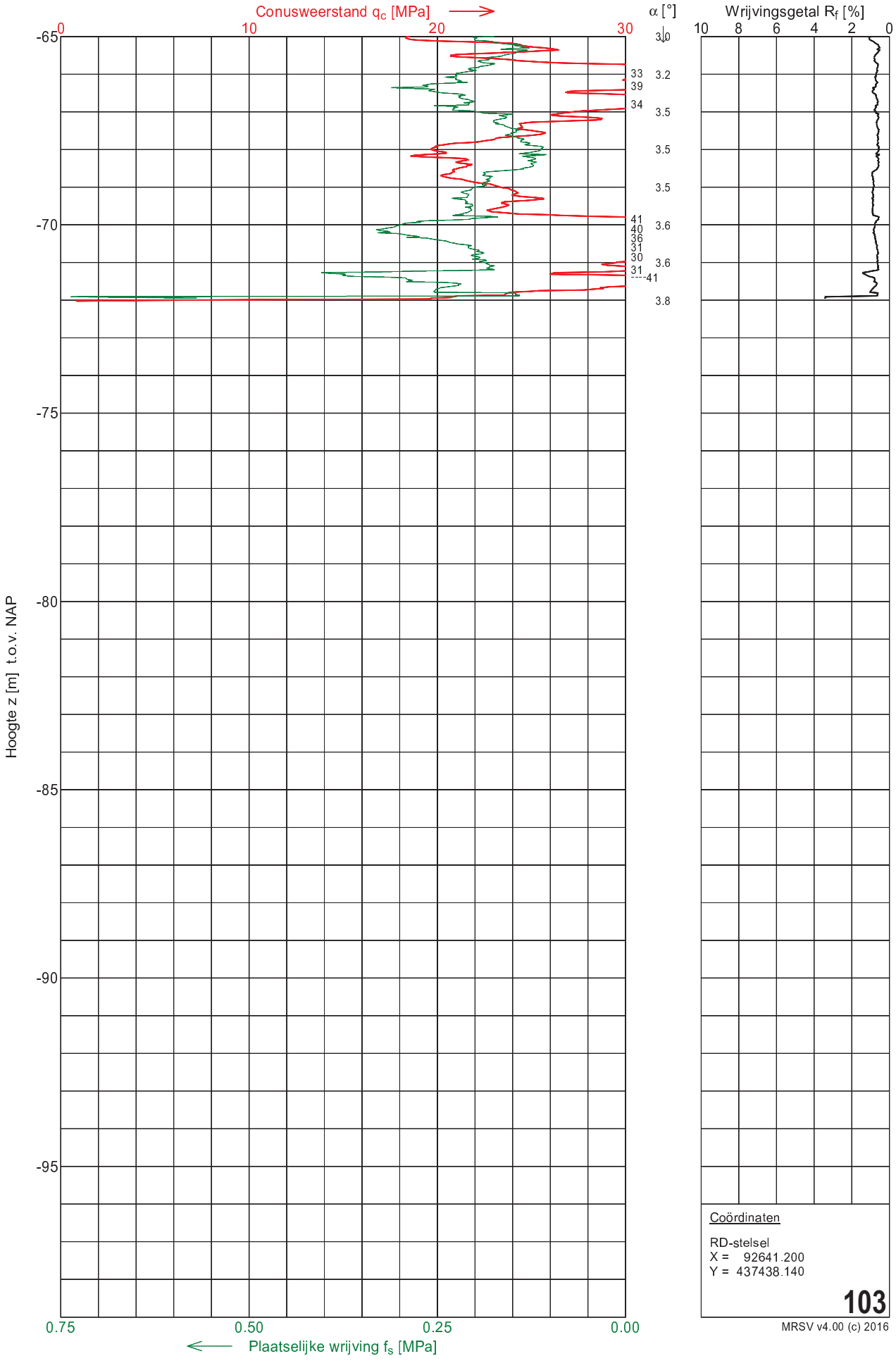

Coördinaten

RD-stelsel
X = 92641.200
Y = 437438.140

103

MRSV v4.00 (c) 2016

MOS GRONDMECHANICA

Sondering 204

Opdracht	: 2100886	Conus nummer	: S15-CFII.1970	NEN-EN-ISO-22476-1	
Plaats	: Rotterdam	Soort conus	: Elektrisch	Klasse 3, type TE1	
Datum	: 08-07-2021	Opp. conuspunt	: 1500 mm^2	Sondeerunit	: SW11
Project	: Postoffice			Blad	: 1 van 3

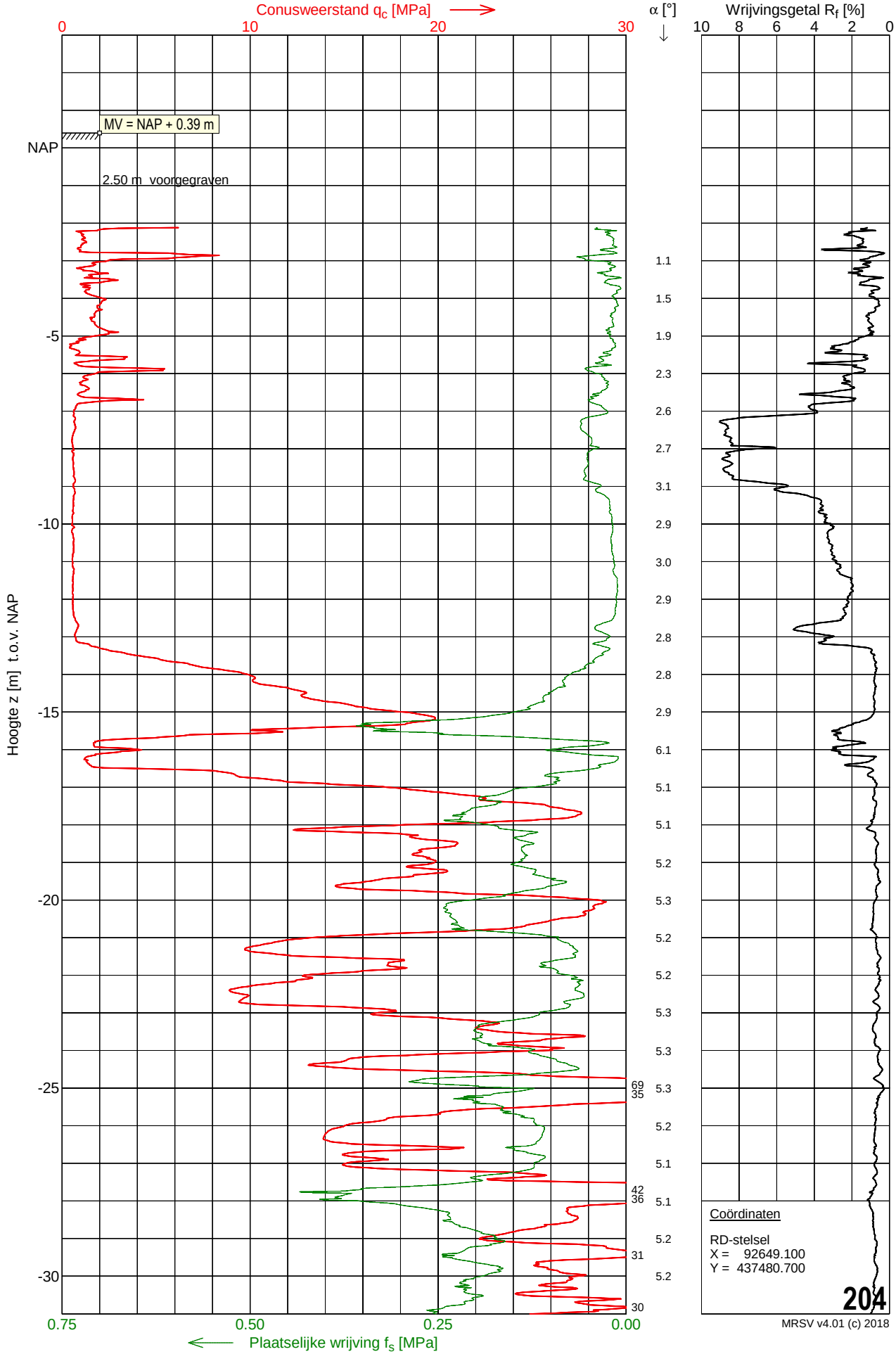

Sondering 204

Opdracht	: 2100886	Conus nummer	: S15-CFII.1970	NEN-EN-ISO-22476-1	
Plaats	: Rotterdam	Soort conus	: Elektrisch	Klasse 3, type TE1	
Datum	: 08-07-2021	Opp. conuspunt	: 1500 mm^2	Sondeerunit	: SW11
Project	: Postoffice			Blad	: 2 van 3

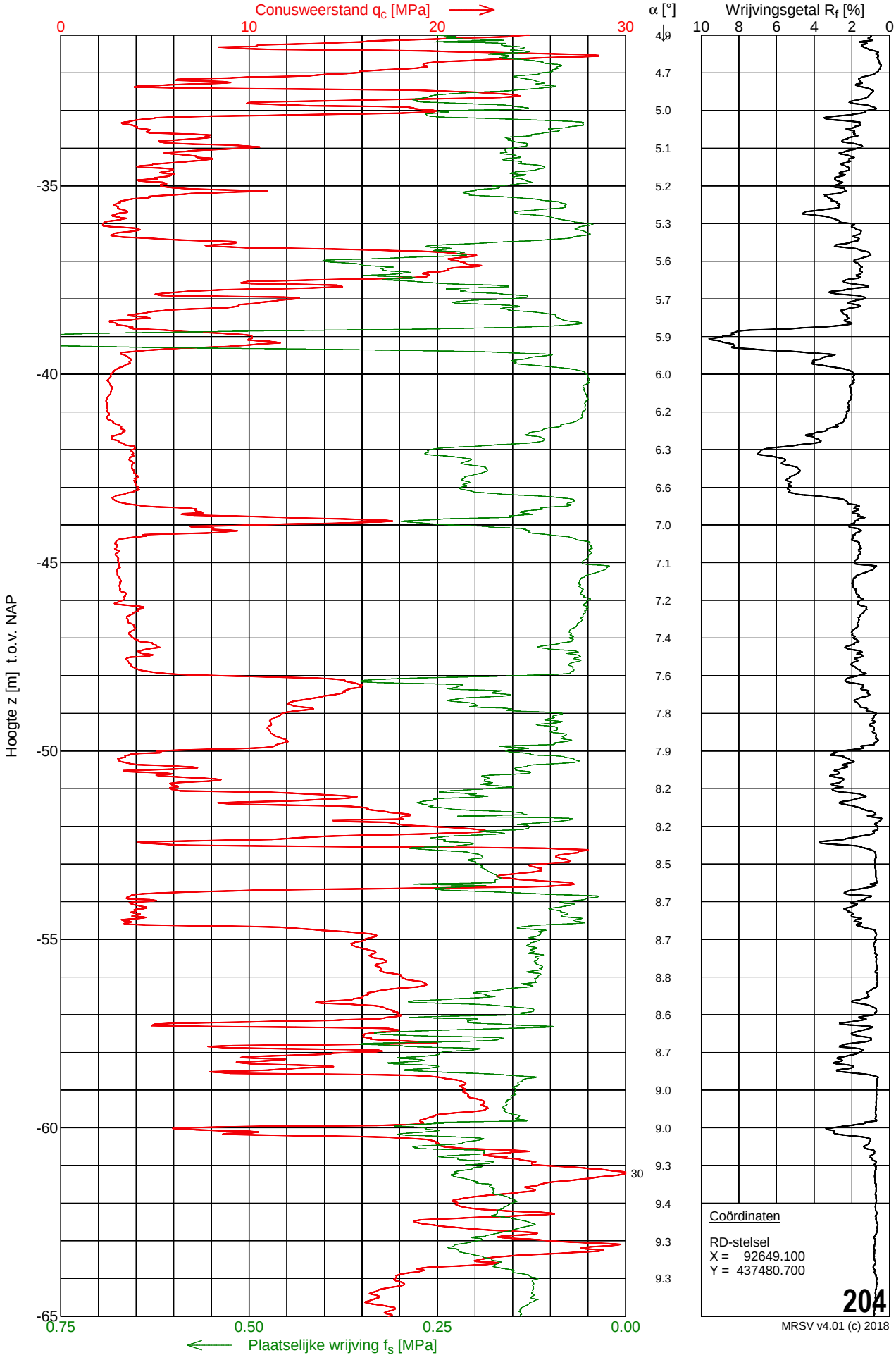

Sondering 204

Opdracht	: 2100886	Conus nummer	: S15-CFII.1970	NEN-EN-ISO-22476-1	
Plaats	: Rotterdam	Soort conus	: Elektrisch	Klasse 3, type TE1	
Datum	: 08-07-2021	Opp. conuspunt	: 1500 mm^2	Sondeerunit	: SW11
Project	: Postoffice			Blad	: 3 van 3

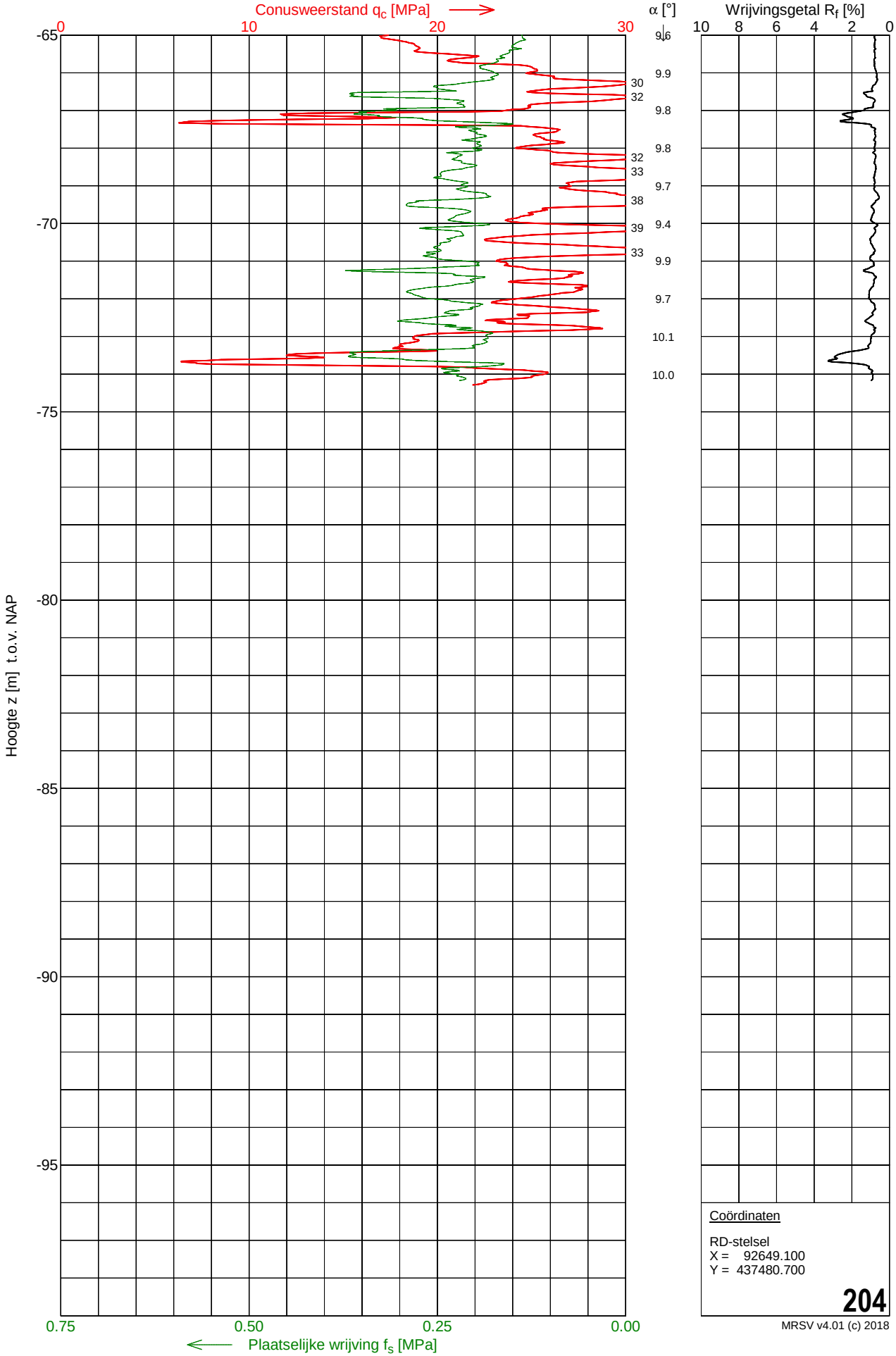

Coördinaten

RD-stelsel
X = 92649.100
Y = 437480.700

204

MRSV v4.01 (c) 2018

Sondering 305

Opdracht	: 2100886	Conus nummer	: S15-CFII.1759	NEN-EN-ISO-22476-1	
Plaats	: Rotterdam	Soort conus	: Elektrisch	Klasse 3, type TE1	
Datum	: 07-09-2021	Opp. conuspunt	: 1500 mm^2	Sondeerunit	: SR2
Project	: Postoffice			Blad	: 1 van 3

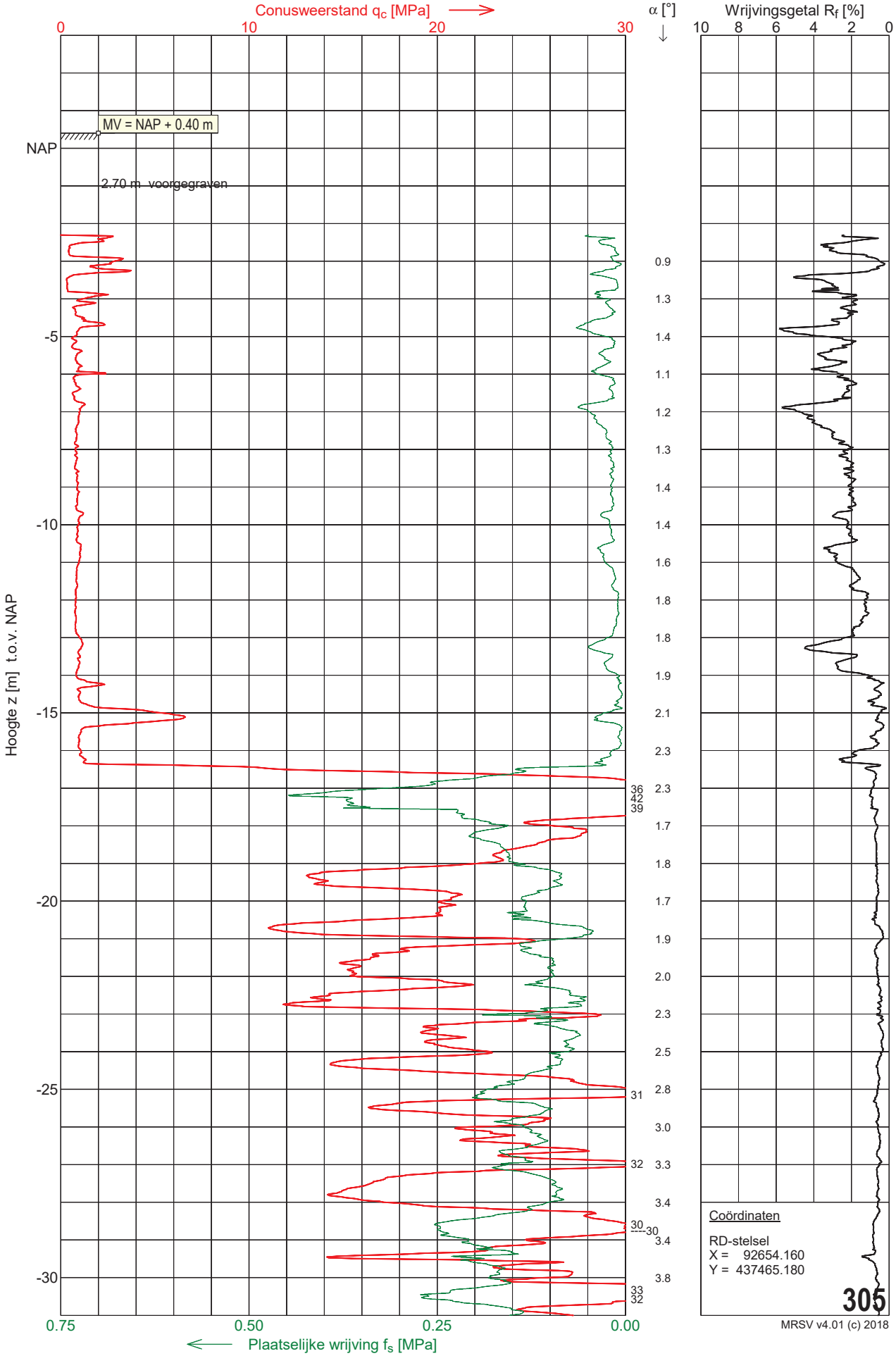

Sondering 305

Opdracht	: 2100886	Conus nummer	: S15-CFII.1759	NEN-EN-ISO-22476-1	
Plaats	: Rotterdam	Soort conus	: Elektrisch	Klasse 3, type TE1	
Datum	: 07-09-2021	Opp. conuspunt	: 1500 mm^2	Sondeerunit	: SR2
Project	: Postoffice			Blad	: 2 van 3

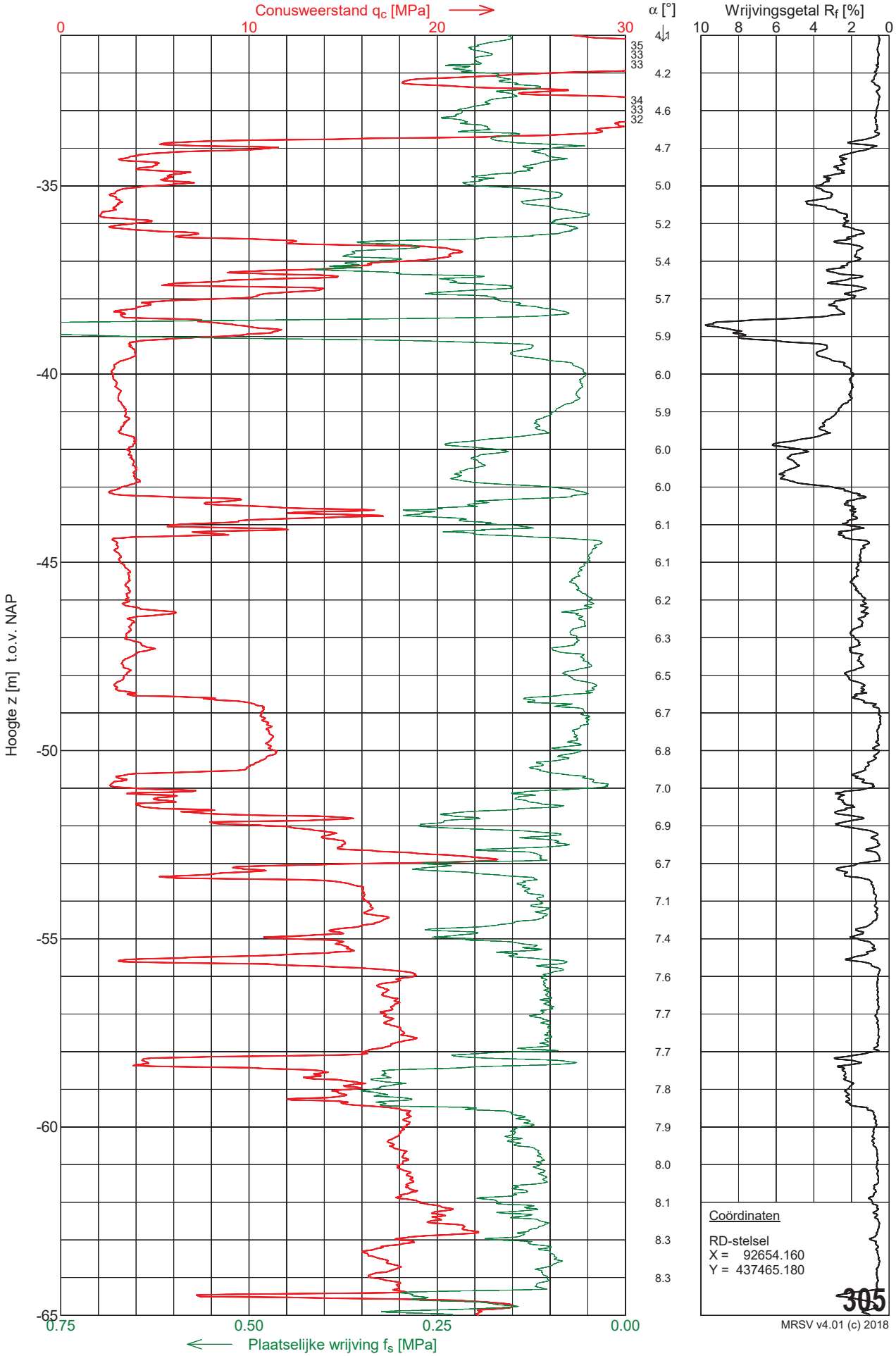

Sondering 305

Opdracht	: 2100886	Conus nummer	: S15-CFII.1759	NEN-EN-ISO-22476-1	
Plaats	: Rotterdam	Soort conus	: Elektrisch	Klasse 3, type TE1	
Datum	: 07-09-2021	Opp. conuspunt	: 1500 mm^2	Sondeerunit	: SR2
Project	: Postoffice			Blad	: 3 van 3

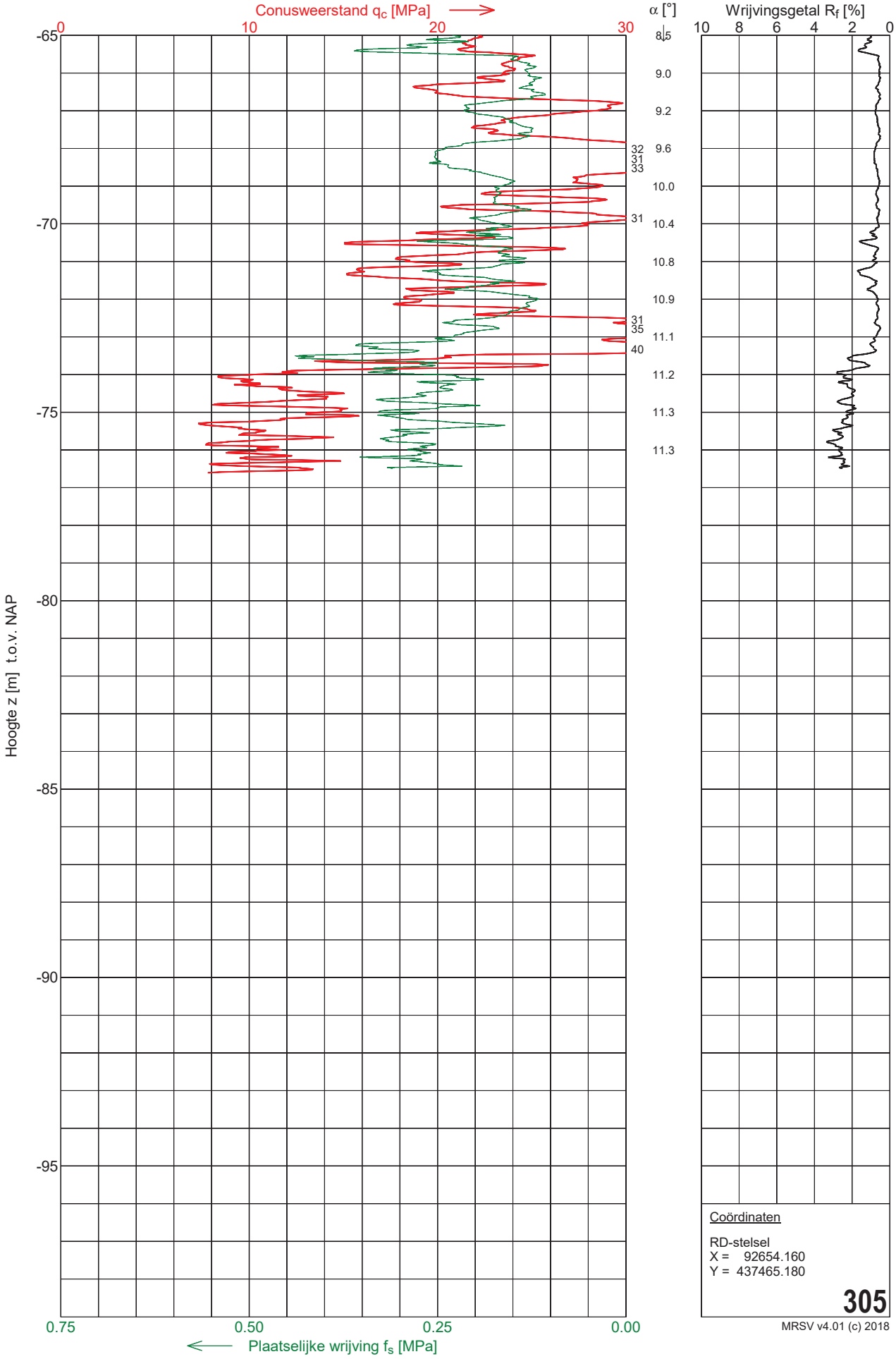

Coördinaten

RD-stelsel
X = 92654.160
Y = 437465.180

305

MRSV v4.01 (c) 2018

MOS GRONDMECHANICA

Sondering 206

Opdracht	: 2100886	Conus nummer	: S15-CFII.1970	NEN-EN-ISO-22476-1	
Plaats	: Rotterdam	Soort conus	: Elektrisch	Klasse 3, type TE1	
Datum	: 07-07-2021	Opp. conuspunt	: 1500 mm^2	Sondeerunit	: SW11
Project	: Postoffice			Blad	: 1 van 3

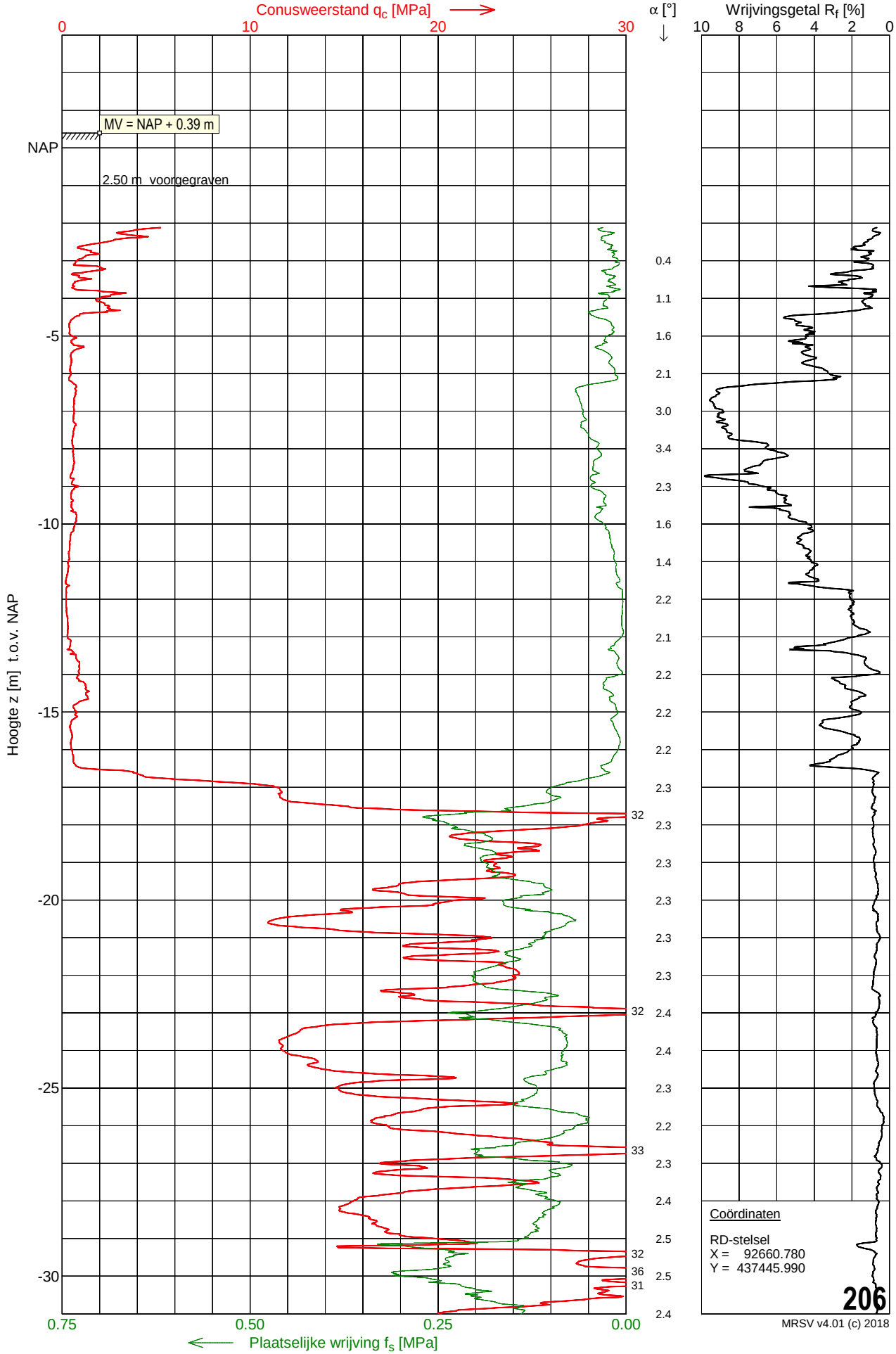

MRSV v4.01 (c) 2018

Sondering 206

Opdracht	: 2100886	Conus nummer	: S15-CFII.1970	NEN-EN-ISO-22476-1	
Plaats	: Rotterdam	Soort conus	: Elektrisch	Klasse 3, type TE1	
Datum	: 07-07-2021	Opp. conuspunt	: 1500 mm^2	Sondeerunit	: SW11
Project	: Postoffice			Blad	: 2 van 3

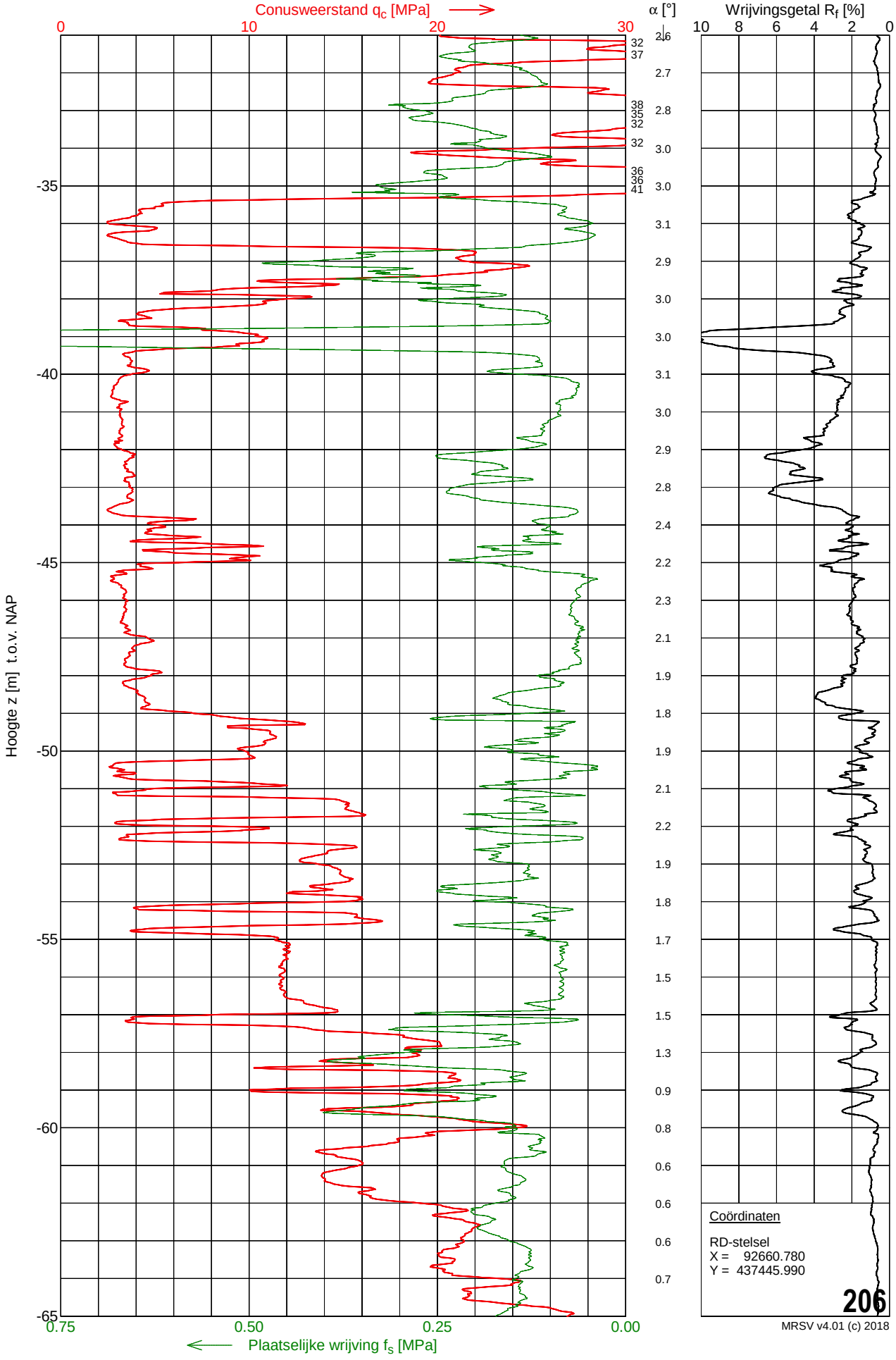

Sondering 206

Opdracht	: 2100886	Conus nummer	: S15-CFII.1970	NEN-EN-ISO-22476-1	
Plaats	: Rotterdam	Soort conus	: Elektrisch	Klasse 3, type TE1	
Datum	: 07-07-2021	Opp. conuspunt	: 1500 mm^2	Sondeerunit	: SW11
Project	: Postoffice			Blad	: 3 van 3

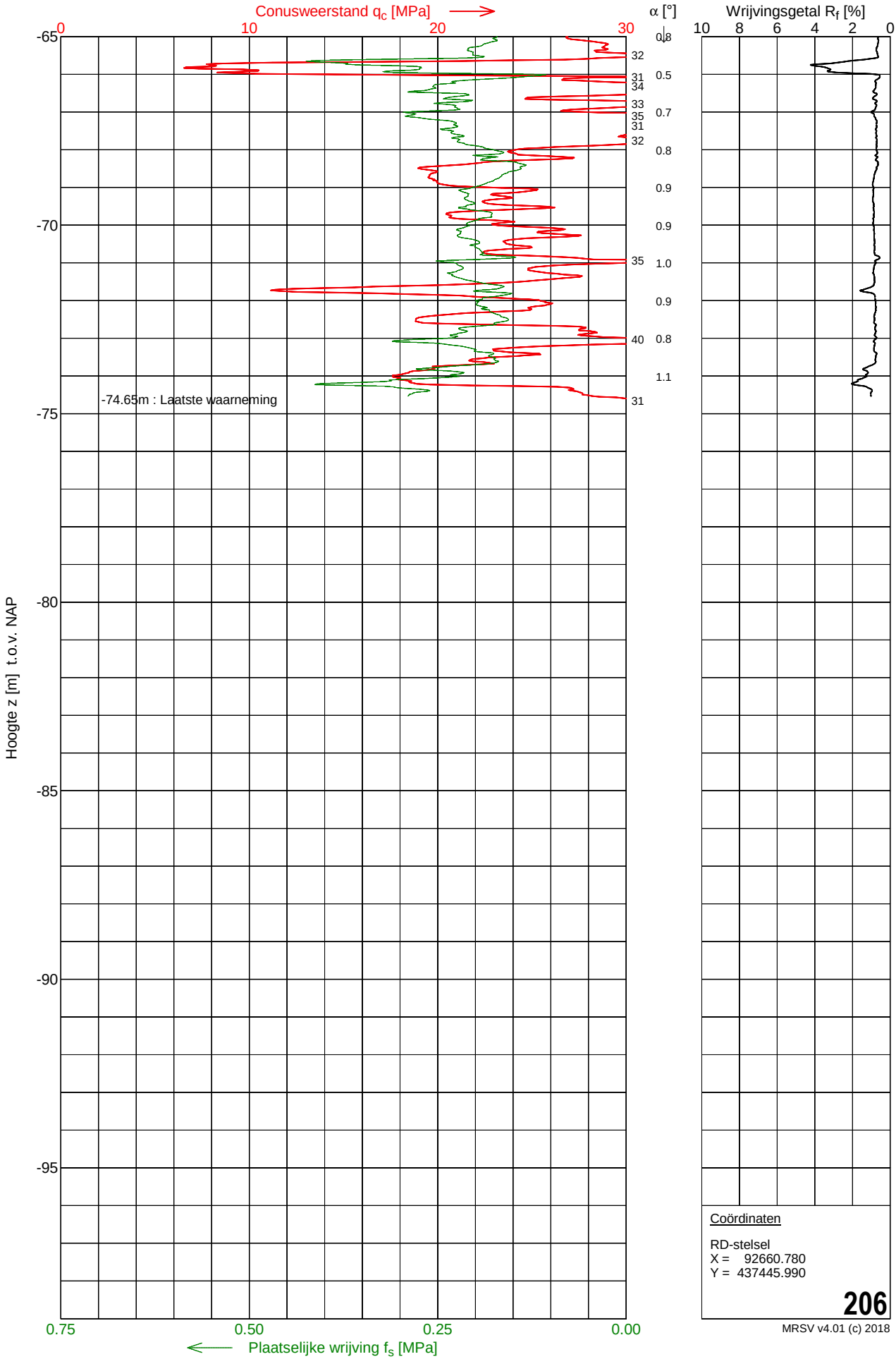

Coördinaten

RD-stelsel
X = 92660.780
Y = 437445.990

206

MRSV v4.01 (c) 2018

B

Construction progress of POST Rotterdam

This appendix includes an up-to-date photographic report of the construction progress of POST Rotterdam. Images hereby presented were collected from online archives as well as taken during site visits while developing this thesis.

Figure B.1: Demolition of the existing wall adjacent to Rodezand street and preparation of the work site (from Arch Daily, 2023).

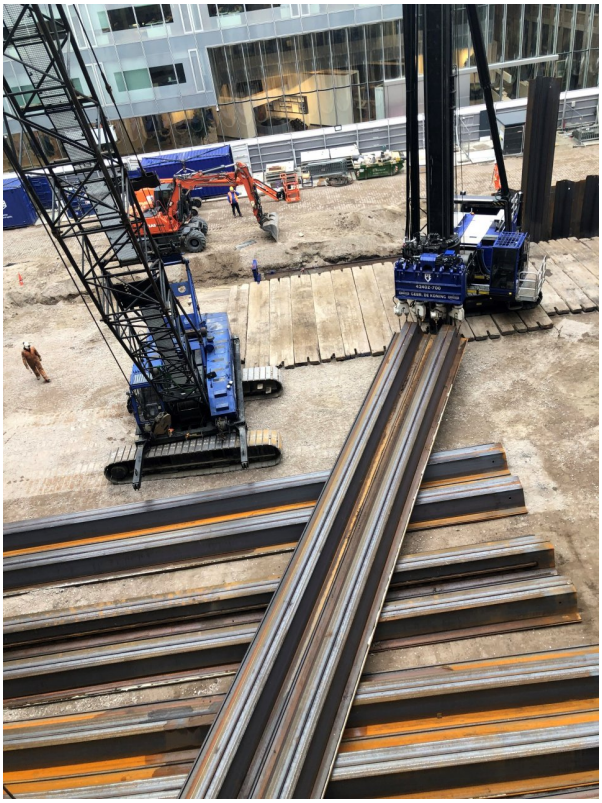

Figure B.2: Installation of the sheet piles and delimitation of the building pit (from The POST Bouw, 2023).

Figure B.3: Installation (and instrumentation) of screw-displacement piles. Excavation level at -2 m NAP is taking place.

Figure B.4: Installation of struts at -2.0 m (from The POST Bouw, 2023).

Figure B.5: Excavation up to -5.6 m. Pile heads become visible at this depth.

Figure B.6: Basement slab is visible.

Figure B.7: Installation of reinforcement for future casting of basement and ground floor.

Figure B.8: Groundfloor and first two floors are built (from Arch Daily, 2023).

C

Fibre optic interpretation process

This appendix includes an additional explanation of the interpretation process of the FO strain measurements on-site (Figure C.1), in accordance with Chapter 6. To this date, the baseline measurement was taken in all four piles after their respective installation (September 2022). Further, measurement 2[1] was carried out on July 2023 for three piles: 97, 31 and 18, as pile 92 was inaccessible on site at that moment. Both measurements are considered for the data processing hereby presented, thus this section contains results of piles 97, 31 and 18.

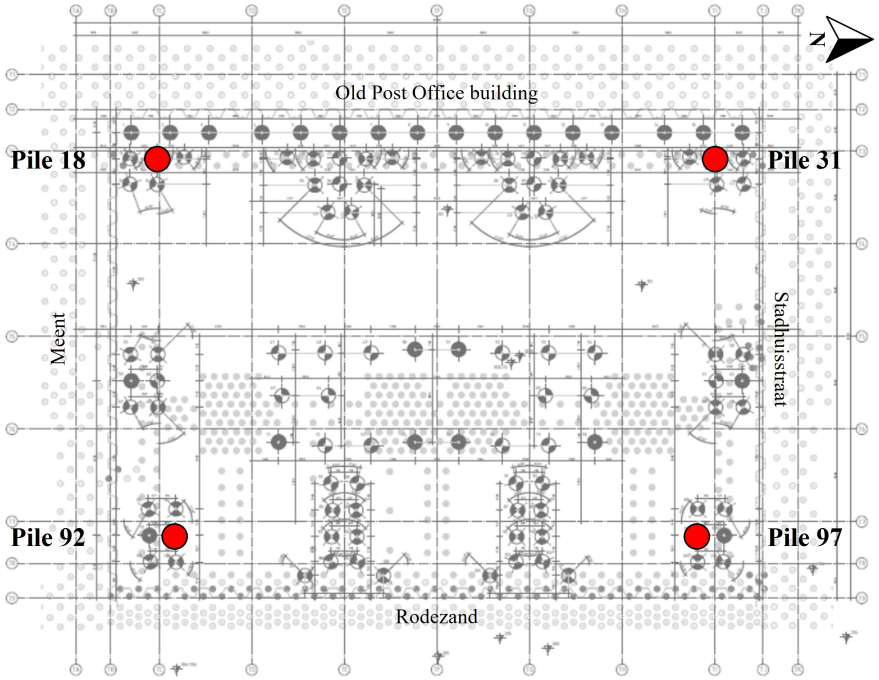

Figure C.1: Location of instrumented piles.

[1]It is called measurement 2, as in January there was a failed attempt to measure pile 97. While the latter is not considered in this interpretation explanation, it still produced (incorrect) results.

C.1. Pile 97

First, the baseline measurements of pile 97 are presented in Figure C.2. Three readings were obtained and later averaged.

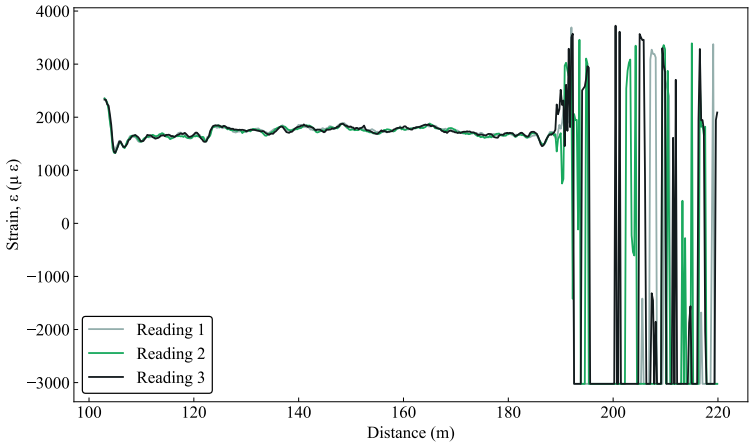

Figure C.2: Distance vs baseline strain measurements of pile 97.

Following, the second measurements are presented in Figure C.3. It should be noted that readings on site were taken separately from the two fibres inside the cable, as a way of verification of results, and due to this, it can be seen two sets of magnitudes of strain in Figure C.3, which, at the measurement stage, there is uncertainty of which one is correct. However, when comparing these results to the baseline measurement, the first set (Readings 1, 2 and 3) is approximately 1000 $\mu\varepsilon$ larger than it, which would lead to an unrealistic result of approximately 17,000 kN when transformed to axial force. Therefore readings 4, 5 and 6 are taken as the correct measurement, which lead to an average difference of 140 $\mu\varepsilon$ with the baseline measurement.

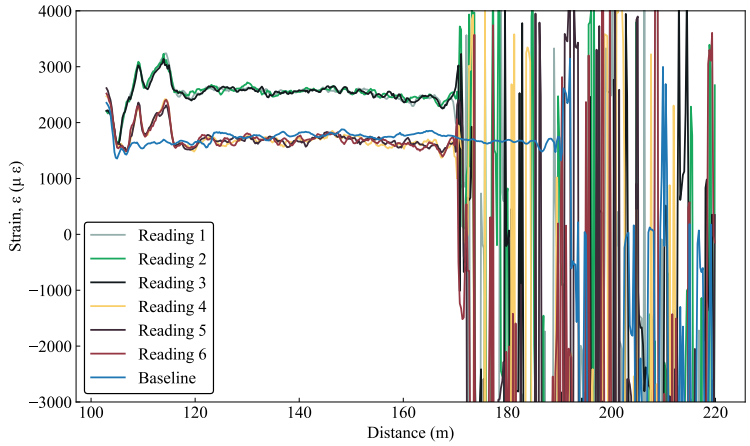

Figure C.3: Distance vs second strain measurements of pile 97.

Next, the distance results of measurement 2 were shifted to match the strains of the baseline measurement, and further cut to account for the length of the pile and eliminate readings of

the rest of the cable. When shifting measurement 2, it was important to match specifically the bottom of the graphs, under the hypothesis that the pile tip is expected to have almost null displacement during the construction stage of the building. To achieve this, the shift was indicated with a millimetric precision. Further, the strain of measurement 2 is interpolated to depths specified by the baseline measurement. The strain difference is calculated and used to get the axial force as expressed in Equation 3.1. Figures C.4a and C.4b show the results of strain and force for pile 97, respectively. These plots are also shown in Chapter 6.

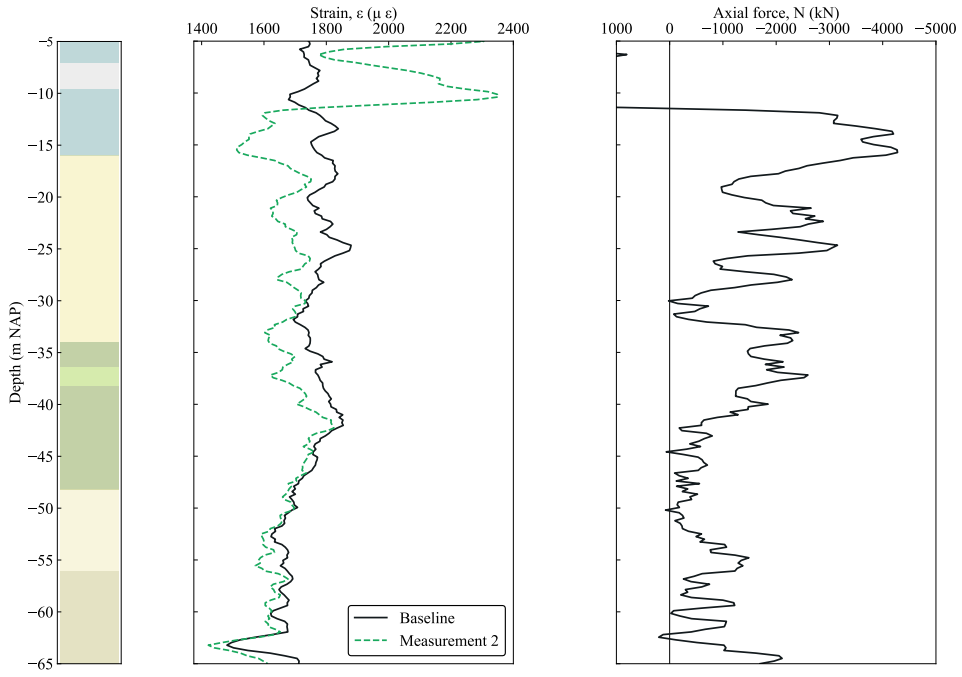

(a) Strain measurements vs depth. **(b)** Axial force results vs depth.

Figure C.4: Strain and axial force results of pile 97.

C.2. Pile 31

Pile 31 has a full loop of FO cable and therefore every reading outputs twice the pile profile. Therefore, the interpretation of readings is divided into measurement (a) and measurement (b) as shown in Figure C.5.

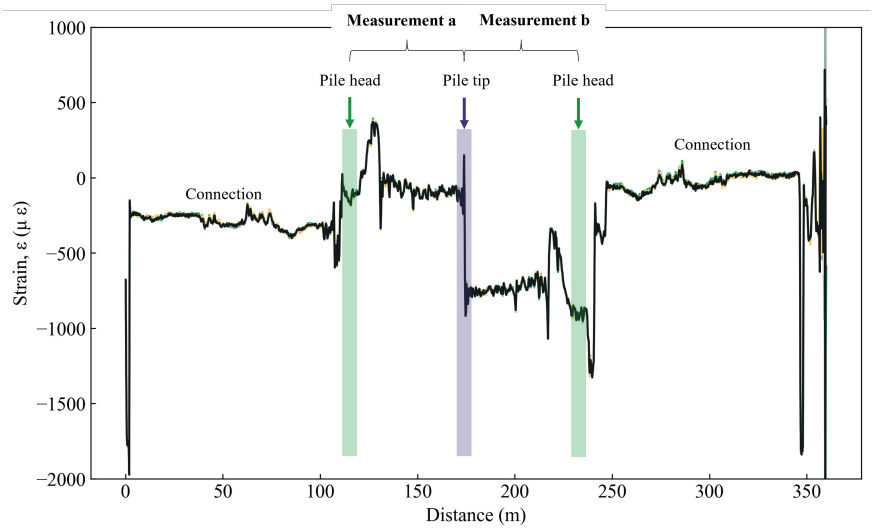

Figure C.5: Scheme of the full loop readings.

Baseline measurement readings are shown in Figure C.6. It can be seen that the results are consistent except for reading 1, which was eliminated from the average calculation of baseline measurement readings.

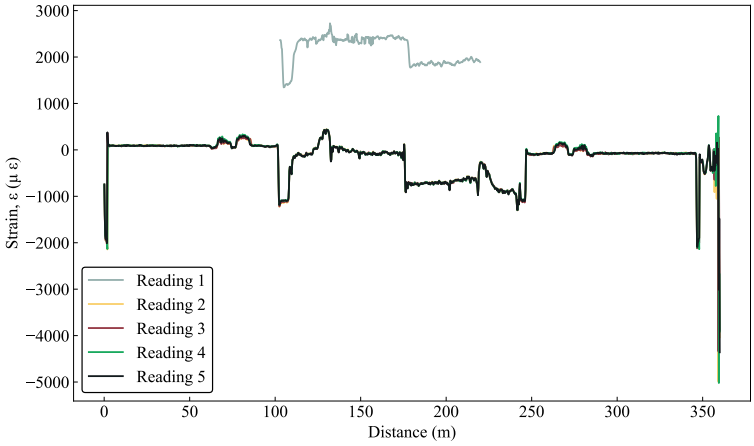

Figure C.6: Distance vs baseline strain measurements of pile 31.

Readings of measurement 2 are shown in Figure C.7. It can be seen there is a slight offset between measurements (a) and (b), and therefore both will be processed to verify the final accuracy of axial force calculation.

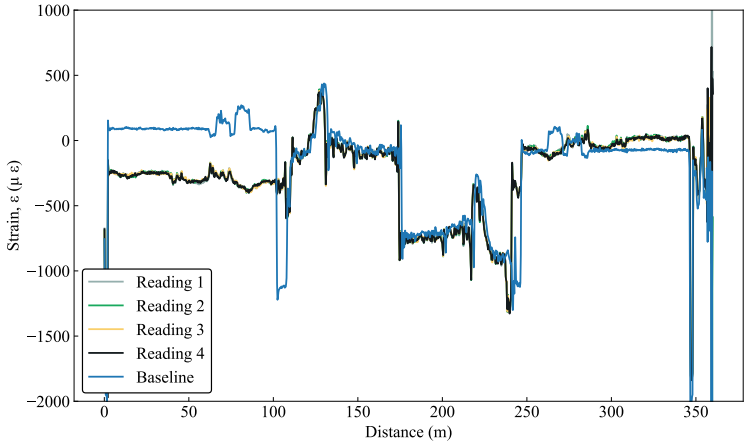

Figure C.7: Distance vs second strain measurements of pile 31.

Next, the results of measurement 2 were shifted to match the shape of the baseline measurement on a millimetric precision, and further cut to account for the length of the pile and eliminate readings of the rest of the cable. When shifting measurement 2, it was important to match both pile tips. Further, the strain of measurement 2 is interpolated to depths specified by the baseline. The strain difference is calculated and used to get the axial force. Figure C.8 shows the results of strain for pile 31, showing both profiles built with measurements (a) and (b), while Figure C.9 show the resultant force profiles, which are analysed in Chapter 6.

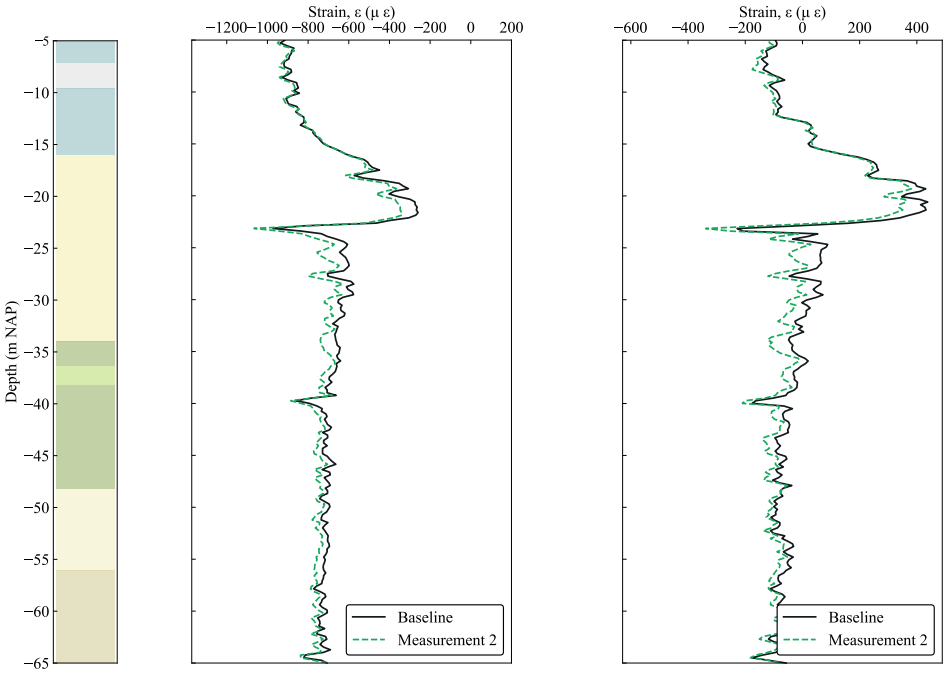

(a) Strain vs depth: Measurement (a). **(b)** Strain vs depth: Measurement (b).

Figure C.8: Strain results of pile 31.

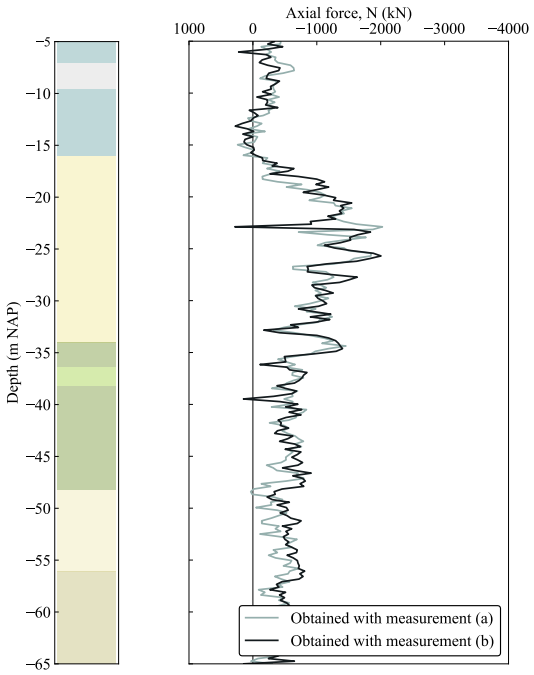

Figure C.9: Axial force results of pile 31.

C.3. Pile 18

Baseline measurements of pile 18 are presented in Figure C.2. Three readings were obtained and later averaged.

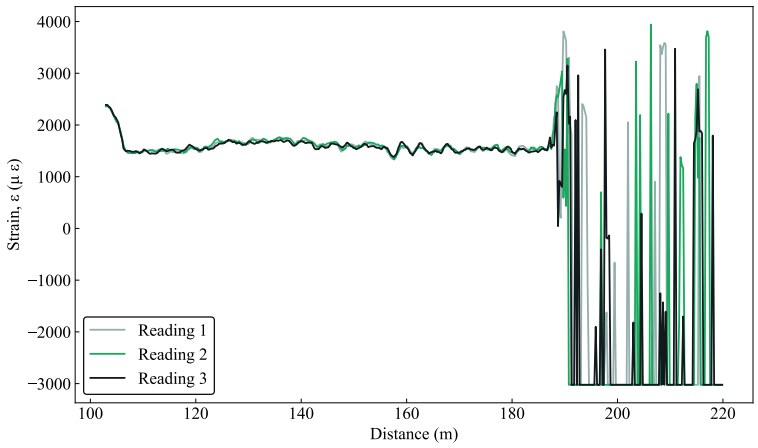

Figure C.10: Distance vs baseline strain measurements of pile 18.

Following, the second measurements are presented in Figure C.11. Similarly to pile 97, readings on site were taken separately from the two fibres inside the cable, resulting in two sets of magnitudes of strain as seen in Figure C.3. When comparing these results to the baseline measurement, it can be seen readings 5 to 8 are the ones to be considered for further study.

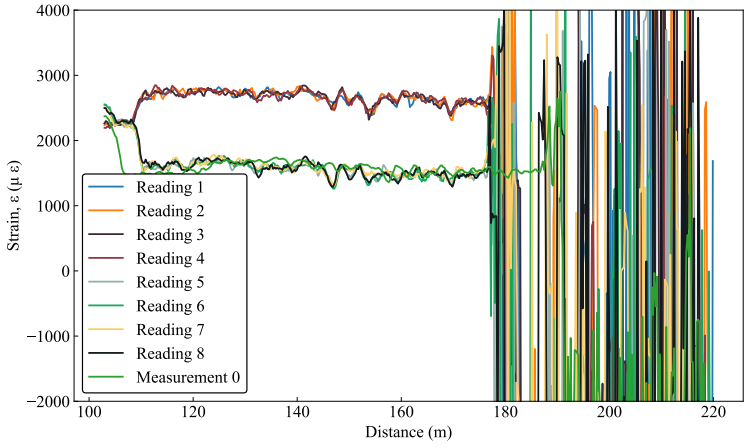

Figure C.11: Distance vs second strain measurements of pile 18.

Next, the distance results of measurement 2 were shifted to match the tip of the strains of the baseline measurement, and further cut to account for the length of the pile and eliminate readings of the rest of the cable. Finally, the strain of measurement 2 is interpolated to depths specified by the baseline measurement. The strain difference is calculated and used to get the axial force. Results are shown in Figure C.12 and evaluated in Chapter 6.

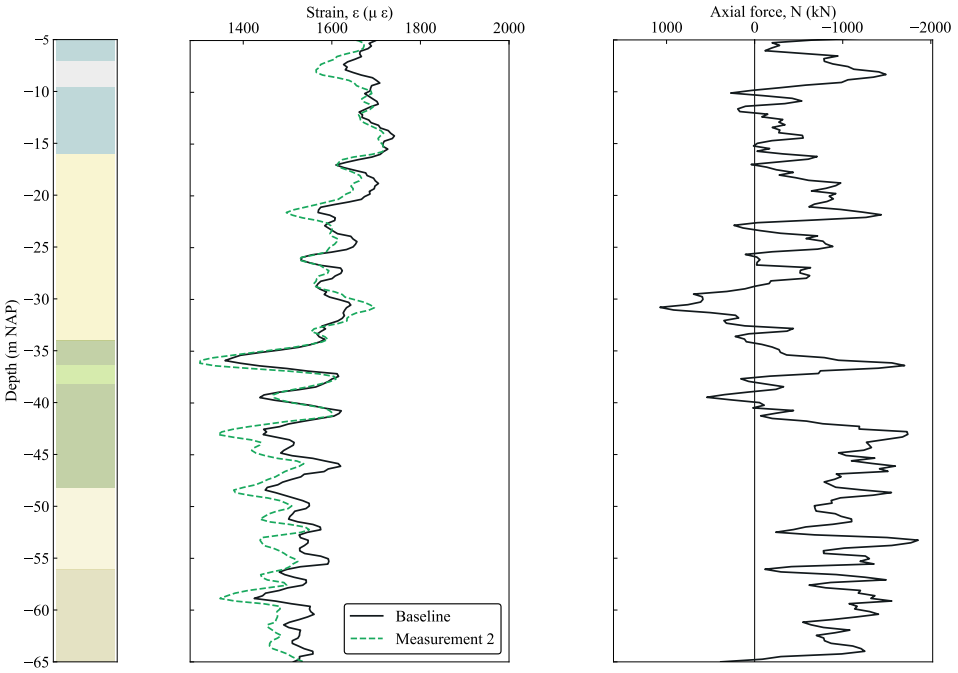

(a) Strain measurements vs depth. **(b)** Axial force results vs depth.

Figure C.12: Strain and axial force results of pile 18.